Advancing Microfluidic-based Protein Biosensor Technology for Use in Clinical Diagnostics

by

Seokheun Choi

A Dissertation Presented in Partial Fulfillment
of the Requirements for the Degree
Doctor of Philosophy

Approved July 2011 by the
Graduate Supervisory Committee:

Junseok Chae, Chair
Nongjian Tao
Hongyu Yu
Erica Forzani

ARIZONA STATE UNIVERSITY

August 2011

ABSTRACT

Demand for biosensor research applications is growing steadily. According to a new report by Frost & Sullivan, the biosensor market is expected to reach $14.42 billion by 2016. Clinical diagnostic applications continue to be the largest market for biosensors, and this demand is likely to continue through 2016 and beyond. Biosensor technology for use in clinical diagnostics, however, requires translational research that moves bench science and theoretical knowledge toward marketable products.

Despite the high volume of academic research to date, only a handful of biomedical devices have become viable commercial applications. Academic research must increase its focus on practical uses for biosensors.

This dissertation is an example of this increased focus, and discusses work to advance microfluidic-based protein biosensor technologies for practical use in clinical diagnostics. Four areas of work are discussed: The first involved work to develop reusable/reconfigurable biosensors that are useful in applications like biochemical science and analytical chemistry that require detailed sensor calibration. This work resulted in a prototype sensor and an in-situ electrochemical surface regeneration technique that can be used to produce microfluidic-based reusable biosensors. The second area of work looked at non-specific adsorption (NSA) of biomolecules, which is a persistent challenge in conventional microfluidic biosensors. The results of this work produced design methods that reduce the NSA. The third area of work involved a novel microfluidic sensing platform that was designed to detect target biomarkers using

competitive protein adsorption. This technique uses physical adsorption of proteins to a surface rather than complex and time-consuming immobilization procedures. This method enabled us to selectively detect a thyroid cancer biomarker, thyroglobulin, in a controlled-proteins cocktail and a cardiovascular biomarker, fibrinogen, in undiluted human serum. The fourth area of work involved expanding the technique to produce a unique protein identification method; Pattern-recognition. A sample mixture of proteins generates a distinctive composite pattern upon interaction with a sensing platform consisting of multiple surfaces whereby each surface consists of a distinct type of protein pre-adsorbed on the surface. The utility of the "pattern-recognition" sensing mechanism was then verified via recognition of a particular biomarker, C-reactive protein, in the cocktail sample mixture.

To My Wife ***Kyoungmi*** *and my daughter* ***Sua***

ACKNOWLEDGEMENTS

First and foremost, I would like to thank God for giving me strength and courage to pursue my doctoral program and to see it to completion. I would like to thank my wife, Kyoungmi, for all of her love, patience, support and the home cooked meals; and my lovely daughter, Sua, for her unconditional love and self-discipline in my absence. I really appreciate Soonwhan Choi and Sunae Kim, my parents. Their positive attitude towards education encouraged me to pursue a higher education. I am very happy to dedicate this dissertation to them.

I would like to express my deep and sincere gratitude to my Ph.D. advisor, Dr. Junseok Chae. Throughout my four-year Ph.D. study, his advice, support, and encouragement have always helped me in several arenas, including my study, my research, my scientific presentation and writing, and my creative thinking. I also thank my other committee members, Dr. Nongjian Tao, Dr. Hongyu Yu and Dr. Erica Forzani for taking interest in my work and giving me valuable advice.

I am grateful to members of my group: Dr. Sang-Soo Je, Dr. Yongmo Yang, Dr. Wencheng Xu, Xu Zhang, Helen Schwerdt, Sangpyeong Kim, Ran Wang and Arad Lajevardi-Khosh. I especially thank Rhonda Steele and Dr. Philip Bernick, who taught me how to improve my technical writing skills.

TABLE OF CONTENTS

Page

CHAPTER Page

CHAPTER Page

LIST OF TABLES

Table Page

LIST OF FIGURES

Figure Page

Figure Page

Figure Page

Figure Page

1 INTRODUCTION

1.1 Biosensor technologies

A recent advance in molecular biology has led to a better understanding of biomolecular interactions. The interactions of specific ligands, such as DNA-DNA, RNA-DNA, antibody-antigen, enzyme-substrate, and protein-aptamer, involve formation of a strong and specific chemical bond, allowing biosensors in detecting target biomolecules (Mohanty and Kougianos, 2006; Powner and Yalcinkaya, 1997; Skottrup et al., 2008; Wu et al., 2007). The basic structure and function of a biosensor is shown in Figure 1.1. A biosensor has a specific biomolecular recognition element (or Bioreceptor) that selectively recognizes a target analyte, and a transducer to monitor the recognition event. Recognition elements, such as antibodies, enzymes, aptamers, or DNAs, are immobilized on a solid surface and maintain permanent bonding through linker molecules.

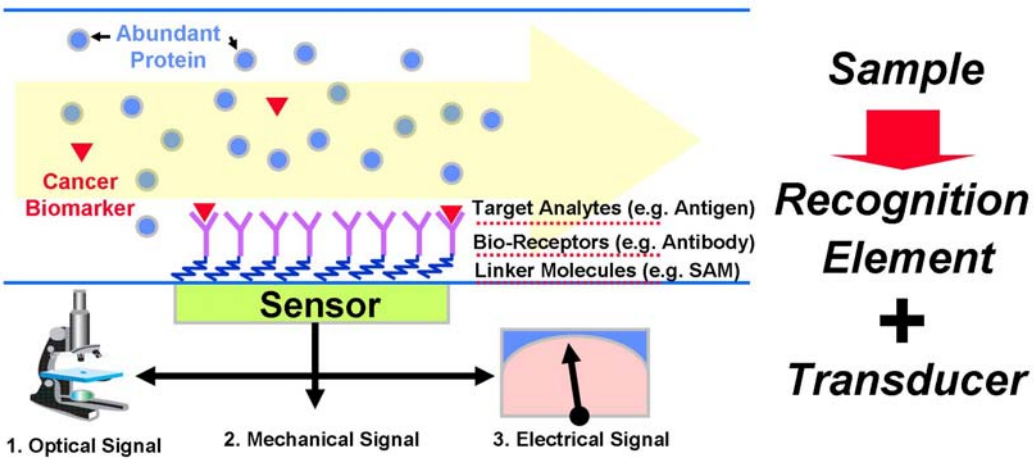

Figure 1.1 A general scheme of a protein biosensor.

Target disease-related biomarkers are captured by the recognition elements, which induce an optical, mechanical or electrical signal and it is then converted by a transducer into an output-readable signal. Biosensors can be either labeled or label-free systems. Labeling techniques have been broadly employed for biological/chemical analysis, but labeling may modify a target protein's characteristics, altering its behavior (Haab, 2003). Moreover, the labeling procedure is time-consuming and labor-intensive, and it is often difficult to achieve accurate quantification due to variable labeling efficiency for different proteins. The label-free technique, on the other hand, can eliminate the labeling process and is becoming a rather attractive alternative for biological analysis (Yu et al., 2006).

In clinical diagnostics, the analyte to be detected is a disease-related biomarker. By measuring levels of certain proteins expressed and/or secreted by infectious/cancer cells, biosensors provide information of the presence of a specific disease or the effectiveness of a treatment. However, there is a significant challenge for biosensors as diagnostic and therapeutic tools in clinics; the biosensors should be able to detect and characterize relevant biomarkers, comparable to or even better than conventional analytical systems. Biosensor technologies are currently deployed for clinical applications like blood glucose or blood gas measurement, but relatively few biosensors have been developed for disease-related diagnosis/prognosis. This is mainly because their combined performance of sensitivity and selectivity does not meet the clinical requirements. Recently, however, a number of novel biosensor technologies have been proposed,

and their practicality has been demonstrated by detecting actual disease biomarkers in a complex media such as serum.

1.1.1 Target biomarkers

Scientists have reported potentially fast, simple and inexpensive test techniques to detect disease-associated biomarkers (Rifai et al., 2006). Biomarker is an important parameter to assess the progress of disease and monitor the effects of treatment. For instance, molecular biomarkers allow early diagnosis of bladder cancer. Many genomics and proteomics techniques are available for biomarker detection (Khan, 2003; Tyers and Mann, 2003). Although both genomics and proteomics are used to correlate biomarkers to specific diseases, genomics are often limited in providing a predictable and reliable diagnosis. This is because the correlation in the levels of expression between mRNAs and corresponding proteins is still ill-defined (Huber, 2002). Moreover, one gene may express multiple proteins with variable biological function, and the proteins expressed from the genes may undergo a number of post-translational modifications which may be important in disease processes. Proteomics, on the other hand, has been considered as an effective diagnostic tool. This is because proteins are the final form of the gene product and hence directly associated with biological function. Many protein biomarkers have been discovered for aid of early diagnosis in the past (Sahab et al., 2007). Nevertheless, existing diagnostic approaches based on proteomics are still limited partially due to (i) low sensitivity at ultra low concentration biomarkers, (ii) complex three-dimensional protein conformation, and (iii) diverse forms of proteins.

1.1.2 Biomolecular recognition element

A recognition element is a critical component of any biosensor. These elements have a specific affinity site that captures the target analyte, and this determines the selectivity of the biosensor. Many different biomolecules have been used as recognition elements, including antibodies, enzymes, aptamers, and DNAs. Initially, biosensors used naturally-occurring recognition elements, purified from living systems. With advances in technology and synthetic chemistry, many biosensor recognition elements are now synthesized in the laboratory to support improved stability, and reproducibility for biosensing functions (Chambers et al., 2008).

Antigen- or antibody-based elements have been extensively studied in biosensor research. A distinct advantage of these elements is the inherent specificity of antibody-antigen interactions. This specificity precludes the need for purification prior to detection. This method became very popular significantly after monoclonal antibody technology was established.

Enzymes are very attractive as recognition elements because a variety of measurable reaction products arise from the catalytic process: protons, electrons, light, and heat. One of the most advanced sensors currently based on enzymes is the glucose sensor, which uses glucose oxidase as the recognition element. In the presence of oxygen glucose oxidase catalyzes glucose oxidation, producing gluconolactone and hydrogen peroxide. An amperometric transducer measures oxygen elimination or hydrogen peroxide formation, and converts that rate into a glucose reading.

Aptamers are nucleic acid ligands isolated from libraries of oligonucleotides by an in-vitro combinatorial chemistry-based technology. Aptamers can be synthesized from commercial sources with high reproducibility and purity, and they tend to be highly chemically stable compared to antibodies or enzymes.

1.1.3 Transducer technologies

Transducers convert recognition events into measurable signals. Many different transducing techniques exist, including mechanical, electrical, and optical. Mechanical sensors monitor stress or mass changes caused by molecular adsorption and interactions on a sensing surface. In stress sensing modes, molecular recognition events induce stress on the surface, resulting in mechanical bending of the surface. In mass sensing modes, transducing materials are brought into resonance. Mass variation induced by the recognition events on the materials is then correlated to the concentration of the target analyte. Film bulk acoustic resonators (FBARs) (Xu et al. 2010), quarts crystal microbalances (QCMs) (Aizawa et al. 2001) and microcantilever techniques (Wu et al. 2001) are well established as mechanical transducers, and have proven useful in identifying cancer biomarkers, including as prostate-specific antigen (PSA) and C-reactive protein (CRP). Wu *et al.* demonstrated that a microcantilever-based biosensor achieved a 0.2 ng/mL PSA detection rate from samples containing human serum and plasminogen (Wu et al. 2001). Kurosawa *et al.* reported a QCM immunosensor that provided pg/mL CRP detection directly from serum samples (Kurosawa et al. 2004).

Optical biosensors are light-based sensors that measure changes in optical characteristics. The transducer can be divided into two categories based on optical characteristics: optical intensity-based, and surface plasmon resonance (SPR)-based. Optical intensity-based measurements characterize some of the simplest and most widely used biosensors today. The optical signal can be either fluorescent or luminescent. Fluorescence detection is used mainly to identify the availability of labels with a large spectral range and different functional groups. Gervasis *et al.* demonstrated an impressive fluorescence-based microfluidic device that yielded a ng/mL detection limit for serum sample analysis, and contained various concentrations of the cardiac biomarker, CRP (Gervasis and Delmarche 2009). Luminescence detection relies on the enzymatic reaction of a luminogenic substrate solution, or activation following a highly energetic electron transfer process (during the application of a potential at an electrode surface). More recently, luminescent techniques have been utilized for detecting cardiac-specific biomarkers such as cTnI, myoglobin and CRP, at clinically significant concentrations. Surface plasmon resonance (SPR) is a very attractive optical transducer that allows real-time monitoring of biochemical interactions without the need for reagent labeling. SPR provides high analyte sensitivity up to few ppt (pg/mL) (Li et al. 2007). Recently, several research groups have been investigating the use of modified gold surfaces and gold nanoparticle-based sensors to improve detection sensitivities. SPR-based technology has been used to detect several cancer biomarkers: cTnI (cardiac troponin I), PSA, CRP, BNP

(brain natriuretic peptide), and fibrinogen (Mohammed and Desmulliez 2011, Choi et al. 2010).

Portability, miniaturization and cost effectiveness have led the development of electrical or electrochemical detection techniques over the past decades. Electrical biosensors have been downscaled to nanometer dimensions using silicon nano-wires or carbon nanotubes, demonstrating integration into CMOS technology up to 512 array positions (Simon 2010). Electrical biosensors fall into four categories: potentiometric, amperometric, conductometric and impedimetric sensors. Potentiometric biosensors are based on measuring changes in the potential induced by recognition events between bioelements and target analytes. The most common form of potentiometric sensors is ion-sensitive field effect transistors (ISFETs). Kamahori *et al.* demonstrated ISFET-based potentiometric immunosensors, which allowed detection of Interleukin 1β, an inflammatory biomarker, at a range of 1 ~ 250 pg/mL (Kamahori et al. 2007). Amperometric biosensors measure the current generated when electro-active species are either oxidized or reduced at the electrode at a fixed potential. The most widely used examples are glucose biosensors monitoring hydrogen peroxide formation when the hydrogen peroxide is reduced at -600 mV at Ag/AgCl reference electrode. Conductometric biosensors measure the conductance changes associated with changes in the overall ionic medium between two electrodes. Conductometric techniques are attractive due to their simplicity and ease of use since no specialized reference electrode is required. Zheng *et al.* reported detection of a cancer marker, PSA, using a silicon-nanowire conductometeric biosensor (Zheng

et al. 2005). They identified a detection limit of 0.9 pg/mL in undiluted serum samples. Last but not least, impedimetric sensors monitor any change in resistance or capacitance at the sensor surface on which biomolecular reaction occurs. Billah *et al.* presented a microfluidic impedimetric biosensor capable of detecting the cardiac biomarker, myoglobin, of 15 ng/mL (Billah et al. 2006). The transducer techniques and specifications reviewed here are summarized in Table 1.1.

Table 1.1 Summary of various transducer techniques

Transducer type		Target Analyte	Recognition element	Labeling	Limit of detection	Real-time detection	Ref.
Mechanical	QCM	CRP	Anti-CRP	No	10 pg/ml	Yes	Kurosawa et al. 2004
	Cantilever	PSA	Anti-PSA	No	0.2 ng/ml	Yes	Wu et a. 2001
Optical	Fluorescence-based	CRP	Anti-CRP	Yes	1 ng/ml	No	Gervasis and Delmarche 2009
	Luminescence-based	cTnI	Anti-cTnI	Yes	0.1 ng/ml	No	Cho et al. 2009
	SPR	cTnT	Anti-cTnT	No	10 pg/ml	Yes	Dutra and Kubota 2007
Electrical	Potentiometric sensor	IL-1β	Anti-IL-1β	Yes	1 pg/ml	No	Kamahori et al. 2007
	Amperometric sensor	H-FABP	Anti-H-FABP	Yes	4 ng/ml	No	O'Regan et al. 2002
	Conductometric sensor	PSA	Anti-PSA	No	0.9 pg/ml	Yes	Zheng et al. 2005
	Impedimetric sensor	Myoglobin	Anti-Myoglobin	No	15 ng/ml	Yes	Billah et al. 2008

1.1.4 Surface plasmon resonance

Among various transducer techniques, SPR (Surface plasmon resonance) has been one of the leading techniques due to its extremely high sensitivity, offering detection limits up to few ppt (pg mL^{-1})). SPR is an optical tool that uses the excitation of surface plasmons and it is a surface-sensitive analytical tool

responding to slight changes in refractive index occurring adjacent to the metal film (Figure 1.2). In this way, binding of proteins on the surface and their affinity interactions can be monitored in real-time without labeling.

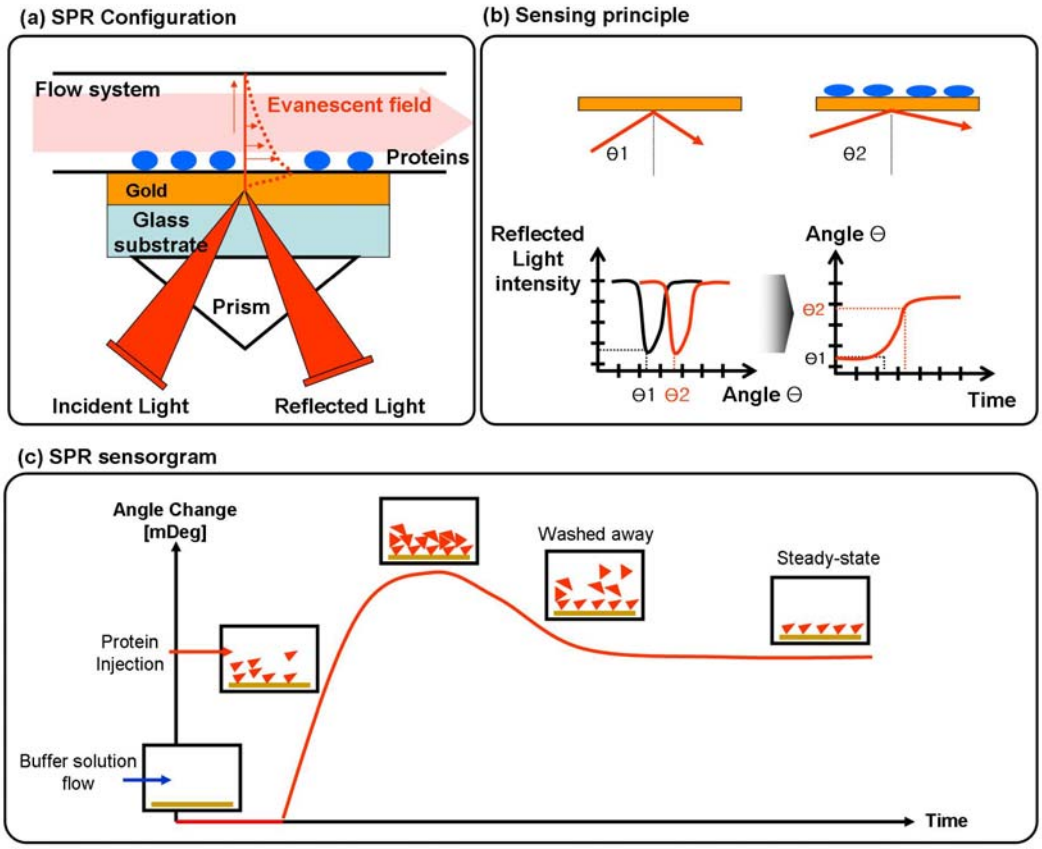

Figure 1.2 (a) Schematic view of the SPR-based biosensor. (b) Molecular interactions on the gold layer produce the SPR angle changes. (c) Typical SPR sensorgram.

SPR can be configured in various ways to monitor the molecular interactions. So far, there are three different optical systems to excite surface plasmons; systems with (i) prisms (ii) gratings and (iii) optical waveguides. Among them, SPR using a prism coupler is most widely adopted, and also called

the “Kretschmann configuration” because of enhanced stability and sensitivity. The SPR using a prism consists of several components; a light source, a prism, a sensing surface, a flow regulator, and a photo-detector. A glass slide covered by a thin gold film is optically coupled to a prism via a refractive index matching liquid. Plane polarized light is directed through a prism to the gold film over a wide range of incident angles and the intensity of the reflected light is detected by a photo-detector. At a certain incident light angle, surface plasmon reaches a maximum and the reflected light becomes minimum, which is denoted as the SPR angle. The propagation constant of the surface plasmon wave propagating at the interface between a dielectric and a metal is given by

$$k_{sp} = k_0 \sqrt{\frac{\varepsilon_{metal}\varepsilon_{sample}}{\varepsilon_{metal} + \varepsilon_{sample}}}, \tag{1.1}$$

where k_0 is the free space wave vector of the optical wave, ε_{metal} and ε_{sample} are the complex dielectric constants of the metal and the sample medium respectively. The enhanced wave vector of incident light (k_x) is given by

$$k_x = k_0 n_{glass} \sin\theta_i, \tag{1.2}$$

where n_{glass} is the refractive index of the prism and θi, the angle of incidence. In order to excite the plasmons at resonance, the two vectors should be matched, i.e.

$$k_{sp} = k_x. \tag{1.3}$$

Therefore, a small variation of ε_{sample}, which is the dielectric properties of the medium adjacent to the sensing surface, will lead to a large change of SPR angle (θ_i). Figure 1.2 (c) shows a typical SPR sensorgram. Initially, PBS (Phosphate

Buffered Saline) is circulated for about 20 min until the angle shift stabilizes. Once the angle shift stabilizes, the protein sample flows through the microfluidic channels, reaches the surface, and generates an angle shift that is proportional to the molecular interactions on the surface. When protein adsorption completes, PBS was flowed to wash the surface to remove excess weakly bound proteins to obtain a steady-state angle value.

1.2 Microfluidics and point-of-care diagnostics

Recently, there has been an increasing interest to integrate advanced biosensors into lab–on-a-chip systems by introducing microfluidics. The lab-on-a-chip systems take advantage of several intrinsic characteristics of microfluidics including laminar flow, low consumption of costly reagents, minimal handling of hazardous materials, short reaction time required for analysis, multiple sample detection in parallel, portability, and versatility in design. With microscale fluid regulators (e.g. valves, mixers and pumps) integrated on the lab-on-a-chip platform, the analytical performance of biosensors towards point-of-care (POC) diagnostics can be greatly enhanced. POC testing is one of the most promising areas for biosensor applications and readily provides the clinician essential information of proper treatments. In developing areas and disaster scenes where only very limited resources are readily accessible, POC system is an attractive tool to diagnose patients for proper clinical management. Nevertheless, the stringent requirement of POC diagnostics presents new challenges for biosensor technologies. For instance, detecting target analytes with high sensitivity and selectivity is a key challenge in microfluidic-based POC because of the ultra-

small sample volumes. Another challenge is to merge the detection component with other fluid regulatory elements on a single platform.

1.3 Goals of dissertation

The overall objective of this dissertation is to advance microfluidic-based protein biosensor technologies for practical use in clinical diagnostics. It is organized as follows: Chapter 1 provides background for the work discussed. Chapter2 discusses an in-situ electrochemical technique to regenerate a protein biosensor surface in microfluidics. This work was motivated by a growing demand for high accuracy, high precision, and increased functionality in these sensors has created a new platform for exploring reusability in microfluidic applications. Chapter 3 explores a persistent challenge in creating widespread commercial protein biosensors: non-specific adsorption of biomolecules, which causes false responses and decreases sensitivity in biosensors. The goal of the work discussed was to reduce the non-specific adsorption in a microfluidic protein sensor by using relatively short-chain self-assembled monolayer as a linker molecule. Chapter 4 describes work on an innovative technology that can be used to detect disease-related biomarkers. This is a fundamentally different protein detection method that relies on the competitive nature of protein adsorption onto a surface instead of immobilized biomolecular recognition elements to detect these biomarkers. Chapter 5 discusses work done to extend the protein adsorption behavior to a novel method of protein identification based on patterns generated from the utilization of multiple types of biosensing surfaces. The pattern generation method will allow the analysis of complex analytes and mixtures. Chapter 6

summarizes the major findings of this dissertation and offers suggestions for further work on these projects.

2 REUSABLE BIOSENOSRS VIA IN-SITU ELECTROCHEMICAL SURFACE REGENERATION IN MICROFLUIDIC APPLICATIONS

2.1 Introduction

There are three main approaches to biosensor applications; qualitative, semi-quantitative and quantitative sensor (Kissinger, 2005). While Qualitative sensors only provide existence of target analytes (pregnancy test), semi-quantitative ones can detect and quantify the analytes in sub-threshold level (DUI test). Both techniques are commercially available now and have proved very useful for many areas of clinical specialty (i.e glucose monitoring), food industry, and environment monitoring. In those cases, disposable biosensors have been the more successful ones to date, taking advantage of low cost materials and batch fabrication (Nakamura and Karube, 2003). On the other hand, quantitative sensors are required to cover a wide dynamic range and have high resolution and accuracy to produce large signal to noise ratio data. In particular, with the growth of genomics and proteomics, there is an increasing need for more quantitative analysis which can elucidate the mechanisms that regulate the formation and activities of specific biomolecular complexes (Lee et al., 2005).. In the quantitative technique, detailed calibration of biosensors is required. So far, quantitative results have been typically obtained using a series of measurements with disposable sensor units (Asanov, et al., 1998). However, variation coming from batch-to-batch irreproducibility and uncontrollable experimental condition generates unalterable false-positive/negative responses. This motivates this work

to design a reusable/regenerative or even reconfigurable biosensor, especially in a microfluidic device.

Reusable biomolecular sensors are very useful; yet there has been little practical success despite many attempts thus far. These approaches can be summarized into two ways. First technique is to dissociate the target-bioreceptor complexes. Once target analytes bind to the specific bioreceptor and the recognition event is transduced, the target analytes are removed and the remaining bioreceptors are reused as a probe for detecting the same target molecules. The extreme pH, temperature, and chaotropic agents to detach the target from the bioreceptor have been used. As a consequence of the strong agents a significant loss of biospecific activity occurs (Asanov et al., 1998). Moreover, some biomolecules cannot be dissociated because of the high affinity of biomolecular interactions and their stability in extreme conditions (Asanov et al., 1998). Recently, Chen et al. reported that low frequency AC electric field dissociates the C-reactive proteins from antibodies (Chen et al., 2006). The loss of affinity from multiple use and the possibility of reductive or oxidative desorption of linker molecules induced by the low frequency AC electric field were not addressed (Oldham and Asanov, 1999). These approaches impose limitations in dissociating the target-bioreceptor complexes and reduce the activity of biomolecular receptors (Saerens et al. 2008). Second technique of implementing reusable sensors is to remove the linker molecules with all bounded biomolecules (Yuan et al., 2008; Raiber et al., 2005; Kim et al., 2008).. Generally linker molecules are used to immobilize the bioreceptors on a solid surface to maintain permanent

bonding. Self-assembled monolayer is a good candidate as a linker molecule because it is easy to be formed spontaneously and be used to control the orientation of the bioreceptors. To remove the linker molecules, existing techniques use acid, base or detergent (Deval et al., 2004; Limbut et al.,2006; Minunni et al., 2004; Gau et al., 2001; Zhang et al., 2008). However, the extreme solutions damage the sensing sites and have a fatal impact on the next regeneration step. Recently, an alternative method has been proposed using electrochemical desorption of SAMs (Balasubramanian et al., 2006; Canaria et al., 2006; Mirsky, 2002). Its theoretical mechanism has long been studied and well established (Han et al., 2008; Imabayashi et al., 1997; Lee and Lennox, 2007; Oyamatsu et al., 2008; Vericat et al., 2001; Widrig et al., 1991). Electrochemical desorption of SAMs on metal surfaces occurs at negative potential or positive potential. At negative potential, a reductive desorption on a metal (Au) surface occurs according to the following reaction

$$R - S - Au + e^- \rightarrow R - S^- + Au, \quad (2.1)$$

where R and S represent an n-alkanethiols, i.e., alkanethiolates are desorbed from a gold surface by the one-electron reduction process in an electrolyte (Figure 2.1).

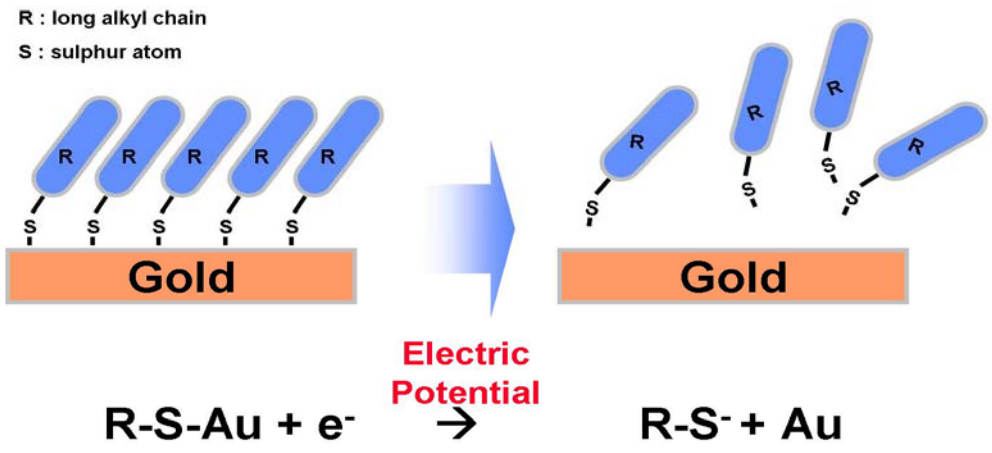

Figure 2.1 A schematic of SAM desorption

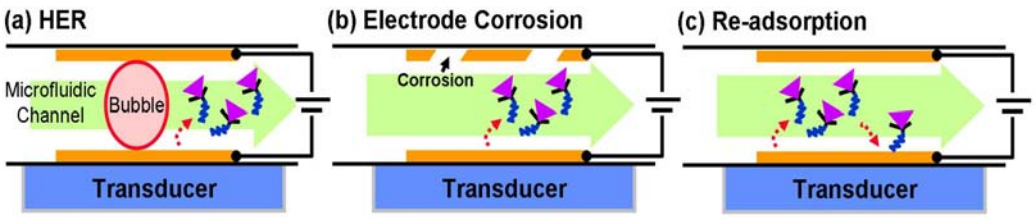

Figure 2.2 Three challenges in developing a reusable microfluidic biosensor

At voltammograms measured in 0.5 M KOH solutions (versus Ag/AgCl), reductive peak potential, Ep, ranges from -0.7 V to -1.2 V depending upon the thiol derivatives, length of the alkyl chain, the metal substrates and the electrolyte solutions. Also, an oxidative desorption occurs at positive potential (+0.8 V ~ +1.2 V) but this process has been studied less extensively.

Recently, many applications have been proposed using the desorption of SAMs. Riepl et al. suggested an electrical control method for addressable immobilization of different bioreceptors on electrode arrays (Riepl et al., 1999).

Balasubramanian et al. gauged the general applicability of SAM desorption to reusable biosensor devices (Balasubramanian et al., 2006). However, fewer studies have attempted to apply the SAM desorption to the microfluidic systems. This is because i) hydrogen evolution reaction (HER) occurs at a similar potential to the potential of the SAM desorption reducing the sensitivity of the biosensor (Schilardi et al., 2006) (Figure 2.2 (a)) and (ii) when reductive potential is applied to the SAM-coated electrode, the opposite electrode suffers from corrosion (Santini et al., 2000; Lukaszewski and Czerwinski, 2006) (Figure 2.2 (b)). In addition, (iii) reductively desorbed SAMs can be re-adsorbed onto the sensing surface (Shepherd et al., 2004), posing a practical obstacle to reuse (Figure 2.2 (c)). Overcoming those issues in microfluidic applications is the focus of this work.

2.1.1 Electrode corrosion and hydrogen evolution reaction

Both electrode corrosion and hydrogen evolution reaction **(**HER) are the main challenges to develop a reusable/reconfigurable biosensor because the issues not only damage the sensing surface itself but also reduce the sensitivity, reliability and the accuracy of the biosensors. In particular, it is difficult to remove hydrogen bubbles by low flow rate of solution; typically several 10's of μl/min is used in microfluidic devices. The bubbles reduce the sensitivity, reliability, and accuracy of the biosensor. Several groups desorbed SAM in a strong alkaline electrolyte to avoid HER (Lee and Lennox, 2007); however, most biosensors need to operate in a physiologically relevant medium such as PBS (pH=7.4) and few research activities exist to explore SAM desorption in such physiological solutions.

Electrode corrosion and HER are attributed to high reductive potential for electrochemical desorption of SAMs, especially in a physiological solution. In order to minimize these limitations, the reduction potential is shifted less than -1.0V using short chain SAMs ($COOH(CH_2)_nSH$, n=2 and $CH_3(CH_2)_nSH$, n=3). SAMs desorb in sharp voltammetric peaks whose peak potentials shift in the negative potential direction as the hydrocarbon chain length of the alkanethiol molecule increases; thus the shorter the chain length is, the lower the reduction potential is (Imabayashi et al., 1997). Linear sweep voltammetry is used to characterize the desorption of SAMs as a function of the length of the alkyl chain, the type of terminal groups and the binding of proteins. Ellipsometry are used to evaluate the desorption of SAMs before and after the desorption. SPR in-situ monitors successive experimental procedure of reconfigurable biosensor in real time, including SAM formation, protein modification, and SAM desorption in the microfluidic device.

2.1.2 Re-adsorption of detached molecules

SAMs with intermediate ($8 < n < 16$) or long chain lengths ($n \geq 16$) are commonly used as linker molecules in existing biosensor applications to immobilize biomolecules. They offer a high degree of surface coverage with little defect (Anandan et al., 2009), but their detached SAMs have significant re-adsorption rates, posing a practical obstacle to reuse the sensing surface (Shepherd et al., 2004; Pesika et al., 2006). Accumulation is significant because re-adsorption prevents complete regeneration of the biosensor surface, interferes with subsequent immobilization cycles, and degrades sensor sensitivity. This

results in the use of short-chain SAMs as linker molecules to immobilize molecular probes. They promote higher detection sensitivity than long chain SAMs (Anandan et al., 2009), and have lower steric hindrance, leading to the ordering of the structures by the terminal groups (Jang and Keng, 2008). In addition, they require shorter incubation time (~ 6 hours) for their full formation than that of the long chain SAMs (~ 24 hours) (Anandan et al., 2009). Above all, short-chain SAMs rapidly diffuse away from the electrode surface under the desorption conditions, resulting in little or no re-adsorption (Pesika et al., 2006).

2.2 Experimental methods

2.2.1 Chemicals

n-alkanethiols ($CH_3(CH_2)_nSH$) with n=3 (1-butanethiol) and n=11 (1-dodecanethiol) and ω-carboxylic acid alkanethiols ($COOH(CH_2)_nSH$) with n=2 (3-mercaptopropionic acid) and n=10 (11-mercaptoundecanoic acid) are purchased from Sigma Aldrich. PBS 1X. (1.15 g/L-Na_2HPO_4, 0.20 g/L-KCl, 0.20 g/L-KH_2PO_4, 8.0 g/L-NaCl, pH 7.4), sodium acetate (NaAc), absolute elthanol are obtained from Mediatech, Inc. 1-ethyl-3-(3-dimethylaminopropyl) carbodiimide (EDC) and N-hydroxysuccinimide (NHS) are purchased from Fisher Scientific. Streptavidin and fibrinogen are from Calbiochem. All the chemicals are used without further purification.

2.2.2 Surface preparation for ellipsometry and linear sweep voltammetry

Glass substrates (BK7, n=1.517) are first cleaned in piranha solution (a 3:1 ration of H_2SO_4 and H_2O_2) for 10 min. The cleaned glass is coated with Cr/Au (2 nm/47 nm) by thermal evaporation. The substrates are cleaned by oxygen plasma

(Harrick Plasma Inc.) at 18 W for 1 min and then immersed in an ethanol solution of alkanethiols at 2 mM for 1h at room temperature to form SAMs.

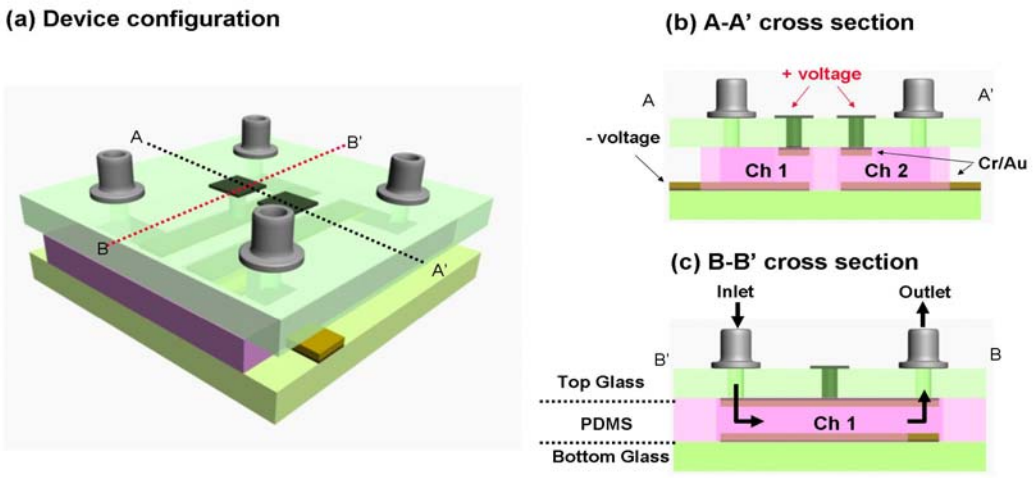

Figure 2.3 A schematic of a microfluidic device. (a) Device configuration (PDMS spacer between glass substrates with Cr/Au electrodes); (b) A-A' cross section; (c) B-B' cross section

2.2.3 Fabrication of microfluidic devices

Figure 2.3 shows the microfluidic device to characterize a reusable and reconfigurable biosensor. Top and bottom glass substrates have Cr/Au electrodes and the spacer between the two substrates is made of PDMS. These layers are bonded all together by using oxygen plasma. Cr/Au of bottom layer (2 nm/47 nm) is evaporated and patterned on a 150 um-thick glass substrate for SPR measurement. 1 mm-thick top glass is mechanically drilled to have six holes including two inlets, two outlets, and two electrical contacts which are filled with silver paste for feedthroughs. The PDMS layer is prepared to be 1 mm in thickness and mechanically cut to have two channels; reference and sample

channels. Electrical potential is applied between the top and bottom electrodes; negative potential to the bottom with respect to the top electrode.

2.2.4 Methods and evaluation

The electrochemical desorption process of SAMs has been investigated by many techniques including electrochemistry, Fourier Transform Infrared Spectroscopy (FTIR), electrochemical Quartz Crystal Microbalance (QCM), in-situ Scanning Tunneling Microscope (STM), Second Harmonic Generation spectroscopy (SHG), Sum Frequency Generation (SFG), ellipsometry, Raman spectroscopy, and SPR (Imabayashi et al., 1997; Yang et al., 1997; Qu and Morin, 2001; Wano and Uosaki, 2001; Buck et al., 1991; Himmelhaus et al., 2000; Bain et al., 1989; Peterlinz and Georgiadis, 1996; Jung and Campbell, 2000; Damos et al., 2005; Bryant et al., 1991).. Among all these techniques, electrochemical method is the easiest way to characterize the electrodesorption process showing a current density (j) vs. potential (E) profile. Ellipsometry is used to evaluate the thickness of SAMs on a metal electrode. SPR is a real time, in-situ optical technique that monitors the incident light angle needed to excite surface plasmons at the interface of a thin film of metal and a dielectric layer, such as a SAM. As the thickness of the dielectric layer increases – for example, as proteins bind to a SAM – the resonance angle decreases. Thus the change in resonance angle shows the amount of protein adsorbing to a SAM . Ellipsometry is usually used to evaluate the thickness of SPR (Balasubramanian et al., 2006).

2.2.5 Linear sweep voltammetry

To obtain the operating potential of SAM desorption in the microfluidic device and confirm that the reductive desorption would not be obscured by HER and the electrode corrosion, ex-situ electrochemical measurement was conduced using linear sweep voltammetry. A custom-made electrodes set was built; electrodes were placed at the bottom hole of the cell with a silicone rubber O-ring and the top hole was tightly fitted with a silicon rubber stopper having a Pt wire counter and Ag/AgCl reference electrodes. Linear sweep voltammetry was conducted using a computer-controlled potentiostat (PGSTAT302N, Eco Chemie).

2.2.6 SPR measurement and surface modification procedure

All surface modification steps upon electrochemical desorption on the metal electrode were monitored by SPR in situ in real time. SPR angle shift was produced by differential measurement using two (reference and sensing) channels in the microfluidic device. As shown in Figure 1, the fabricated microfluidic chip was mounted on the SPR analytical system (Biosensing Instrument Inc.), and the angle shift was recorded in real time as each solution inducing surface modification flows through the microfluidic channels driven by an external syringe pump.

2.3 Results and discussion

2.3.1 Electrode corrosion and hydrogen evolution reaction

2.3.1.1 Reductive desorption of SAMs on the cathode

This section explores two challenges to overcome in order to form the reusable/reconfigurable biosensor; i) electrochemical reductive desorption of SAMs without HER and ii) reductive potential to avoid peeling of the metal electrode. HER is the most challenging problem during the electrochemical desorption process. Electrolysis is a process to produce hydrogen at the cathode and oxygen at the anode when electrodes are in an aqueous solution and current runs through the solution. When reductive potential is applied on the cathode, it is difficult to measure reductive peak potential, E_p, since electrodesorption of SAMs and HER occur simultaneously. HER can be fatal in a microfluidic channel because the bubbles generated by HER tend to stay on the cathode and interfere with transduction signal. SPR measurements also produce unreliable data by a tiny bubble in a channel. All baseline data are lost even after the bubble is removed by the buffer solution. Electrodesorption and HER are monitored by voltammetry, measuring the current density vs. potential profile in the negative direction. The potential for the reductive desorption of thiol SAMs depends on the length of the alkyl chain, the type of terminal groups and the binding of proteins. On COOH-teminated SAMs, streptavidin is covalently immobilized using EDC/NHS mixture. On CH_3-terminated SAMs, fibrinogen is adsorbed through hydrophobic attraction. Figure 2.4 shows linear sweep voltammograms of Au electrodes coated with SAMs in PBS solution, having different alkyl chain

lengths and different terminal groups. The DC potential was swept from 0 V to -1.2 V at the rate of 20 mVs^{-1}. Figure 2.4 (a) shows the voltammograms of $COOH(CH_2)_nSH$ for n=2 and 10. E_p of the reductive desorption of adsorbed thiols appears at -0.7680 V for n=2 and -0.8887 V for n=10 (Table 2.1). On the other hand, E_p of the corresponding n-alkanethiols, $CH_3(CH_2)_nSH$, appears at -0.8047 V for n=3 and -0.9072 V for n=11 as shown in Figure 2.4(b) and in Table 2.1. Two reductive potential peaks are observed in short chain SAMs whereas long chain SAMs show only one peak in the voltammetry.

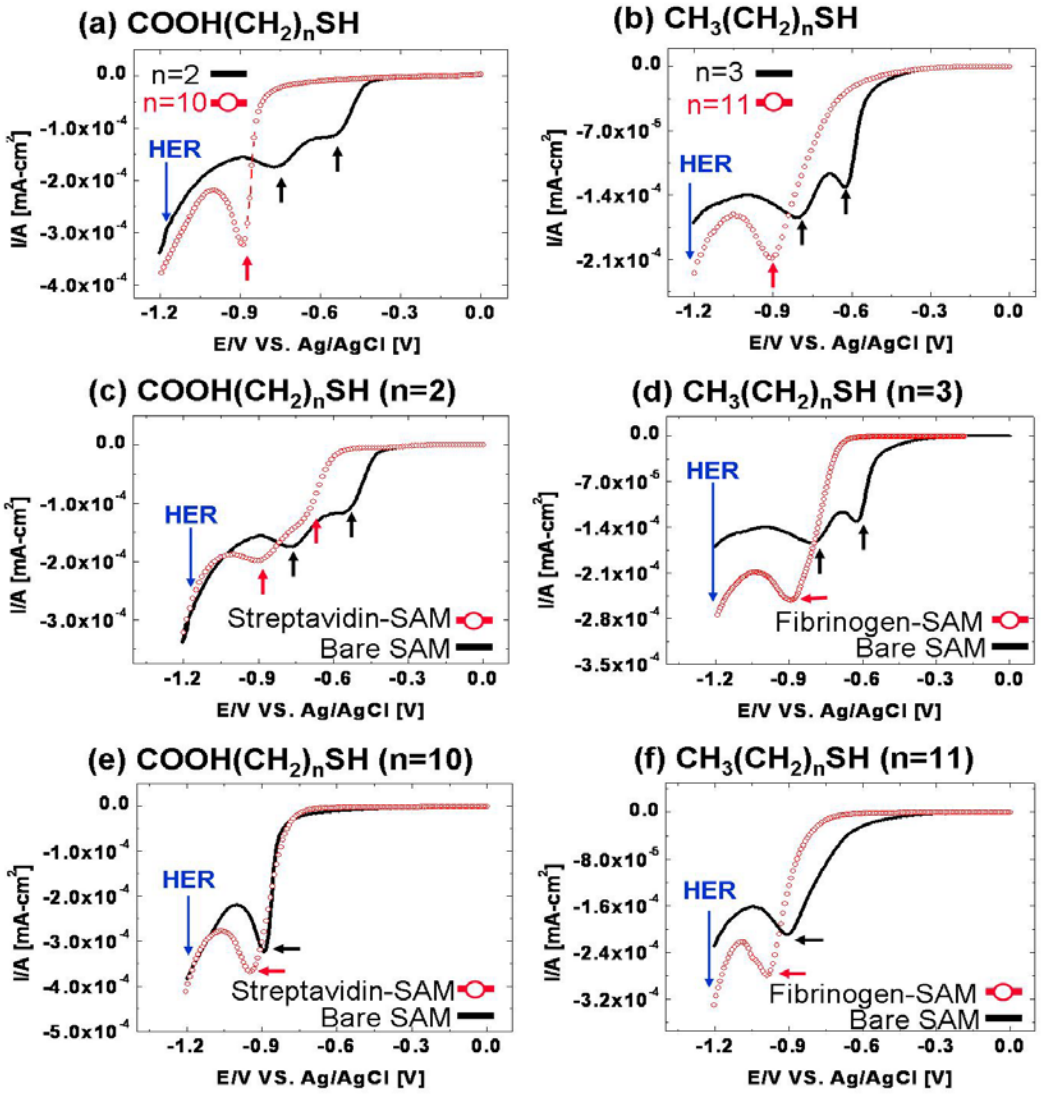

Figure 2.4 The reductive desorption of (a) $COOH(CH_2)_nSH$ for n=2 and 10, (b) $CH_3(CH_2)_nSH$ for n=3 and 11(c) & (e) $COOH(CH_2)_nSH$ modified by Streptavidin and (d) & (f) $CH_3(CH_2)_nSH$ modified by fibrinogen

Table 2.1 Reductive peak potential of SAMs and protein-bound SAMs

Monolayer	E_{peak} (E/V vs Ag/AgCl)
$COOH(CH_2)_nSH$, n=2	- 0.7680
$COOH(CH_2)_nSH$, n=10	- 0.8887
$CH_3(CH_2)_nSH$, n=3	- 0.8047
$CH_3(CH_2)_nSH$, n=11	- 0.9072
Streptavidin-bound $COOH(CH_2)_nSH$, n=2	- 0.8965
Streptavidin-bound $COOH(CH_2)_nSH$, n=10	- 0.9471
Fibrinogen-bound $CH_3(CH_2)_nSH$, n=3	- 0.8971
Fibrinogen-bound $CH_3(CH_2)_nSH$, n=11	- 0.9909

The separated desorption peaks are reported to be due to the differences in the type of binding site and the subsequent strength of the interactions of the sulfur atom with gold surface. Among the two peaks the final reductive desorption of the SAMs occurs at the second peak potential. It is shown that E_p of the reductive desorption varies depending on the length of alkyl chain and the type of terminal group of SAMs. The longer the alkylchain, the more negative E_p becomes, reflecting the stronger van der Waals attractive interaction among alkylchains. E_p is also dependent on the terminal groups; E_p of the reductive desorption of $COOH(CH_2)_nSH$ is more positive than that of $CH_3(CH_2)_nSH$. This is due to the repulsive interaction between the negatively charged carboxylate groups in a COOH-SAM.

Figure 2.4 (c) and (e) present the voltammograms of covalent bond of streptavidin to $COOH(CH_2)_nSH$ by formation of an amide bond. Reductive desorption peak potentials are more negatively shifted by 128 mV for n=2 and by

58 mV for n=10 when the surface is modified by streptavidin. Figure 2.4 (d) and (f) show the voltammograms of adsorption of fibrinogen on $CH_3(CH_2)_nSH$ by hydrophobic attraction. The desorption peak potentials are also shifted to more negative values by 92 mV and 84 mV for n=2 and 11, respectively, after the surface is modified by fibrinogen. Regardless of bonding mechanism of proteins, more potential is required to desorb the protein-bound SAMs than that of unmodified SAM. Anderson et al. reported similar findings, stating that the SAM modified by 1,3- and 1,4-phenylenediamine had more negatively shifted reductive desorption (Anderson and Baltzersen, 2003). Figure 2.4 (e) and (f) show that proteins-bound long chain SAMs need approximately -1.0 V to desorb the SAMs and such high potential seriously damages the opposite top electrode, especially when the electrode is a thin metal film. Following section addresses this issue. For all different SAMs in Figure 2.4, HER occurs at approximately -1.2 V, which does not overlap the reductive desorption potential. Thus, short chain SAMs have a much less chance to encounter HER.

2.3.1.2 Oxidative desorption of SAMs on the anode

This biosensor experiences both reductive and oxidative processes on electrodes; reductive process on the cathode and oxidative process on the anode. Figure 2.5 shows the voltammogram of unmodified short chain SAMs where the potential is swept between 0 V to +1.2 V. At +0.9 V, oxidative desorption of SAMs occurs and Au electrodes begin to corrode over +1.0 V. As the potential further increases, the gold film peels off from the glass substrate. In order to remove longer chain SAMs bound by proteins on the cathode (figure 2.4), more than DC

1.0 V is required, which induces corrosion of gold on the anode. This is why the short chain SAMs is used for the reusable/reconfigurable biosensor; to minimize HER on the cathode and prevent the corrosion of a metal film.

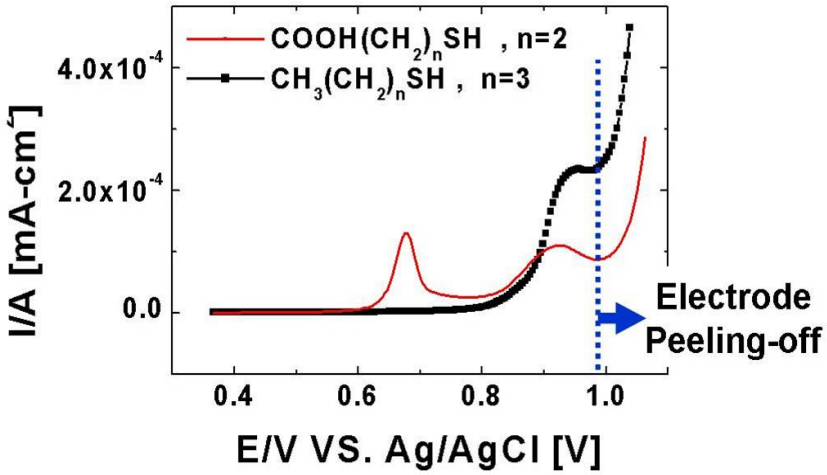

Figure 2.5 Current density vs. potential profiles for the oxidative desorption of $COOH(CH_2)_nSH$ for n=2 and $CH_3(CH_2)_nSH$ for n=3

2.3.2 Re-adsorption of the desorbed SAM molecules

This section investigates another issue in developing a reusable microfluidic biosensor; re-adsorption of detached SAMs. Reductive potentials of -0.9 and -1.0V were applied to the bottom electrode for the ω-carboxylic acid alkanethiols [$COOH(CH_2)_nSH$] with n=2 (3-mercaptopropionic acid) and n=10 (11-mercaptoundecanoic acid), respectively. *In-situ* SPR sensograms of two chain lengths (n = 2, 10) was observed, shown in Figure 2.6. SAM formation solution was introduced from the inlet port, and the COOH-terminated SAM [$COOH(CH_2)_2SH$] was formed on the bottom gold electrode. Variable parameters were the duration of the voltage application and the flow of the buffer solution. Before applying the reductive potential, SPR angle values of intermediate and

short chain SAMs were established at approximately 200 mDeg and 100 mDeg, corresponding to surface coverages of 1.67 ng/cm^2 and 0.83 ng/cm^2, respectively.

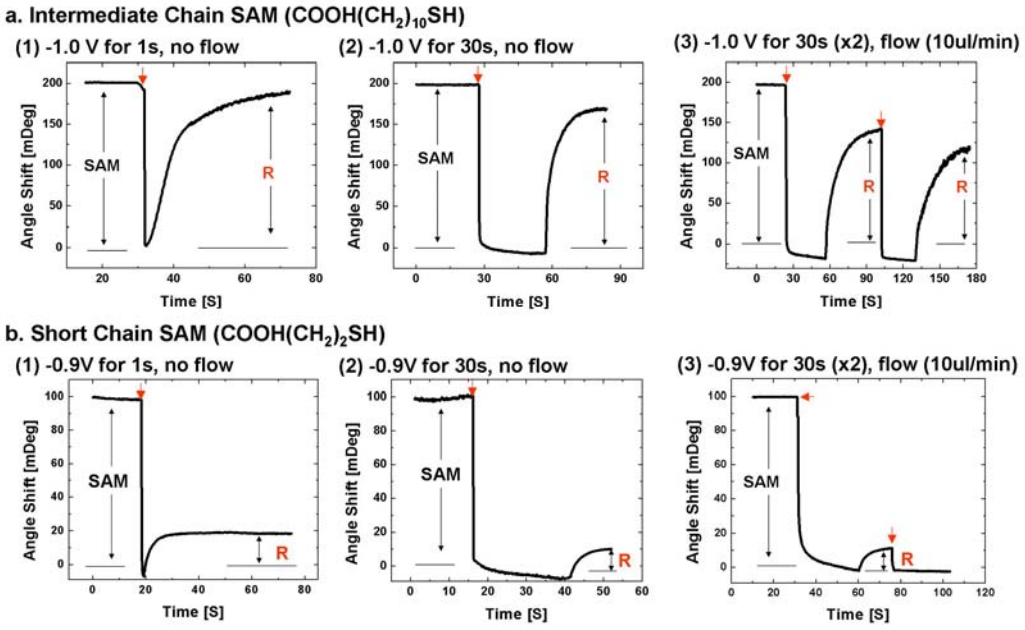

Figure 2.6 (a) Re-adsorption of Intermediate chain COOH-SAM (n = 10) (b) Re-adsorption of short-chain COOH-SAM (n = 2) (Red arrow: reductive potential application, R: re-adsorption.)

These numbers indicate tightly packed SAMs formation (alkanethiol monolayer, 7.6 x 10^{-10} mol/cm^2) (Balasubramanian et al., 2006). Figure 2.6 shows that the intermediate chain SAMs suffer from extensive re-adsorption reaction. Upon -1.0 V for 1s with no flow, most of the detached SAM readily re-adsorb onto the surface within tens of seconds (Figure 2.6a(1)). The duration of the voltage application was increased to 30 s, yet the SPR angle value returned to 169 mDeg, which means that 83 % of the desorbed SAM species were re-adsorbed on the same surface (Figure 2.6a(2)) . A flow of 10 µl/min did not help reducing the re-adsorption. Figure 2.6a(3) shows that two consecutive potential applications with

the flow at 10 μl/min have the re-adsorption of 58.5 %. On the other hand, only 18 % of the detached short-chain SAMs (-0.9 V for 1 s) re-adsorbs with no flow and the re-adsorption reduces to 10 % as the duration of the voltage application increases (Figure 2.6b(1) & 2.6b(2)). When -0.9 V was applied for twice for 30 seconds with the flow of 10 μl/min, re-adsorption of the detached SAM was almost negligible (Figure 2.6b(3)).

Pesika et al. explained the reductive desorption by a simple model that takes into account diffusion of the thiolate into the bulk solution, stating that the solubility of the thiolate increases as the chain length decreases (Pesika et al., 2006), which is in good agreement with the results. Beside, Figure 3.6 shows that the flow of the buffer solution does not seem to increase the solubility for both intermediate and short chain SAMs. Therefore, the re-adsorption decreases significantly as the chain length decreases and the duration of the potential application increases.

The surface stability was studied by repeating the formation and removal cycles of the short chain COOH-SAM up to 50 times. SAMs were repeatedly formed for 1h and removed by applying -0.9 V for 30-second twice on the working electrode. Figure 2.7 shows the surface reproducibility data generated by SPR. The repeated angle shift of the recycled SAM formations was 2.43 % of RSD (Relative Standard Deviation) during 50 cycles. No sign of re-adsorption occurs throughout the repeated formation and removal of the COOH-SAM. After the 50th SAM removal, the SPR baseline shifted by merely 3 mDeg.

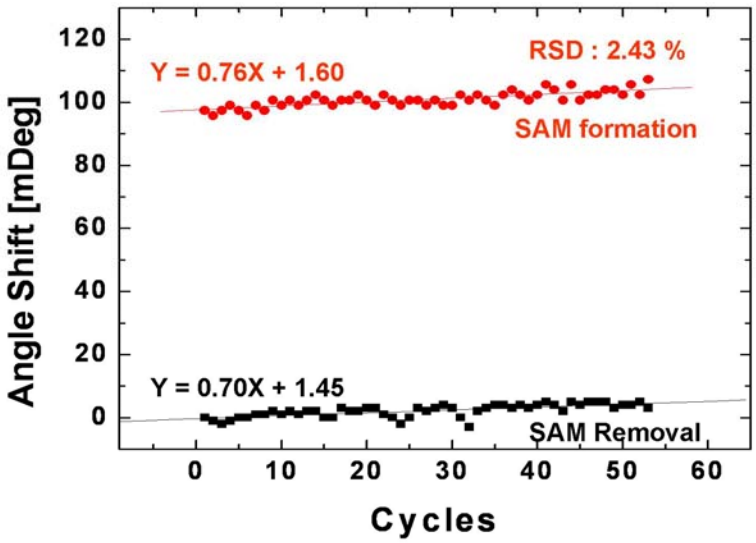

Figure 2.7 Surface reproducibility with short-chain SAM (n = 2)

2.3.3 Real time monitoring of SAM desorption in a microfluidic device

SPR and ellipsometry are used in concert throughout this study to verify assembly and removal of molecules in the microfluidic device. Electrochemical reduction is performed in-situ in a two electrode set-up and SPR monitors the molecular interactions in real-time. Ellipsometry is performed ex-situ to confirm the assembly of multiple layers on the bottom Au electrode surface. From SPR angle shift, proteins' and SAMs' thicknesses and their refractive indices are calculated according to the method of de-Feijter, hence allowing the transformation of a film thickness parameter into an amount of adsorbed protein per unit area

$$\Gamma\ (ng \bullet \mathrm{mm}^{-2}) = d\ [\ (\ n_f - n_m\ )\ /\ (\ \mathrm{d}n\ /\ \mathrm{d}C\ )\ ], \qquad (2.2)$$

where d is the film thickness (nm), n_f is the refractive index of the film, n_m is the refractive index of the ambient, and $\mathrm{d}n/\mathrm{d}C$ is the refractive index increment (de Feijter et al., 1978). This method is based on the assumption that the refractive

index of a protein solution is a linear function of the protein concentration. This formula for the air/solid measurement is as follows

$$\Gamma\ (ng \bullet mm^{-2}) = K \bullet t, \tag{2.3}$$

where K is the density of the protein and SAMs and t is the thickness (nm). The density of protein and SAMs are 1.36 g/cm^3 (proteins), 0.842 g/cm^3 ($CH_3(CH_2)_3SH$), 0.845 g/cm^3 ($CH_3(CH_2)_{11}SH$), 1.218 g/cm^3 ($COOH(CH_2)_2SH$), 0.792 g/cm^3 ($COOH(CH_2)_{10}SH$), respectively. For the SPR instrument, an increase in the plasmon resonance angle of 120 mDeg corresponds to an average material layer growth of 1 ng/mm^2.

Figure 2.8 shows SPR profiles as a sequence of surface modification steps. Table 2.2 summaries the SPR angles from Figure 2.8, the thicknesses converted from SPR and ellipsometry results. First, COOH-terminated SAM is formed by flowing 40 ul of 2 mM MPA in ethanol at the rate of 10 ul/min. SPR angle shift increases by 1800 mDeg. When the value stabilizes, the flowing was stopped for 1 hour to form SAMs. SAM formation is a two-step process, where thiol molecules first adsorb on a solid surface and then rearrange to become a packed monolayer (Damos et al., 2005). 40~50 % of the adsorption occurs very rapidly within ~ 10 s and over 90 % of formation is completed in 10-100 min (Pan et al., 1996). After 1 hour, PBS was reflowed to thoroughly wash unformed SAM residues. The thickness of the SAM is measured by ellipsometry to be 4.06 Å, which is in good agreement with SPR; 58.2 mDeg shift, corresponding to 3.98 Å. Then EDC/NHS mixture activates carboxylic acid groups of MPA monolayer to effectively immobilize streptavidin. Streptavidin containing amine groups on the

surface interact readily with the activated MPA intermediates and form covalent amide linkages, showing 11.95 Å thick from SPR converted values. Reductive desorption of the immobilized proteins is performed by applying -0.9 V to the cathode against Au top electrode for 30 seconds.

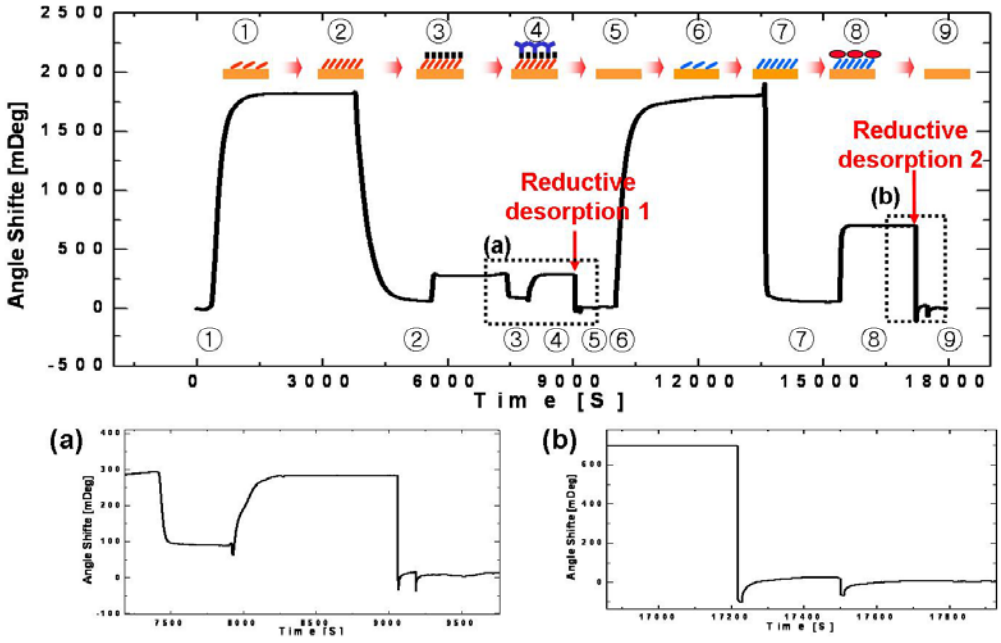

Figure 2.8 SPR profiles with schematics of step-by-step procedure of surface modification. (a, b) The enlarged SPR sensorgram of reductive desorption 1 and 2, respectively.

Table 2.2 SPR angle shift and thickness

Adlayer	Step no. in Fig. 3.6	SPR angle (mDeg)	Thickness (Å, SPR)	Thickness (Å, Ellipsometry)
COOH-SAM	②	58.2	3.98	4.06 ± 0.2
EDC/NHS	③	88.1	-	-
Streptavidin	④	283.2	11.95	14.33 ± 0.1
Desorption	⑤	2.8	0.02	0.3 ± 0.08
CH_3-SAM	⑦	52.8	4.98	5.22 ± 0.2
Fibrinogen	⑧	697.3	42.7	49.5 ± 0.4
Desorption	⑨	1.3	0.01	0.2 ± 0.06

During the desorption process, PBS keeps flowing to avoid re-adsorption of the detached SAMs. The amplitude of the desorption potential is based on the data from linear sweep voltammetry measurement. By applying reductive desorption potential twice, almost complete removal of adlayers is achieved (⑤ in Figure 2.8 and Table 2.2). The cycle was repeated using CH_3-terminated short chain SAM ($CH_3(CH_2)_3SH$) and capture the second target molecule, Fibrinogen, to demonstrate a reconfigurable biosensor. The bond between fibrinogen and CH_3-terminated SAM is formed by a strong hydrophobic attraction. These phenomena are attributed to the characteristic structure of proteins. Generally, proteins have hydrophobic residues buried within the core of the proteins and their hydrophilic residues facing outside. The adsorption of any protein onto a solid surface is a strong function of hydrophobic attraction. Hydrophilic residues form the orientation of the adsorbed protein and do not take part in the adsorption process itself (Latour, 2005). Therefore, proteins rapidly adsorb onto a hydrophobic surface, unfold and spread their hydrophobic core over the surface (Choi et al., 2008). The solid surface, CH_3-terminated SAM, employed here shows high hydrophobicity of 102° in contact angle measurement. As a result of fibrinogen adsorption, strong bonding occurs between the protein and the surface. Figure 2.8 shows that even PBS flow does not dissociate the protein-surface binding. The Fibrinogen-bound SAM is also completely desorbed at -0.9 V (⑨ in Figure 2.8 and Table 2.2). This demonstrates that the sensing surface resets to be reusable/reconfigurable by undergoing electrochemical desorption of short chain

SAMs while avoiding electrode corrosion, HER and re-adsorption of detached molecules.

One thing to note is that SAM formation and dissociation may occur on top Au electrode (anode) if high enough potential is applied. Figure 2.5 shows that $COOH(CH_2)_3SH$ has two oxidative peaks at +0.6756 V and + 0.913 V while a desorption peak of $CH_3(CH_2)_2SH$ is shifted to more positive values, +0.9502 V. Therefore, DC 0.9 V for the reductive desorption of SAMs on the cathode does not completely remove the SAMs formed on the top Au electrode. However, it is expected that this imperfect desorption at the anode has no effect on the reductive desorption or adsorption of SAM on the cathode since SPR only measures biomolecular interactions within approximately 200 nm from the cathode. Moreover, 30 sec of DC is unlikely to re-adsorb newly detached alkyl molecules on both electrodes because the flow rate of 10 ul/min is fast enough to completely flow the dissociated residues out of the channel. Five measurements of the procedure above were performed in the same microfluidic device and the change of the SPR signal was monitored (two cycles: COOH-SAM formation → Streptavidin immobilization → regeneration → CH_3-SAM formation → Fibrinogen adsorption → regeneration). Figure 2.9 and Table 2.3 show absolute angle values of the SPR after each protein modification and regeneration, respectively. The binding activity of streptavidin and fibrinogen retained over 95 % of the original SPR change signal after 10 cycles of regeneration. The result indicated that the microfluidic device can be reused with good reproducibility with an RSD lower than 1.86 %.

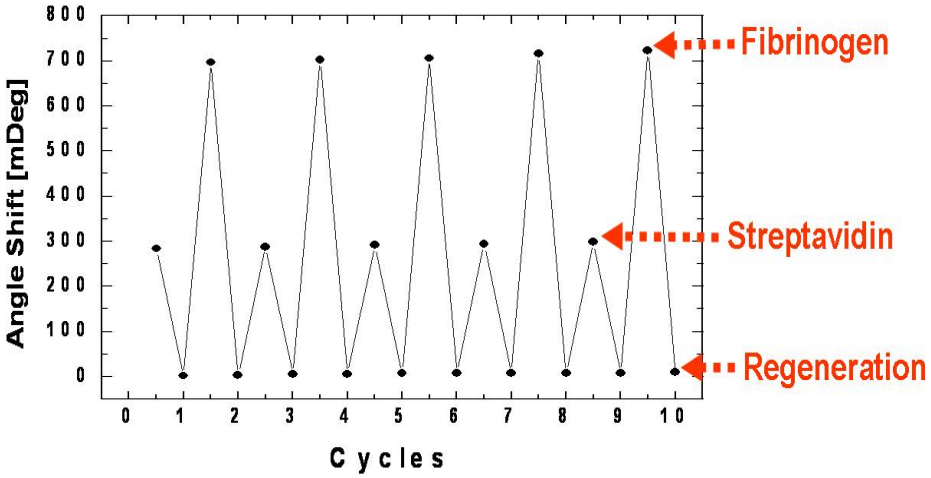

Figure 2.9 Reproducibility of the SPR response from the protein modifications with regeneration using SAM desorption

Table 2.3 SPR angle shift and thickness of Figure 2.9

	Streptavidin		Fibrinogen	
	SPR angle	Thickness (nm)	SPR angle	Thickness (nm)
1 cycle	283 mDeg	1.73	696 mDeg	4.26
2 cycle	287 mDeg	1.76	702 mDeg	4.30
3 cycle	290 mDeg	1.78	705 mDeg	4.32
4 cycle	293 mDeg	1.79	715 mDeg	4.38
5 cycle	297 mDeg	1.82	722 mDeg	4.42
Average	290 mDeg	1.78	708 mDeg	4.34
SD	5.39 mDeg	0.034	10.42 mDeg	0.064
RSD	1.86		1.47	

SD standard deviation, *RSD* relative standard deviation

2.4 Conclusion

Many biosensors are designed to be disposable, taking advantage of low cost materials and batch fabrication. Disposable biosensor chips are very attractive for many applications where it is difficult to wash all residues in microfluidic channels and sensing surfaces. On the other hand, reusable and reconfigurable biosensors are useful where detail calibration of sensors is required such as in biochemical science and analytical chemistry. This chapter reports a new biosensor platform for reusable/reconfigurable sensing surfaces using electrochemical reductive desorption of linker molecules. Electrode corrosion, HER, and re-adsorption of the detached molecules occurring in microfluidic systems are solved by using short chain linker molecules. The linker molecules bound to proteins are desorbed by applying very small DC potential, which are characterized by ellipsometry, voltammetry, and SPR in real time. This technique can be comprehensively utilized in all communities where linker molecules need to immobilize biomolecular receptors. Further research is required to determine how many times the device can be used while maintaining reliable formation and desorption of SAMs.

3 NON-SPECIFIC ADSORPTION IN MICROFLUIDIC BIOSENSORS

3.1 Introduction

Label-free biosensors, including SPR biosensors, currently suffer from severe non-specific adsorption (NSA) of proteins (Oliva et al., 2001). Protein NSA causes "false positive" errors in detection through overestimation of the affinity value (Ogi et al., 2009); this tendency often limits the use of SPR-based biosensors. Overcoming this technical hurdle is what motivates this research. Biological samples consist of a complex mixture of compounds, including abundant proteins (on the order of mg/ml) that tend to adsorb nonspecifically to surfaces (Bolduc and Masson, 2008). When other abundant nonspecific proteins are present, however, it is extremely challenging to detect target biomarkers at concentrations typically on the order of ng/ml or less. Many useful SPR applications are currently limited by NSA, and so far, no study has yet reported SPR analysis in whole blood, blood plasma, or serum (Masson et al., 2006). This further motivates this research, as it is crucial in such applications to have a highly active but low-fouling sensing surface for a microfluidics-based SPR immunosensor (Lee et al., 2007; Luo et al., 2008). The ideal SPR biosensor surface would immobilize a maximal density of bioreceptors to increase the signal while simultaneously and effectively minimizing NSA.

Alkanethiol SAMs are among the most widely-used bioreceptor linker molecules, partially because they offer two major advantages: abundant functional groups to immobilize bioreceptors, and a fully packed monolayer that results in little NSA (Bolduc and Masson, 2008; Masson et al., 2006; Chaki and

Vijayamohanan 2002; Lahiri et al., 1999). Biosensing surfaces functionalized with alkanethiol SAMs, however, suffer from NSA for three main reasons (Figure 3.1): non-immobilized bioreceptors, imperfectly-formed monolayers, and polycrystalline gold grain structure (Love et al., 2005). NSA occurs on the activated head group of the SAM where bio-receptors are not immobilized (Figure 3.1, ①). Many techniques have reportedly reduced this source by de-activating the head group with Ethanolamine-HCl, or by using mixed SAMs composed of hydrophilic resist film such as Polyethylenglycol (PEG) or OH-terminated SAMs (Masson et al., 2006; Chapman et al., 2000; Sasaki et al., 1998; Frederix et al., 2004; Furuya et al., 2006).

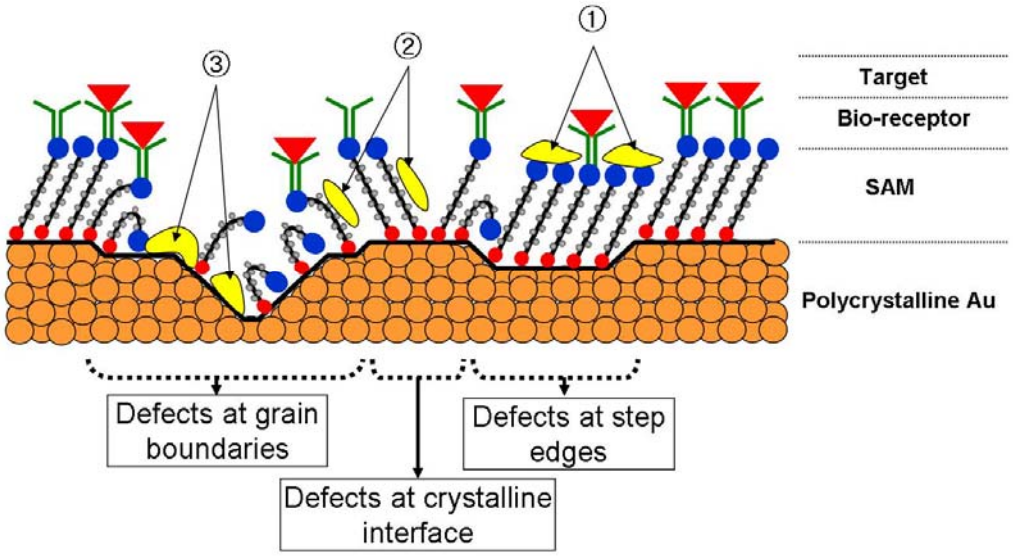

Figure 3.1 A schematic illustration of the defects found in SAMs formed on a polycrystalline gold surface and resultant non-specific adsorption (NSA).

Recently, Bolduc et al. reported that amino acids attached to 3-mercaptopropionic acid significantly mitigate NSA from serum proteins (Bolduc and Masson, 2008). NSA also occurs when imperfect monolayers form on polycrystalline gold surfaces (Figure 3.1, ② & ③). SPR requires an ultrathin gold film (~50 nm) to be deposited on a transparent amorphous substrate, but it is difficult and costly to form a single crystalline gold film on the glass-like substrate (Love et al., 2005). Most SPR substrates have polycrystalline gold films formed by evaporative or sputtering processes (Bolduc and Masson, 2008; Lahiri et al., 1999; O'Dwyer et al., 2004). The grain structure of polycrystalline gold substrates is characterized by dense arrangements of inter-grain boundaries, steps, facets, and other structural irregularities, and these impact the structures and defects of the SAMs (Love et al., 2005). Imperfect SAMs result in NSA on the irregular monolayer where the SAMs have alkane chains exposed on the surface (Figure 3.1, ②) and are not fully formed (Figure 3.1, ③). One alternative that minimizes NSA includes blocking the vacant sites using bovine serum albumin (BSA) (Ogi et al., 2009; Bolduc and Masson, 2008; Masson et al., 2006). This method, however, may interfere with interactions between the biosensor and molecules of interest, thereby resulting in false negative responses (Bolduc and Masson, 2008). BSA can also be displaced by other proteins, or form a multilayer with oppositely charged proteins (Figure 3.2), again resulting in false positive responses.

This chapter reports three design parameters to minimize NSA on polycrystalline gold surfaces: i) SAM formation time, ii) gold surface roughness

and iii) gold (111) crystal orientation. A set of experiments was conveyed to show how the three parameters impact NSA on two different chain lengths of SAMs. This paper is organized in sections addressing experimental approaches, results and discussion, and directions for further research.

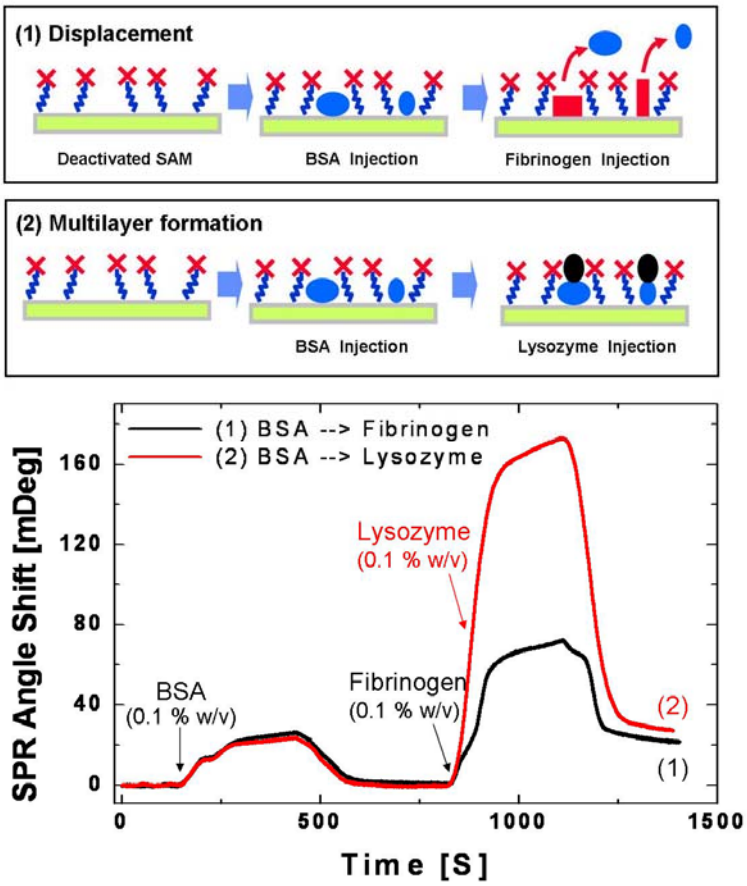

Figure 3.2 A schematic illustration and SPR sensorgrams of the displacement and multilayer formation on the BSA adsorbed surfaces.

3.2 Experimental methods

3.2.1 Chemicals

The analytes for this protein adsorption study were a large blood plasma protein, fibrinogen (340 kDa), and a small protein, lysozyme (14.7 kDa). Fibrinogen (from

Calbiochem) was used as a model for "sticky" and "large" serum proteins (Chapman et al., 2000), while lysozyme (from Sigma Aldrich) was used as a model for "tiny" serum proteins. Anti-fibrinogen antibody was purchased from Calbiochem. Mediatech, Inc. supplied the phosphate buffer solution (PBS) 1X (1.15 g/L-Na_2HPO_4, 0.20 g/L-KCl, 0.20 g/L-KH_2PO_4, 8.0 g/L-NaCl, pH 7.4) and absolute ethanol. The protein samples were prepared as 0.1 % (w/v) concentrations in PBS 1X. 1-ethyl-3-dimethylaminopropyl carbodiimide (EDC), N-hydroxysuccinimide (NHS), sodium acetate (NaAc) and ethanolamine-HCl (GE Healthcare) were used. Both ω-carboxylic acid alkanethiols [$COOH(CH_2)_nSH$] with n=2 (3-mercaptopropionic acid, 3-MPA) and n=10 (11-mercaptoundecanoic acid, 11-MUA) were from Sigma Aldrich. All chemicals were used as purchased from suppliers, without additional purification.

3.2.2 Alkanethiol SAMs with different chain lengths

Two different chain length alkanethiol SAMs (n=2 & 10) were used in the experiments. Long-chain SAMs (11-MUA) have been widely used as linker molecules due to the strong van der Waals forces among their chain molecules, which yield high packing density and well-ordered structures (Masson et al., 2006; Jang and Keng, 2008). High densities in surface terminal groups, however, lead to steric hindrance and disordered bio-receptors. To overcome these limitations, short-chain SAMs have recently been suggested as alternative linker molecules (Choi and Chae, 2009a; Choi and Chae, 2009b; Jang and Keng, 2008). Short-chain SAMs offer higher sensitivity and require shorter incubation time than long-chain SAMs. However, short-chain SAMs are less stable due to the lack

of van der Waals attraction force. Recently, mixed SAMs have been broadly deployed to prepare biosensing surfaces; their powerful versatility regulates the concentrations of functional groups on those surfaces (Frederix et al., 2003). However, mixed SAMs require lengthy incubation periods to engineer the preferred component adsorption and optimize the desired concentration ratio. This is because, on mixed SAM surfaces, the terminal functional group concentrations and the molecular domain distribution do not necessarily depend linearly on the concentration ratios of the mixed solution. Both long-chain (n = 10) and short-chain (n = 2) SAMs were chosen for the NSA study, since different chain lengths and mixed SAMs have been used for different applications (Anandan et al., 2009).

3.2.3 Surface preparation

Glass substrates (BK7, n=1.517) were first cleaned for 10 min in piranha solution. The cleaned glass was then coated with Cr/Au (2 nm/47 nm) by a sputter. Oxygen plasma treatment controlled surface roughness. The gold oxide layer formed during oxygen plasma treatment was removed by a 10 min ethanol treatment (Peterlinz and Georgiadis 1996). Au(111) orientation was enhanced by thermal annealing using a hydrogen flame for several seconds. To form SAMs, Au substrates were immersed in a room-temperature ethanol solution of ω-carboxylic acid alkanethiols at 2 mM.

3.2.4 Fabrication of microfluidic devices

The microfluidic device was fabricated using a standard soft-lithography technique. First, a silicon wafer was patterned by Deep Reactive Ion Etch (RIE), ~ 100 μm deep. Two 2.1 mm-wide channels were separated by 1.3 mm. PDMS

solution was poured and cured on the silicon wafer, then peeled off. The molded PDMS layer was approximately 1 cm, and it became the top structure. Inlet/outlet tubes from Upchurch Scientific (Inner diameter: 25 μm, Outer diameter: 360 μm) were inserted through the PDMS top using a syringe needle, then fixed by an adhesive. The bottom substrate had patterned Cr/Au (2nm/47nm) pads on the glass substrate, which formed two sensing surfaces: reference and sample surfaces. The fabricated microfluidic chip is shown in Figure 3.3.

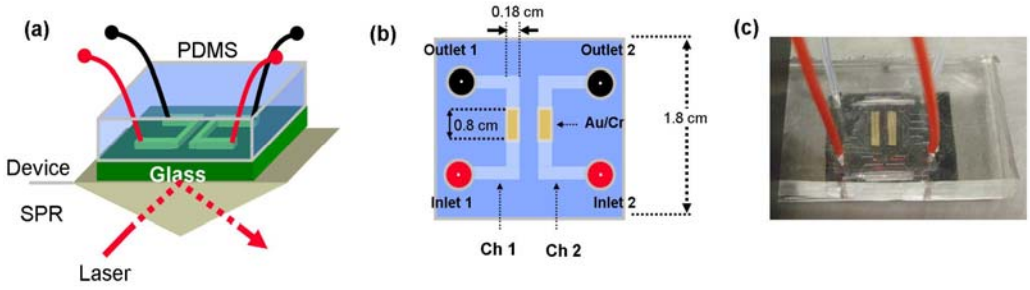

Figure 3.3 Microfluidic device used to characterize NSA in this study. (a) the microfluidic device chip on SPR and (b) its top view. (c) photo-image of the chip mounted on the SPR

Its sensing surfaces are 1.8 mm wide and 8.0 mm long. The width of the channel is slightly wider than that of the gold surface to ensure a complete bond of the two substrates via oxygen plasma treatment.

3.2.5 SPR setup and surface modification

To monitor NSA in situ and in real time, the substrates formed by SAMs were mounted on an SPR analytical system (Biosensing Instrument Inc.). Angle shifts recorded the surface modification as each solution was delivered through the microfluidic channels by an external syringe pump. All flow rates were set at 10

μl/min. To study the effect of NSA due to imperfect SAM formation and alkane chains on the exposed gold surface, the COOH-SAM was first activated by flowing freshly mixed 0.4 M EDC/ 0.1 M NHS (1:1) in water for 10 min (step ①-② in Figure 3.4), then quenched the activated carboxyl groups using 1M ethanolamine-HCl (pH 8.5) for 10 min to block biomolecule adsorption on the SAM (step ②-③ in Figure 3.4). This process allowed for distinguishing NSA from biomolecules (fibrinogen or lysozyme) being adsorbed on the empty spaces or exposed SAM chains (since the quenched surface in the study is neutral, electrostatic force does not exist between the quenched carboxyl groups and proteins). When proteins were injected in step ③, for example, negligible SPR angle shift (a) showed that little NSA occurred. When many proteins adsorb non-specifically on the surface, the angle shift is large (b). As shown in Figure 3.4, final angle shift values (a) and (b) were used throughout the entire course of experiments to quantitatively evaluate NSA, and to compare the two different chain-length SAMs across the three critical design variables: SAM formation time, Au roughness, and Au (111) orientation.

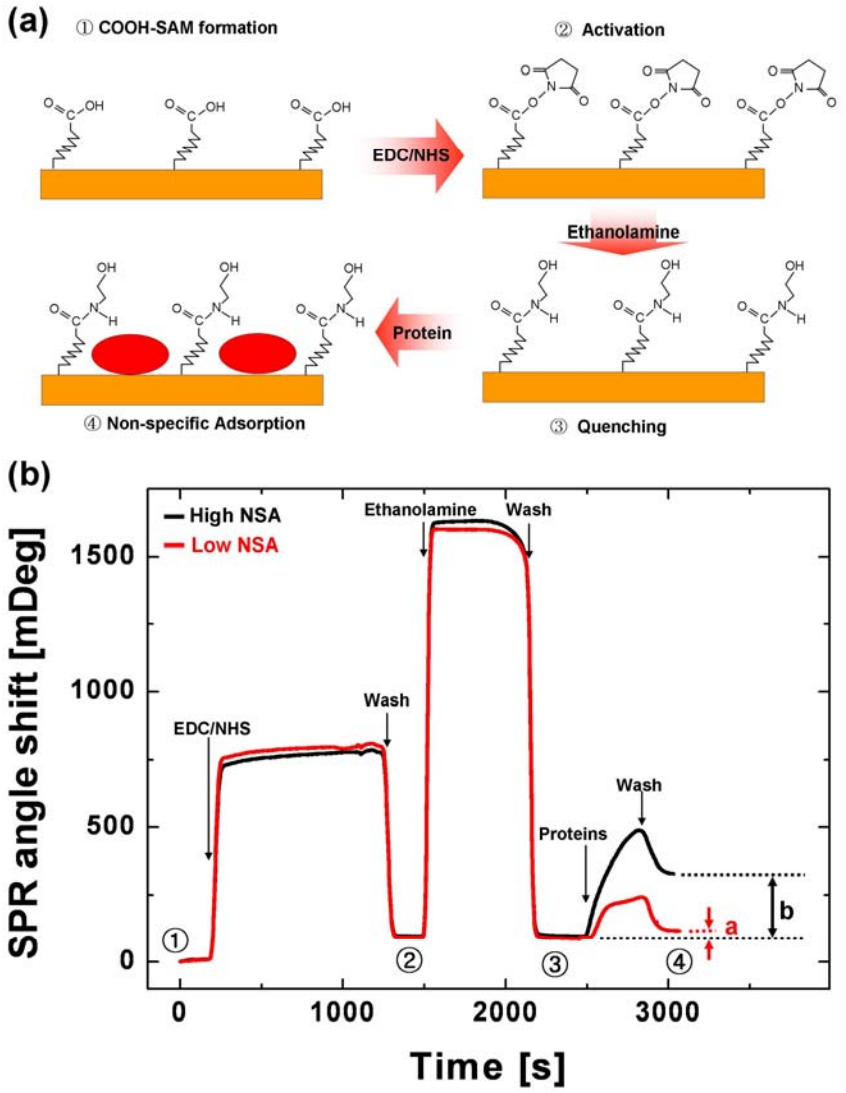

Figure 3.4 Surface modification procedure for NSA monitoring and SPR sensorgrams. Final angle shift values (a) and (b) were used to quantitatively evaluate NSA.

3.2.6 Evaluation using atomic force microscopy

An AFM (Digital Instruments Nanoscope IIIs multimode AFM) was used to evaluate the protein absorption ex situ. Surface morphology changes were observed as protein absorption occurred. Measurements were performed at air-ambient (25 °C and 35% relative humidity). 42 N/m silicon AFM tips were

utilized with a resonance frequency of 250~390 kHz, and a scanning rate of 2 Hz (lines per second).

3.3 Results and Discussion

3.3.1 Effect of SAM incubation time on NSA

Figure 3.5 describes NSA as a function of SAM incubation time. As the structure of SAMs changes from low to saturated phases, NSA decreases; proteins simply have fewer places to adsorb non-specifically. The long-chain SAM with 2 sec formation time has a large NSA for fibrinogen [586 mDeg (4.88 ng/mm2)] and lysozyme [467 mDeg (3.89 ng/mm2)], while the short-chain SAM shows only 244 mDeg and 256 mDeg NSA, respectively. AFM images of surface coverage (%) also demonstrate substantially more NSA on long-chain SAMs for the short formation time than NSA on short-chain SAMs. Although NSA on long-chain SAMs significantly decreases as incubation time increases, non-negligible NSA exists even after 24-hour formation time: 20 mDeg (0.17 ng/mm2) for fibrinogen, and 12 mDeg (0.1 ng/mm2) for lysozyme. By contrast, after a 3-hour formation time for the short-chain SAM, little NSA was observed: 6 mDeg (0.05 ng/mm2) for fibrinogen and 9 mDeg (0.075 ng/mm2) for lysozyme. AFM images confirm the substantial NSA reduction after full monolayer formation.

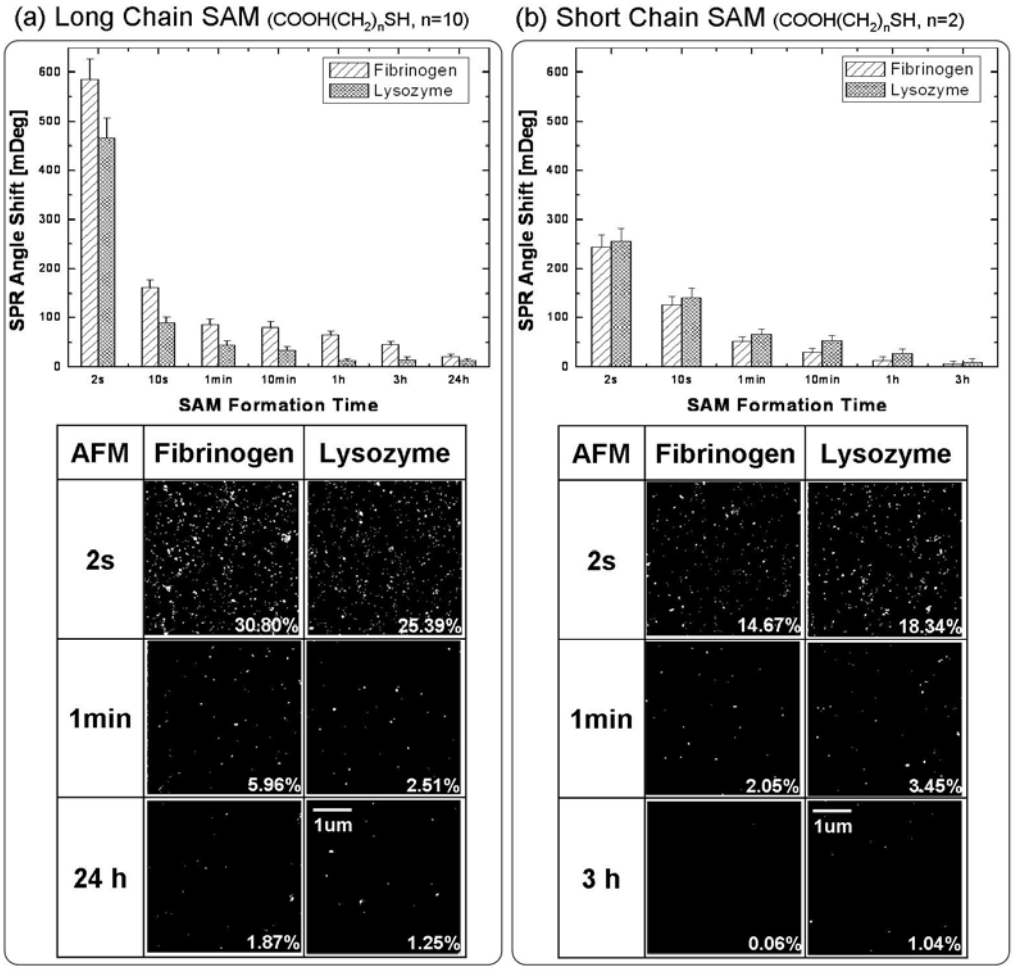

Figure 3.5 NSA behavior of proteins as a function of SAM formation time. NSA was monitored by *in-situ* SPR and *ex-situ* AFM. (The percentages indicate that the NSA portion within the measured area by AFM.)

The NSA behavior of the different chain length SAMs is explained in Figure 3.6. Many prior arts report the kinetics of alkanethiol adsorption as a function of incubation time (Peterlinz and Georgiadis, 1996; Jakubowicz et al., 2005; Pan et al., 1996). For long-chain SAMs (n > 8), 80 – 90% of SAMs are formed in the initial stage within a few minutes (Pan et al., 1996). In the first stage, chemisorption of the thiol head group forms a "lying down phase" on the surface

of the substrate. The second and third stage formations occur over the longer period of incubation, and involve reorienting hydrocarbon chains and ordering the SAM terminal functional groups (Henderson et al., 2009). Short-chain SAMs exhibit a different formation phase. They tend to stand up from the initial stage, but the weak van der Waals force between chains makes a less dense monolayer (Desikan et al., 2007). Those different formation stages result in different NSA, and the following is one possible explanation.

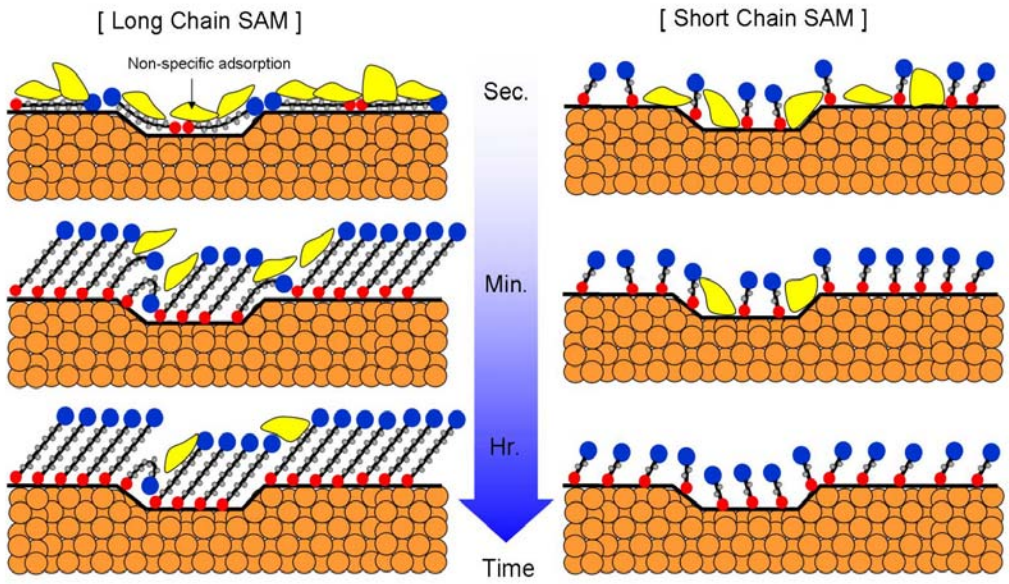

Figure 3.6 The NSA behavior of the different chain length SAMs according to the formation time

For the initial stage, long-chain molecules lie down randomly on the surface, exposing many empty gold surfaces and alkane chains. As those exposed surfaces are hydrophobic (Lam et al., 1999), many proteins tend to adsorb non-specifically. However, short-chain molecules stand up on the surface so significantly fewer empty gold surfaces are exposed. Therefore, there is substantially less NSA on the

short-chain SAM than on the long-chain SAM for the same formation duration. A few seconds later, however, long-chain molecules start to stand up from the van der Waals attraction force between chains, allowing them to form a dense monolayer. Consequently, NSA dramatically reduces for long-chain SAMs after 10 s. Nevertheless, the NSA of long-chain SAMs incubated for 24 hr is higher than that of the short-chain SAM incubated for 3 hr. This difference is because the long-chain SAM on the polycrystalline gold surface does not completely follow the structural irregularities on the gold surface while the short-chain SAM covers most gold surfaces. This is further addressed in the next section. One thing to note is that NSA is a function of the size of proteins. Fibrinogen on the long-chain SAM, for instance, adsorbed more than lysozyme did, while short-chain SAM showed the opposite trend. Sparsely-formed short-chain molecules allow small lysozyme proteins to adsorb on the empty space where fibrinogen cannot enter, while sticky fibrinogen tends to adsorb more on long, exposed hydrophobic alkane chains.

3.3.2 Effect of Au roughness on NSA

The surface roughness of sensing surfaces substantially impacts NSA. The roughness of the thin gold film is determined by the substrate material and lattice matching between the substrate and gold crystals. Conventional techniques producing smooth gold surfaces use an atomically flat substrate such as mica. As a result of epitaxial growth on the cleaved mica, one can deposit a single-crystal Au (111) layer either by evaporation or sputtering (Tsuneda et al., 1999). Here, this study focuses on non-crystalline glass rather than mica substrates because

glass offers several practical advantages over mica, including high stability at high temperature, easy handling for SPR monitoring, and low cost (Tsuneda et al., 1999). However, a gold film deposited onto a glass substrate has higher roughness, which leads to formation of defects in alkanethiol SAM, consequently causing severe NSA (Yang et al., 2003). Figure 3.7 shows that as the surface roughness decreases, NSA is consistently reduced. Using oxygen plasma treatment, two gold substrates were prepared with different roughnesses. One has 4.4 nm of Root Mean Square (RMS) roughness while the other has 0.8 nm (Figure 3.7 (a)). NSA on long-chain SAMs is a strong function of the roughness. Fibrinogen adsorption (80 mDeg) on a high-roughness surface significantly reduces to 20 mDeg on a low-roughness surface. Lysozyme adsorption also decreases as the roughness of the gold surface decreases. However, NSA of short-chain SAMs is not sensitive to the surface roughness as much as that of long-chain SAMs. Long-chain SAMs have many defects when they are formed on the polycrystalline gold surfaces because of the van der Waals attraction force between chains (Love et al., 2005). Those defects could increase NSA. By contrast, the surface roughness of short-chain SAMs has little impact due to the very low van der Waals force between chains.

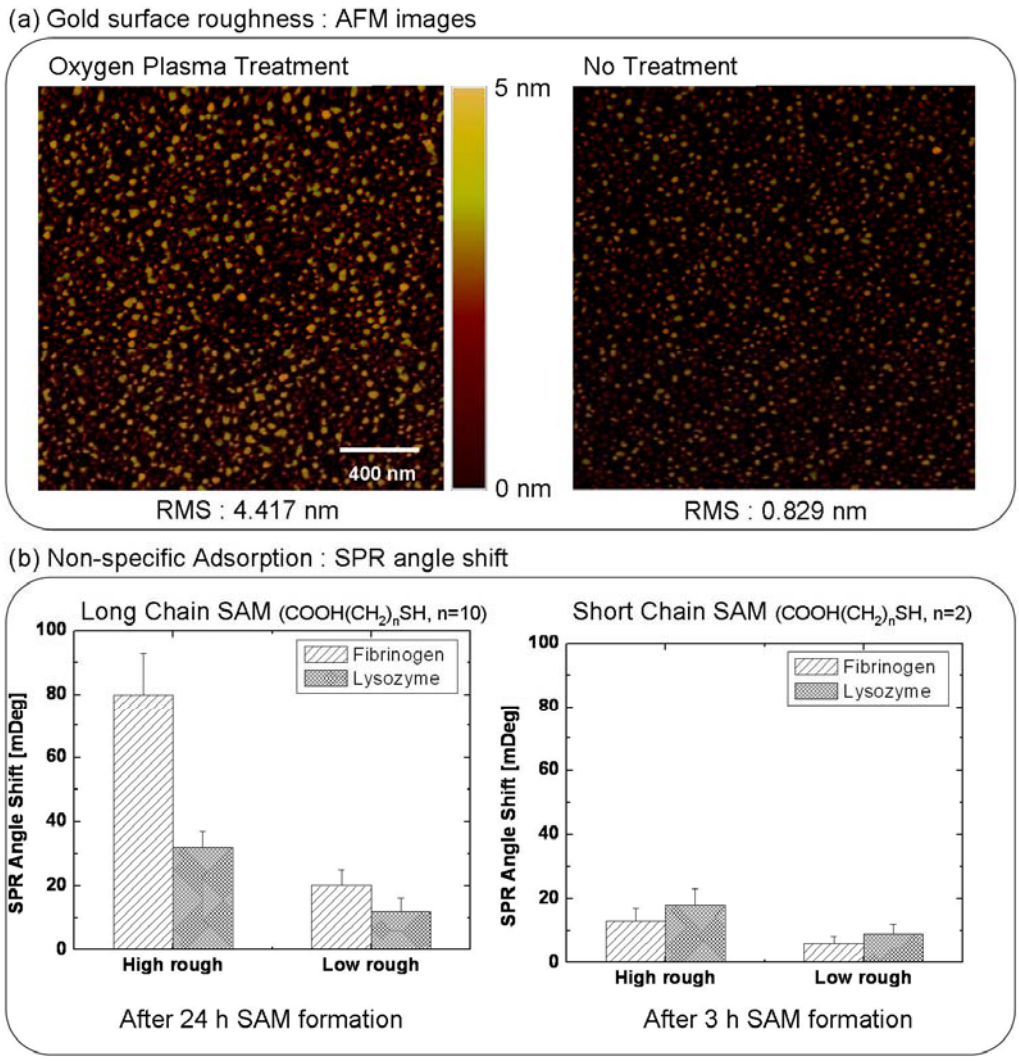

Figure 3.7 (a) AFM images of gold roughness before and after the oxygen plasma treatment. (b) SPR sensorgram of NSA, a function of surface roughness and SAM chain length.

3.3.3 Effect of annealing Au film

The formation of SAMs strongly depends on the crystalline morphology of the underlying gold surface. Annealing Au film changes the morphology by changing the crystallographic orientation and enlarging the grain size. Au (111) yields a monolayer of the highest density and degree of regularity. This is why Au (111) is

the most popular substrate material for SAM applications (Luderer and Walschus, 2005). Single-crystalline Au (111) substrate has been widely used for SAMs in STM or AFM studies (Love et al., 2005; Tsuneda et al., 1999; Wink et al., 1997). Recently, polycrystalline gold has become attractive for biosensor applications because of its practical handling and low cost (Tsuneda et al., 1999). A gold film on a glass substrate cannot grow epitaxially because there is no atomically ordered phase on the glass surface, yet most Au deposition processes tend to produce films with substantial preference for a crystalline gold (111) texture (Twardowski and Nuzzo, 2002). As shown in Figure 3.8 (a), XRD (X-ray Diffraction) of both thermally untreated and treated films have almost exclusively a (111) texture. A series of rocking angle measurements of the Au (111) diffraction peak [inset, Figure 3.8 (a)] show a substantial improvement in FWHM (full width at half maximum) in the thermally treated samples. This suggests that a strong alignment of the crystals along the (111) direction occurs during thermal treatment Figure 3.8 (b)].

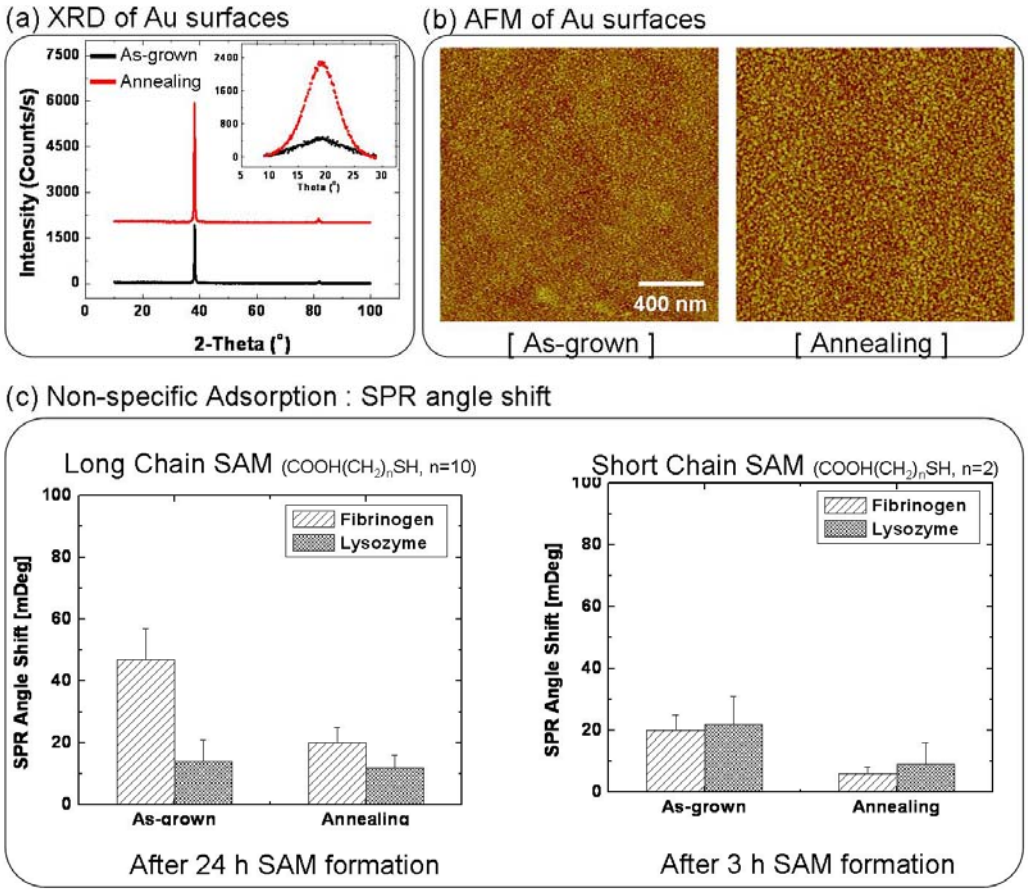

Figure 3.8 (a) XRD and (b) AFM images of gold surfaces before and after the thermal annealing. (b) SPR sensorgram of NSA, a function of Au orientation and SAM chain length.

The growth of the Au crystallites decreases defect density on the SAMs, leading to fewer grain boundaries. Figure 3.8 (c) shows that the untreated sample has approximately twice the NSA of fibrinogen compared to the thermally treated sample; lysozyme adsorption, by contrast, has little dependence on the treatment. Fibrinogen's NSA increase might be due to the roughness change during thermal treatment. NSA on long-chain SAMs is highly dependent on the surface roughness (as discussed in the previous section). After thermal treatment, RMS roughness increased from 0.7 nm to 0.8 nm. NSA for both proteins on the short-

chain SAMs, on the other hand, decreased after thermal treatment, showing a 14 mDeg drop for fibrinogen and 13 mDeg for lysozyme. The angle changes between thermally untreated and treated samples were larger than those from the surface roughness effect. Therefore, NSA for short-chain SAMs is more strongly dependent on Au film annealing than that of long-chain SAMs. Figure 3.9 shows the potential explanation of the relationship between the NSA behavior of the different chain length SAMs and crystalline gold (111) texture. In the long chain SAM, the strong van der Waals force between chains makes a denser monolayer decreasing NSA.

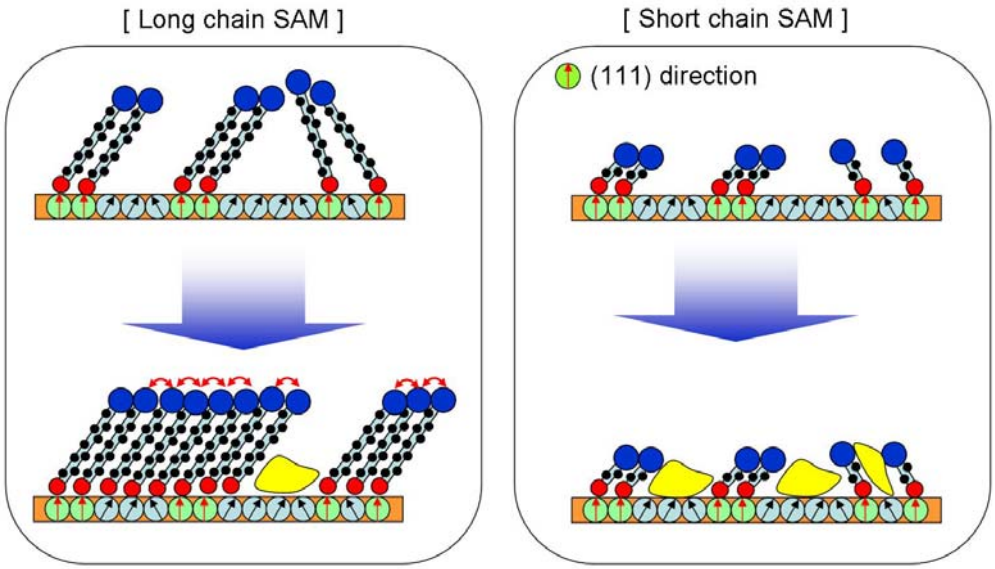

Figure 3.9 The NSA behavior of the different chain length SAMs according to the crystalline morphology of the underlying gold surface

3.3.4 Optimal combination of the three design parameters

The anti-fibrinogen antibody was immobilized on short- and long-chain SAMs by activating the carboxylic acid groups with 400 mM EDC/100 mM NHS in water for 10 minutes. The produced NHS-esters reacted with amine functional groups in the 100 μM anti-fibrinogen in 10 mM NaAc (sodium acetate, pH 5.3) solution. Once protein immobilization was complete, 1M ethanolamine-HCl was used to deactivate and block any remaining active groups on the surface. Then, 1 ng/ml fibrinogen was injected. Figure 3.10 shows the SPR sensorgram of immobilizing anti-fibrinogen antibody to both SAMs and subsequent exposure to fibrinogen in picomolar range (2.94 pM). When 100 μg/ml of anti-fibrinogen in PBS was injected, the angle shifts were 497 mDeg and 381 mDeg for the long- and short-chain SAMs, respectively.

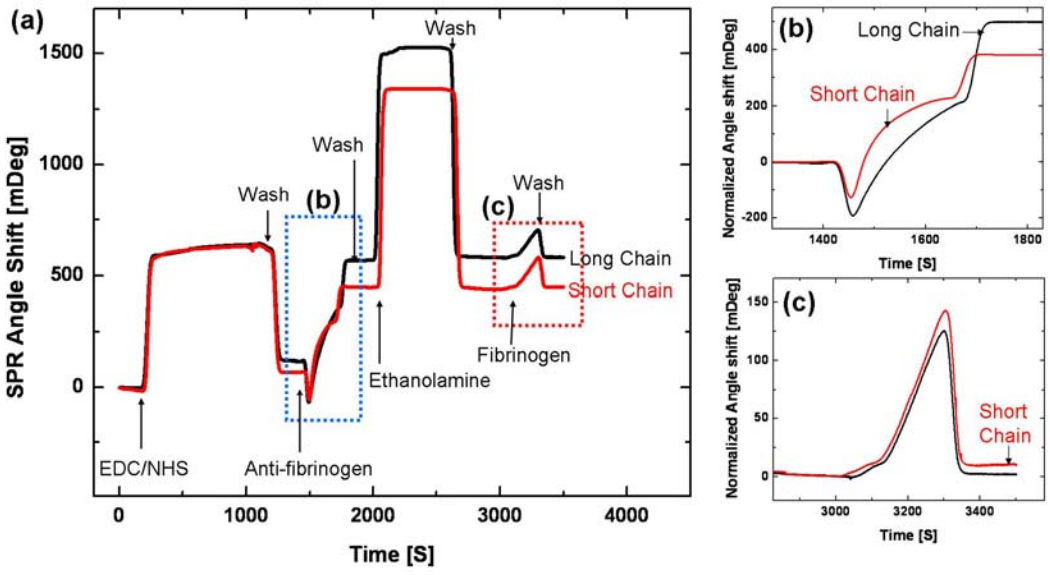

Figure 3.10 (a) SPR sensorgrams of detecting fibrinogen in picomolar range on different chain-length SAMs. Normalized close-up SPR sensorgram after (b) anti-fibrinogen injection and (c) fibrinogen injection.

This suggests that long-chain SAMs are more densely packed and immobilize more antibodies than short-chain SAMs. There might be more NSA due to more defects on the long-chain SAMs. When fibrinogen (1ng/ml concentration) was introduced to the immobilized antibody surfaces, for instance, 1.9 mDeg and 11 mDeg were observed for long and short-chain SAMs, respectively. Considering that long-chain SAMs have more antibodies immobilized than short-chain SAMs, the results suggest the background noise of NSA on the long-chain SAM limits the SPR angle shift. SPR angle shift of the short-chain SAM was five times higher than that of the long-chain SAMs. This demonstrates the optimal combination of the three targeted parameters on the short-chain SAM (incubation time, surface roughness, and crystal direction), producing a signficant SNR (Signal-to-noise ratio) improvement over the conventional long-chain SAM surface.

3.4 Conclusion

This work studied NSA behavior on polycrystalline gold surfaces modified by alkanethiol SAMs with different chain lengths. The purpose of this work is to address a major bottleneck in microfluidic-based biosensor development by providing controllable parameters for reducing NSA on microfluidic-based biosensors. Two different length SAMs were prepared on a microfluidic device, and their NSA was monitored by SPR for each of three different design parameters: i) SAM formation time, ii) gold surface roughness, and iii) gold surface crystal orientation. Results show that long-chain SAMs suffered from NSA even after 24-hour SAM formation time, while short-chain SAMs showed little NSA after just a 3-hour formation time. The gold surface roughness revealed

different NSA patterns for long- and short- chain SAMs: long-chain SAMs were very dependent on roughness, while short-chain SAMs were less dependent. NSA on the short-chain SAMs strongly correlated as a function of gold (111) orientation. For actual antigen detection through immunoreaction, however, background noise from NSA on the long-chain SAMs masked the signal from analytes of interest.

4 A NOVEL PROTEIN DETECTION BASED ON VROMAN EFFECT

4.1 Introduction

A conventional biosensor approach is that a specific bioelement immobilized on a sensing surface recognizes a specific target molecule and a sensor element transduces the change in the biomolecular interactions into an electrical signal. While the extensive research on the transducers has allowed the application of extremely high sensitivity up to the level of fM concentration (Kim et al., 2008), the relatively slow advancements in techniques for bioelements cause an enduring problem in creating widespread commercial protein sensor(Pavlickova et al., 2004; Saerens et al., 2008; Predki et al., 2005; Taussig and Landegren, 2003). First, a large diversity of bioelements is not available for detection of various diseases (Glokler and Angenendt, 2003). Second, general immobilization strategies for high capture capacity are not well defined. Third, some bioelements do not have high specificity and affinity (Taussig and Landegren, 2003). Besides these limitations, integrating them on to the transducer is a time-consuming and labor intensive process and often becomes the bottle neck of high yield sensors. In affinity-based sensing, development of new bioelements and their attachment techniques is currently being pursued to overcome the limitations (Kusnezow and Hoheisel, 2002). To date, few alternative platforms for the protein detection have been active in biosensor communities. Here, this study reports a fundamentally different protein detection method that relies on the competitive nature of protein adsorption onto a surface. The method can be a complementary solution to the conventional affinity-based biosensor.

When more than one type of protein presents in solution, a competitive adsorption process occurs between the different proteins to adsorb on the surface, namely the Vroman effect (Vroman and Adams, 1969; Noh and Vogler, 2007; Green et al., 1999). The key factor that influences the adsorption of proteins is that the mass transfer rate of a given solute molecule to a surface is directly related to its solution concentration and inversely related to its molecular weight. Therefore, when a material is exposed to a solution containing several different soluble proteins, such as human serum, the more concentrated and smaller proteins tend to adsorb to the surface first, and then be displaced by larger, more strongly interacting proteins that may arrive subsequently. Since the effect is first introduced by Vroman and Adams in 1969, the Vroman effect has been studied extensively in the biochemistry community for competitive protein adsorption to materials having different surface chemistries and surface energies (Horbett and Brash, 1995**).**

Figure 4.1 shows the simple schematic of Vroman effect. A weak-affinity protein initially covering the surface is displaced by a strong-affinity protein. However, the reverse sequence does not occur. This process is led by thermodynamics: proteins with different dimensions and morphologies adsorb differently to a surface based upon their thermodynamic energy preferences, and behave in ways that minimize the overall system energy (Choi et al., 2008). This can be interpreted as a natural outcome of surface reorganization to achieve the equilibrium interphase composition.

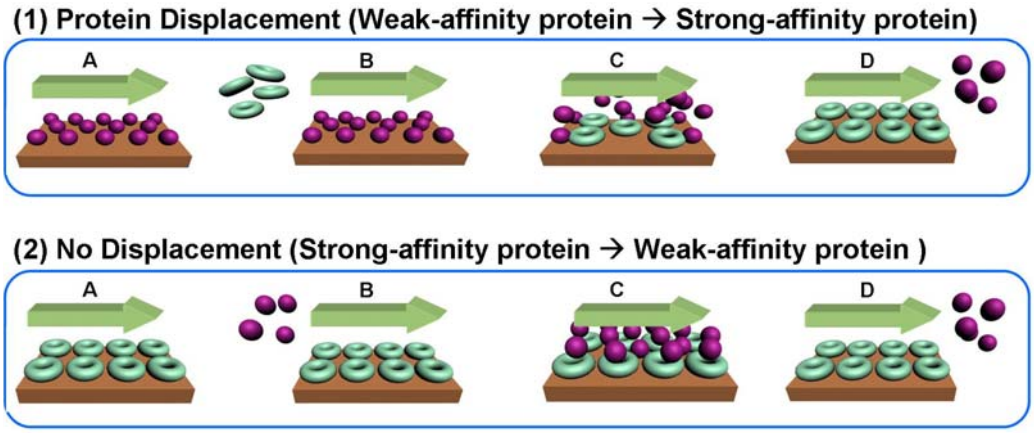

Figure 4.1 A schematic of the Vroman effect on a solid surface: when a weak-affinity protein adsorbs first and then a strong-affinity protein arrives to the surface later, protein displacement occurs. The reverse sequence does not occur

Therefore, the change in the free energy of the protein adsorption process on a certain surface reflects the protein exchange reaction, which can be expressed as

$$\Delta G = \Delta G^{\circ} + RT \ln(\frac{[AB]}{[A][B]}) = -RT \ln K_A = RT \ln K_D, \quad (4.1)$$

where $\triangle G$ and $\triangle G^{\circ}$ represent the changes in adsorption free energy and in standard-state adsorption free energy; R is the ideal gas constant [1.985 cal/K·mol] and T is the absolute temperature [298K]. *[A]* is the molar concentration of the protein in solution and *[B]* and *[AB]* are the mole fraction of surface sites occupied by bare surface and adsorbed protein, respectively (Schubert et al. 2003; Schasfoort and Tudos 2008). The equilibrium association constant K_A and dissociation constant K_D can be acquired from SPR kinetic analysis.

In this chapter, by using the competitive protein adsorption, it is demonstrated that specific target protieins can be identified without using the conventional affinity-based method. In Chapter 4.2, a tyroid cancer biomarker, thyroglobulin (Tg), was detected in a protin mixture. In Chapter 4.3, fibrinogen, a cardiovascular biomarker, was monitored in undiluted human serum.

4.2 Thyroglobulin (Tg) detection

This section presents thyroglobuin (Tg) in three different protein mixture (albumin, haptoglobin and thyroglobulin) can be selectively detected based on the competitive protein adsorption. The concept is that one can engineer a pair of surfaces covered by two known proteins; one is covered by a weaker-affinity protein and the other is covered by a stronger-affinity protein than the target protein. Then, the pair of the surfaces becomes a selective protein sensor since one is displaced and the other is not displaced by the target protein.

4.2.1 Introduction

Thyroid cancer is a cancerous growth of the thyroid gland and the most common endocrine malignancy, accounting for approximately 1% of malignancies worldwide (Park et al., 2006). Thyroglobulin (Tg) concentration in blood is a key parameter in the follow-up of patients treated for differentiated thyroid cancer (DTC) (Krahn and Dembinski, 2009). The power of Tg detection lies in the fact that Tg can only be made by the thyroid gland. Tg is a very specific protein biomarker and can be used for prognosis after the eradication of normal thyroid tissue in thyroid cancer patients. Up to 20% of patients with initial treatment of

thyroidectomy and radioablation therapy show subsequent persistence or recurrence of the disease and 8% of them eventually die (Frasoldati, et al., 2002). Thus, highly sensitive and selective tools to detect Tg is useful for the persistent and recurrent disease.

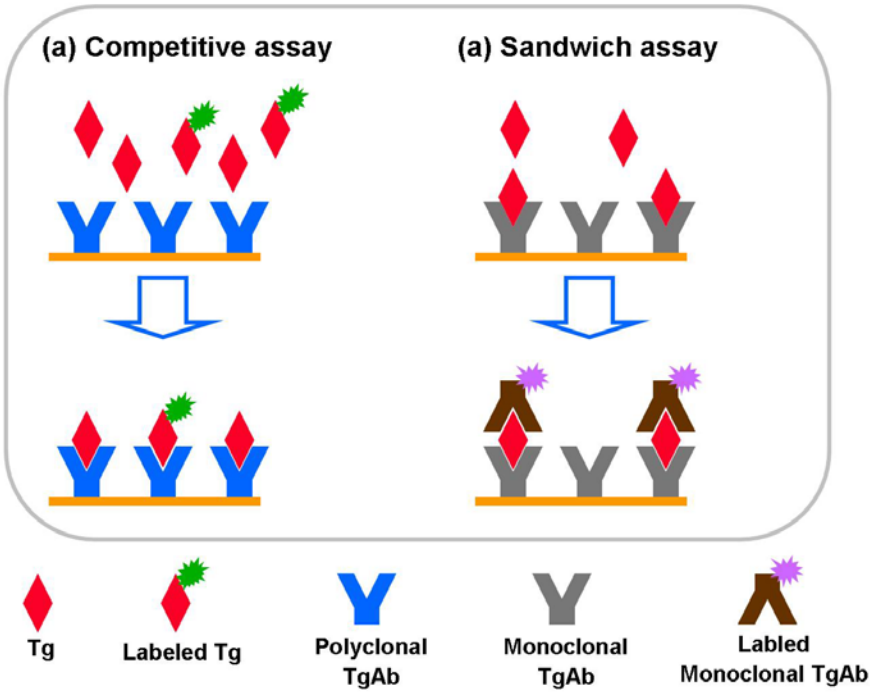

Figure 4.2 Scheme of immunoassay (a) competitive and (b) sandwich immunoassays

Competitive and sandwich immunoassays are common types of assays used to detect Tg (Wartofsky and Nostrand, 2005) (Figure 4.2). Competitive immunoassays use a limited amount of antibody and Tg, labeled with visible markers. By introducing known amounts of unlabeled Tg, a calibration curve is created in which the amount of labeled Tg bound to the antibody is inversely related to the amount of unlabeled Tg in the sample tested. Sandwich

immunoassays begin by having primary Tg antibodies adsorbed onto a surface, which then capture Tg and the additional labeled secondary Tg binds the captured Tg to amplify signal. Both immunoassay methods are well-established for Tg measurement and several kits are commercially available to perform these immunoassays (Wartofsky and Nostrand, 2005).

However, there are two main challenges associated with the immunoassay methods. First of all, both immunoassay methods depend on fluorescence- or radioisotope-labeling or enzymatic amplification to visualize target-antibody binding. The chemical labeling may modify the target proteins' characteristics, altering their behavior (Haab, 2003). Moreover, the labeling procedure is time-consuming, labor-intensive, and it is often difficult to achieve accurate quantification due to variable labeling efficiency for different proteins. On the other hand, the label-free technique can eliminate the labeling process and is becoming an attractive alternative for biological analysis Among various label-free mechanisms, SPR (Surface Plasmon Resonance) has been one of the leading techniques due to its extremely high sensitivity (Ince and Narayanaswamy, 2006).

The second main challenge involves creating highly active and robust sensing surfaces, which is crucial to the performance of the immunoassays. However, developing high-quality antibodies is extremely laborious and expensive. Therefore, the key limiting factor in immunoassays is to develop specific antibodies with sufficient affinity to analytes. Besides these limitations, integrating antibodies on to the surface of a transducer is also a time-consuming

and labor-intensive process, often becoming the bottle neck of high throughput sensing systems (Choi et al., 2008).

Here, this study reports a fundamentally different protein detection method that relies on the competitive nature of protein adsorption onto a surface. The method can be used as a complement to the conventional immunoassay for Tg measurement.

4.2.2 Experimental methods

4.2.2.1 Chemicals

Five human serum proteins were used to characterize the sensor: albumin (66 kDa), haptoglobin (86 kDa), IgG (150 kDa), fibrinogen (340 kDa), and thyroglobulin (660 kDa) (Sigma-Aldrich and CalBIOCHEM). All the chemicals were received as lyophilized powders and used without further purification. The proteins were made up to 0.05 % (w/v) concentrations in PBS 1X (1.15 g/L-Na_2HPO_4, 0.20 g/L-KCl, 0.20 g/L-KH_2PO_4, 8.0 g/L-NaCl, pH 7.4) immediately prior to analysis. The concentration of mixed proteins is 0.05 % (w/v). Fluorescent dyes (Alexa Fluor 488 (green) and 594 (red)) were purchased from Invitrogen, Inc.

4.2.2.2 Sensing surface formation

Glass substrates (BK7, n=1.517, 150 um) were first cleaned in piranha solution (a 3:1 ration of H_2SO_4 and H_2O_2) for 10 min. The substrates were then rinsed with water and ethanol sequentially and were dried under N_2 stream. Using thermal evaporator, Cr layer was coated first on the glass substrates to a thickness of 2 nm

followed by Au to a thickness of 48 nm. Then, the substrates were cleaned by oxygen plasma (Harrick Plasma Inc.) at 18 W for 1 min.

4.2.2.3 Microfluidic device for detecting fluorescent intensity

The microfluidic device was fabricated to evaluate the protein displacement using fluorescent labeling. The device consists of three layers. A 1 mm-thick top glass was mechanically drilled to have two holes; an inlet and an outlet. Bottom glass substrate (100 um-thick) has Cr/Au (2 nm/ 10 nm) electrode, which was evaporated and patterned for inverted microscopy. The spacer between the two substrates was made of PDMS (Polydimethylsiloxane). These layers were bonded all together after oxygen plasma treatment. The PDMS layer was prepared to be 1 mm in thickness and mechanically cut to have a channel.

4.2.2.4 Fluorescent intensity Measurement

The fabricated microfluidic device was mounted onto inverted microscope (Nikon, TE2000-U) with a CCD camera (Photometric). Using a sample injection valve (6-port M-461, Upchurch Scientific), protein and buffer solution selectively flowed through the microfluidic channel driven by two external syringe pumps. Each solution flowed at the speed of 10 μl/min. The captured fluorescent image was analyzed on Image J software provided by NIH Image.

4.2.2.5 Microfluidic device for SPR measurement

The fabrication process is illustrated in Figure 4.3. Soft-lithography was used to fabricate the microfluidic device. For a top layer, photoresist, AZ4330, was spin-coated on a silicon wafer and patterned for channels. Then the pattern was transferred to silicon by Deep RIE, etched ~ 100 um. The width of the channel is

2.1 mm and two channels are separated by 1.3 mm. PDMS solution was poured and cured on the silicon wafer and the molded PDMS was peeled off. The thickness of the layer is approximately 1 cm. Intel/outlet tubes (Upchurch Scientific) (Inner diameter: 25 μm, Outer diameter: 360 μm) were inserted through the PDMS using a syringe needle and fixed by adhesive. A Bottom substrate has patterned Cr/Au (2 nm/ 47 nm) pads on the glass substrate, which are two sensing surfaces for detection of the protein exchange. The size of the sensing surfaces is 1.8 mm wide and 8.0 mm long. The width of the channel is slightly wider than that of the gold surface to completely bond two substrates by using oxygen plasma.

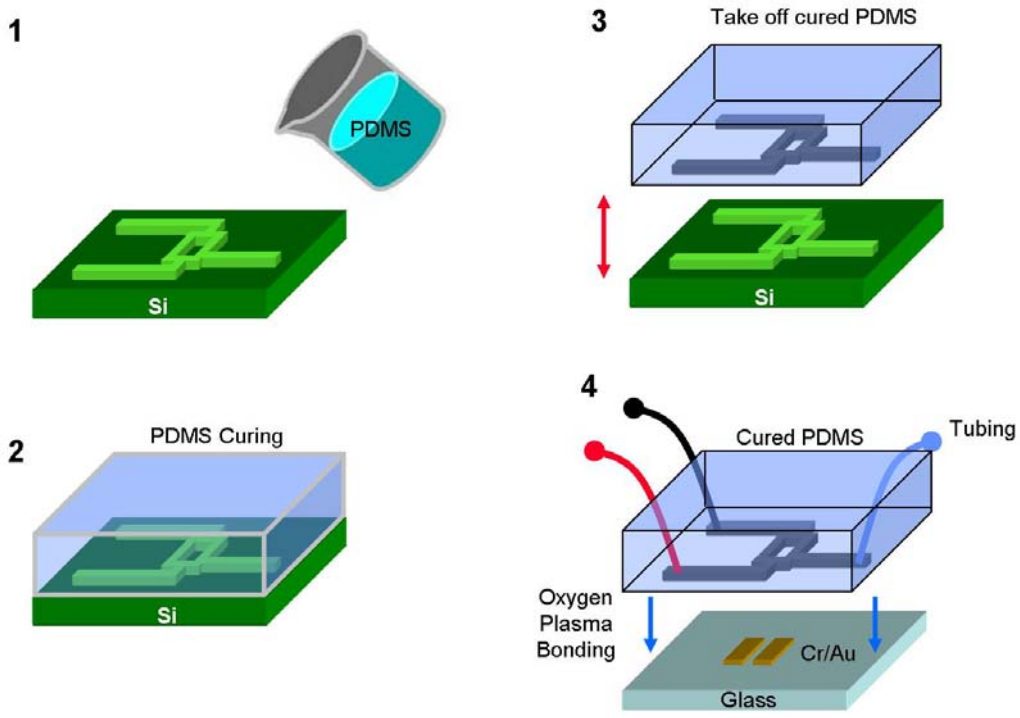

Figure 4.3 Fabrication process

4.2.2.6 SPR setup

The fabricated microfluidic device was mounted to the semi-cylindrical prism of SPR instrument (Bi SPR 1000, Biosensing Instrument Inc.) by using a refractive index matching liquid. The experimental setup is equipped with a computer-controlled data acquisition system. The SPR produces two sensorgrams in real time; one on a reference channel and the other on a sensing channel. Throughout the experiments, room temperature was maintained at 25° C.

4.2.3 Results and discussion

4.2.3.1 Protein displacement

Its first implementation demonstrates that five human serum proteins, albumin (66 kDa), haptoglobin (86 kDa), IgG (150 kDa), fibrinogen (340 kDa) and thyroglobulin (660 kDa), have different adsorption strengths onto the hydrophobic gold surface (contact angle measurement: 83.2°± 0.75°).

Table 4.1 Summary of interaction strengths of five different proteins.

Second	First				
	Albumin	Haptoglobin	IgG	Fibrinogen	Thyroglobulin
Albumin	X (1 mDeg)	X (3 mDeg)	X (-2 mDeg)	X (2 mDeg)	X (-4 mDeg)
Haptoglobin	O (40 mDeg)	X (-1 mDeg)	X (2 mDeg)	X (-1 mDeg)	X (0 mDeg)
IgG	O (90 mDeg)	O (75 mDeg)	X (3 mDeg)	X (0 mDeg)	X (-2 mDeg)
Fibrinogen	O (320 mDeg)	O (249 mDeg)	O (142 mDeg)	X (4 mDeg)	O (90 mDeg)
Thyroglobulin	O (200 mDeg)	O (87 mDeg)	O (62 mDeg)	X (3 mDeg)	X (3 mDeg)

O : Displacement Occurs; X : No Displacement

The different adsorption strengths induce an exchange reaction among them. First, a protein is pre-adsorbed on the surface (row in Table 4.1). Then another protein (column in Table 4.1) subsequently reaches to the surface to interact with the pre-adsorbed protein. The surface was saturated using 0.05 % (w/v) proteins to form a fully packed monolayer (Green et al., 1997), verified by re-injecting the same sets of protein (Table 4.1). Since neutral PBS (phosphate buffered solution, pH 7.4) was used and all the proteins used for experiments have the p*I* (isoelectric point) less than pH 7.0, multilayer formation due to protein-protein electrostatic interaction does not occur (Van der Veen et al., 2004). For example, when IgG is pre-adsorbed on the surface, fibrinogen and Tg displace the IgG producing 142 mDeg and 62 mDeg, which correspond to 2.10 x 10^{11} molecules/cm^2 and 4.72 x 10^{10} molecules/cm^2 (120 mDeg corresponds to 1 ng/mm^2 for the SPR employed here). However the SPR angle change is almost negligible when fibrinogen and Tg are exposed to IgG, hence demonstrating that the angle changes are not due to the multi-layer formation but due to the protein displacement. Table 4.1 shows all the cases of the displacement and the monolayer formation among five different proteins. The displacement strength is ranked in the following order; Fibrinogen (340 kDa) > Thyroglobulin (660 kDa) > IgG (150 kDa) > Haptoglobin (86 kDa) > Albumin (66 kDa). The Vroman effect does not always follow the size of proteins; for instance, thyroglobulin is larger than fibrinogen and yet is being displaced by fibrinogen. This phenomenon may possibly be explained because of their structures and potential conformation at the surface. Fibrinogen has a triad structure tethering two D domains to a central E domain by triple-stranded α–

helical-coiled coils (αC) (Holden and Cremer, 2005). On the neutralized Au surfaces, D and E domains are involved in the strong adsorption and even positively charged αC domains in the neutralized PBS does not have any electrostatic repulsion against the surface. On the other hand, thyroglobulin has a rather high degree of spherical symmetry and compactness. Thyroglobulin is involved in the smaller hydrophobic attraction than fibrinogen because thyroglobulin acts as a compact particle (Bloth and Bergquist, 1968; Deshpande and Venkatesh, 1999).

4.2.3.2 Evaluation

The displacement events were evaluated by using fluorescent labeling of proteins (Figure 4.4). A custom-made microfluidic device was prepared with a 10 nm-thick gold film on a glass slide to observe the proteins adsorption/exchange in real time. The thin film was to form hydrophobic properties and to be transparent to detect fluorescent intensity using inverted microcopy. IgG/fibrinogen and Tg were labeled by green and red fluorescent dyes, respectively. Those dyes are assumed not to interfere in protein displacement process because of their relatively-small size compared to proteins used in the experiment. When Tg flows on the surface of pre-adsorbed by IgG, IgG fluorescent intensity decreases (from 0.453 to 0.015) and Tg intensity remains high (0.202) after washing (Figure 4.4(a)). On the other hand, Figure 4.4(b) shows the reverse consequence; fibrinogen is pre-adsorbed on the surface and Tg arrives later. Fibrinogen fluorescence intensity remains high (0.304) and Tg drops significantly on the washing step (0.081). Tg fluorescent intensity has a larger positive response in

Figure 4.4(a) than it does in Figure 4.4(b), which can be interpreted as a displacement reaction. The fluorescent detection of proteins adsorption/exchange is in good agreement with the results of Table 4.1, demonstrating the Vroman effect.

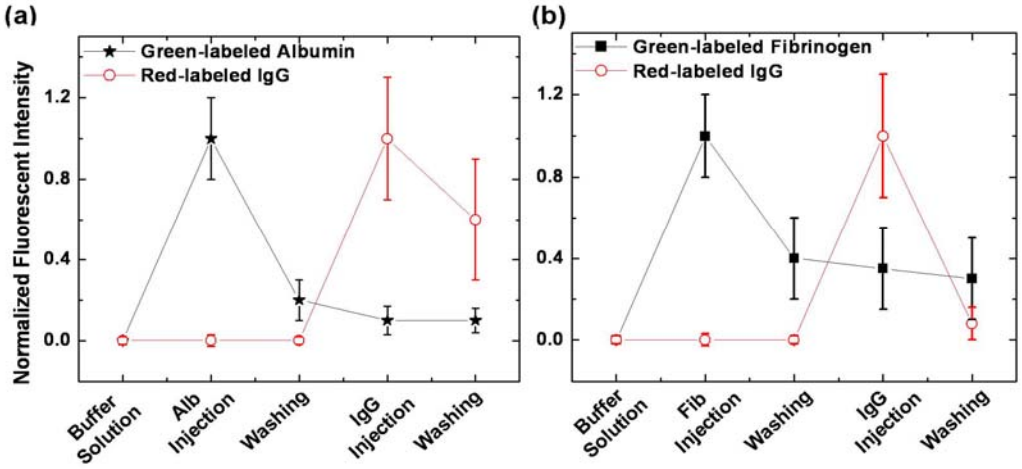

Figure 4.4 Real-time fluorescent intensity changes demonstrate proteins adsorption/ exchange, the Vroman effect.

4.2.3.3 Target protein detection

Based on the data set (Table 4.1), specific target proteins were identified without using the conventional affinity-based method. Figure 4.5 shows how to detect Tg using a pair of surfaces pre-adsorbed by two known-sized proteins; IgG and fibrinogen. Tg displaces IgG in channel 1 but flows through the fibrinogen-covered surface (channel 2) without any exchange reaction. The differential measurement of the SPR angle changes from channel 1 and 2 allows the detection of Tg, and the angle changes indicate the number of Tg molecules displacing IgG.

The sensor is enclosed by microfluidic channels/chambers in order to facilitate potential integration within microfluidic systems (Figure 4.5(a)).

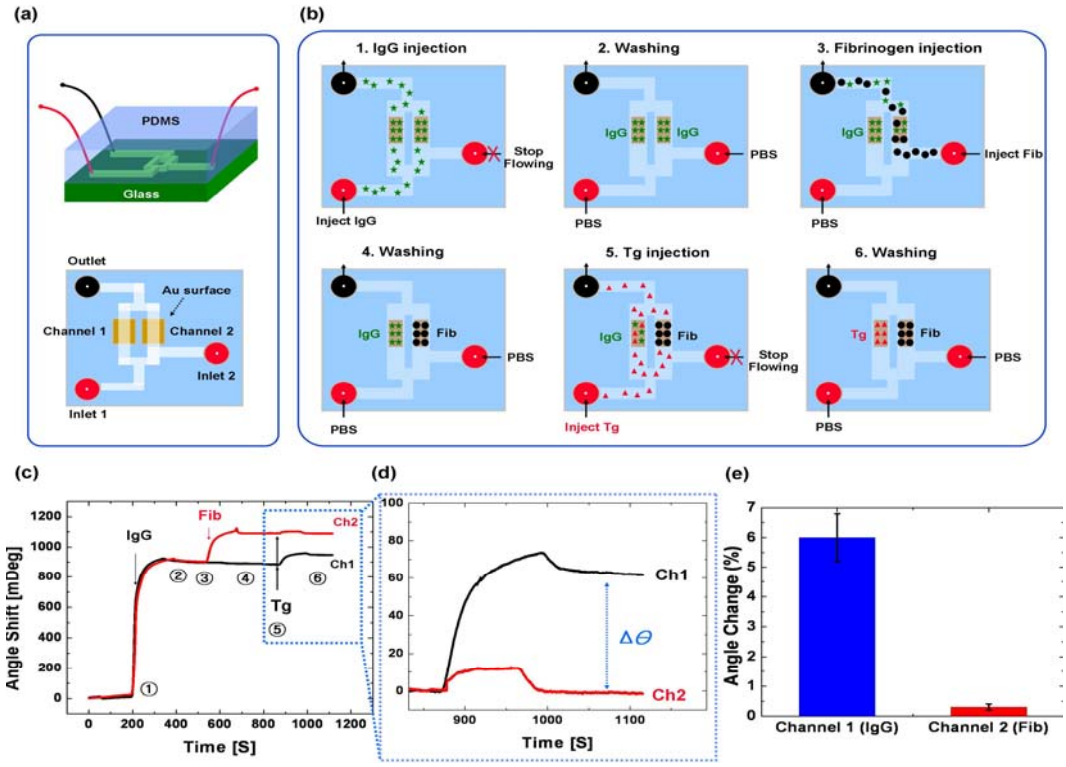

Figure 4.5 (a) A microfluidic device (b) A schematic of operating principle. (c) SPR sensorgram of the displacement event. (d) normalized close-up SPR profile after the Tg injection (e) final angle changes (%) on both surfaces.

The device has two inlets and one outlet unlike the previous approach that has two inlets and two outlets (Choi et al., 2008). A mixture of sample is injected from only one of the two inlets. The three ports microfluidic device allows minimizing baseline discrepancy generated by having the sample injected from two inlets. The angle shift is monitored in real-time as protein solution flows through the microfluidic channels driven by two external syringe pumps from the two inlets. First, PBS is circulated for approximately 20 min until the angle

stabilizes. Once the angle stabilizes, the first protein sample is injected from inlet 1 and flows through both microfluidic channels at 10 μl/min, generating angle changes on both surfaces (Figure 4.5 (b)-1 & (c)). When the protein adsorption completes on both gold surfaces, PBS is flowed to wash the surface to remove excess weakly bound proteins (Figure. 4.5 (b)-2). Then, the second protein sample is injected from inlet 2 and flows only through the channel 2 at the speed of 5 μl/min (Figure 4.5 (b)-3). During the process, PBS keeps flowing from inlet 1 at 10 μl/min to prevent the second protein from flowing back to the channel 1. The second protein is selected to displace the first one in channel 2. For instance, to detect Tg, IgG was first introduced from inlet 1 and adsorbed on both gold surfaces. Then, fibrinogen was injected into inlet 2 while PBS flows from inlet 1. The fibrinogen, then, displaced the pre-adsorbed IgG in the channel 2. When the target molecule, Tg, was introduced from inlet 1, it flowed through both channels and channel 1 had an angle change of 60.1 mDeg and channel 2 showed negligible angle change (Figure 4.5 (d)). This selective displacement offers the selectivity of the sensor. During the surface preparation, fibrinogen completely displaced IgG in channel 2; no angle change occurred after the Tg injection. If IgG residue remained on the surface, while not being completely displaced by fibrinogen, Tg should have displaced the IgG residue and produced angle change in channel 2. Figure 4.5 (e) shows the final angle changes (%) of a series of experiments on both surfaces, which indicates that the sensor has selectivity in the controlled cocktail of proteins.

When a mixture of proteins solution was injected, the sensor only responded to a specific target protein. Figure 4.6 shows that the sensor responds to the target protein, Tg, in a mixture of albumin, haptoglobin and Tg. Upon the mixture reaching the surfaces channel 1 showed 58.9 mDeg angle change and the channel 2 had little angle change (3 mDeg) (Figure 4.6 (b)). This set of experiment demonstrates that fibrinogen (channel 2) remained on the surface whereas IgG (channel 1) was displaced by the mixture. Since albumin and haptoglobin in the mixture cannot displace IgG (Table 4.1) and multi-layer is not formed in the process, only thyroglobulin generates the SPR angle change in the channel 1 (Figure 4.6 (a) & (b)). A series of experiments verified that the sensor had a selectivity (Figure 4.6 (c)).

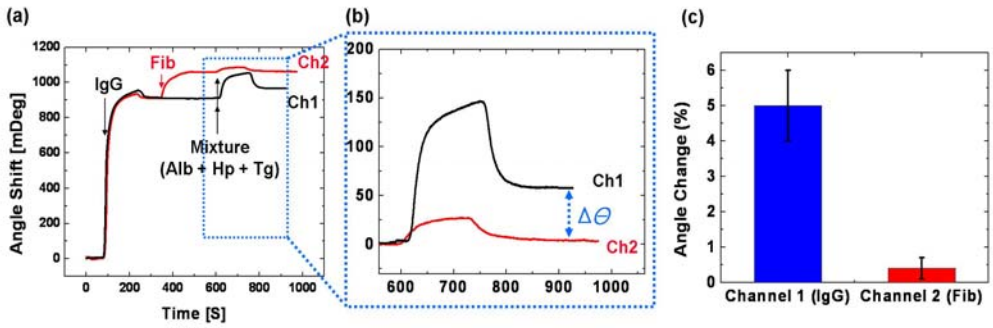

Figure 4.6 (a) Tg detection of pre-adsorbed IgG and fibrinogen surfaces in a mixture of albumin, haptoglobin, and Tg. (b) normalized close-up view (c) SPR angle changes (%) of channel 1 (IgG) and channel 2 (fibrinogen)

When the exchange reaction by the mixtures occurs, many weakly bonded proteins are easily detached by subsequent PBS washing flow because few proteins are involved in the displacement. Also, it is noteworthy to observe the behavior of proteins in channel 2. Although target molecules do not displace pre-

adsorbed proteins on the surface in channel 2, the SPR shows a small increase with moderate slope. However, their interactions to the surface are very weak and they are easily detached by subsequent PBS flow, resulting in a very small hill of SPR angle change. After waiting to be stabilized, the permanent angle change is almost negligible (Figure 4.5 (d) & 4.6 (b)).

4.2.3.4 Selectivity and limit of detection in Tg detection

Figure 4.7 (a) shows the selectivity of Tg on the pre-adsorbed surfaces by IgG and fibrinogen. The selectivity was measured with respect to albumin, haptoglobin and IgG. When Tg was injected, 59 mDeg angle was generated while others had insignificant angle changes, all less than 5 mDeg. This indicates that the Vroman-effect-based biosensor can be configured to selectively detect Tg. Figure 4.7 (b) shows the linear range and LOD by measuring the signal magnitude over a range of Tg loadings (1pg/ml to 1 ug/ml). The plot demonstrates that the assay is linear over 6 orders in concentration (1 pg/ml – 1 μg/ml) and LOD was estimated to be 1.0 pg/ml.

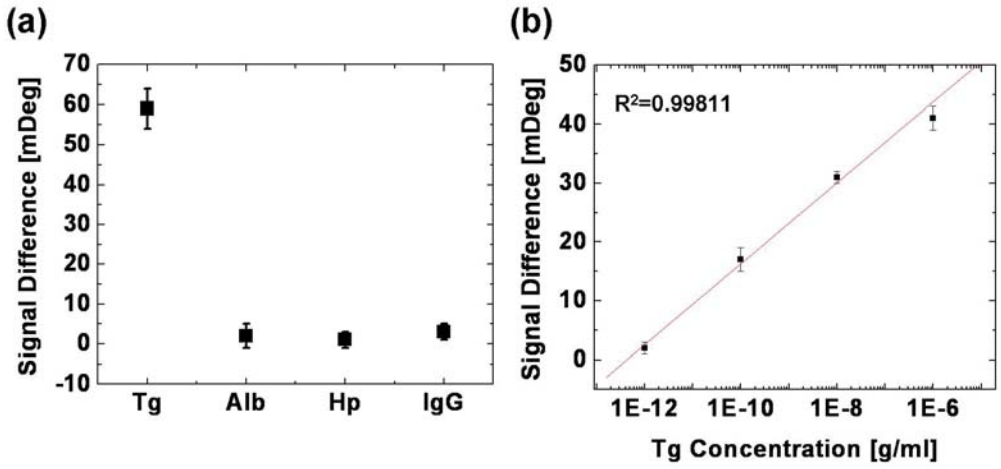

Figure 4.7 (a) Selectivity and (b) standard curve of Vroman effect-based biosensor in a case of thyroglobulin detection.

4.2.4 Conclusion

This chapter demonstrated that the competitive nature of protein adsorption allows selective detection of a cancer biomarker, Tg, in a protein mixture (albumin, haptoglobin, and Tg) without using the antibody immobilization. The sensing method offers multiple advantages over many existing affinity-based detection methods: i) rather expensive, time-consuming and labor-intensive immobilization process can be avoided using hydrophobic physical adsorption of proteins and ii) diverse target molecules can be detected by choosing an appropriate combination of pre-adsorbed protein pairs. The proof-of-concept protein sensor has many challenges to be addressed. The sensor requires extensive sample preparation steps to separate proteins including size exclusion chromatography and electrophoresis since the sensor alone can not detect a protein of interest among a large mixture of proteins with simliar

adsorption properties. These sample preparation steps are currently deployed in analytical instruments, which the sensor needs to be interfaced with.

4.3 Fibrinogen detection

A unique sensing mechanism is reported based on competitive protein adsorption to measure fibrinogen, a cardiovascular biomarker, in undiluted human serum. The method uses physical adsorption of proteins to a surface rather than complex and time-consuming immobilization procedures.

4.3.1 Introduction

High fibrinogen levels are strongly correlated with the frequency of cardiovascular disease. Many studies have reported that fibrinogen concentrations increase by 200 μg/ml for those with heart diseases (Kamath and Lip 2003). Two different concentrations of fibrinogen spiked in human serum (3.0 mg/ml (normal concentration) vs. 3.2 mg/ml (abnormal concentration with heart disease)) were successfully differentiated by monitoring real-time SPR signals as fibrinogen displaced a pre-adsorbed protein, IgM. The technique provides a selective detection of fibrinogen; the relatively strong-affinity protein, IgM, was dominantly displaced by fibrinogen, and significantly less by other proteins in human serum. Using the nature of protein adsorption obviates the need to rely on complex assays and their attachment to transducers. An additional benefit of this method is that, non-specific binding of other proteins in complex mixture does not hamper sensing performance; the sensing surface is pre-adsorbed by relatively high affinity proteins that are eventually displaced by a stronger-affinity target analyte.

4.3.2 Experimental methods

4.3.2.1 Chemicals

Human serum from platelet-poor human plasma, as well as albumin and IgM, were purchased from Sigma-Aldich. The human serum fibrinongen was received as lyophilised powers from CalBioChem and used without further purification. Alubumin and IgM concentrations were up to 0.1 % (w/v) in PBS 1X. (1.15 g/L-Na_2HPO_4, 0.20 g/L-KCl, 0.20 g/L-KH_2PO_4, 8.0 g/L-NaCl, pH 7.4) immediately prior to pre-adsorption. The two human serum samples were prepared by spiking fibrinogen (3.0 mg/ml and 3.2 mg/ml).

4.3.2.2 Surface preparation

Glass slides (BK7, n=1.517, 150 um) were first cleaned in piranha solution (a 3:1 ration of H_2SO_4 and H_2O_2) for 10 min. The slides were then rinsed sequentially with DI water and ethanol and were dried under a N_2 stream. Using sputter, a Cr layer was first coated on the glass substrates to a thickness of 2 nm followed by Au to a thickness of 48 nm. The slides were then cleaned by a hydrogen flame for several seconds. The bare gold surface was moderately hydrophobic (82.6 ± 0.77° of contact angle).

4.3.2.3 SPR setup

Using a refractive index matching liquid, the glass slide was mounted to the semi-cylindrical prism of the SPR instrument (Bi-2000, Biosensing Instrument Inc.). The flow cell with two microfluidic channels was mounted on top of the surface. Then the angle shift was monitored in real time as sample solution driven by an external syringe pump flowed throught the channels. The experimental setup was

equipped with a computer-controlled data acquisition system. SPR was calibrated each time to maintain the sensitivity, 60 mDeg at 1 % ethanol solution. Throughout the experiments, room temperature was maintained at 25 °C.

4.3.3 Results and discussion

Fibrinogen is known to be a "sticky protein" on hydrophobic surfaces, for displacing other serum proteins (Hemmersam et al. 2005). The previous study showed that fibrinogen (340 kDa) has such high adsorption strength on a gold surface that it displaces thyroglobulin, which has higher molecular weight of 660 kDa (Choi and Chae 2009a). It is essential to design a pre-adsorbed surface that fibrinogen displaces yet other proteins do not; the higher the chance of being displaced by other proteins, the lower the selectivity of the sensor for fibrinogen. Figure 4.8 illustrates this sensing scheme. When weak-affinity proteins are pre-adsorbed on a surface, the complex mixture of many proteins in serum tends to displace the pre-adsorbed proteins. By contrast, when the surface is pre-adsorbed by a strong-affinity protein, it is hypothesized that only several types of proteins, including fibrinogen, could displace the pre-adsorbed protein, thereby increasing the chance of measuring fibrinogen. To verify this hypothesis, two proteins were selected as pre-adsorbed known proteins; albumin (67 kDa) and IgM (900 kDa).

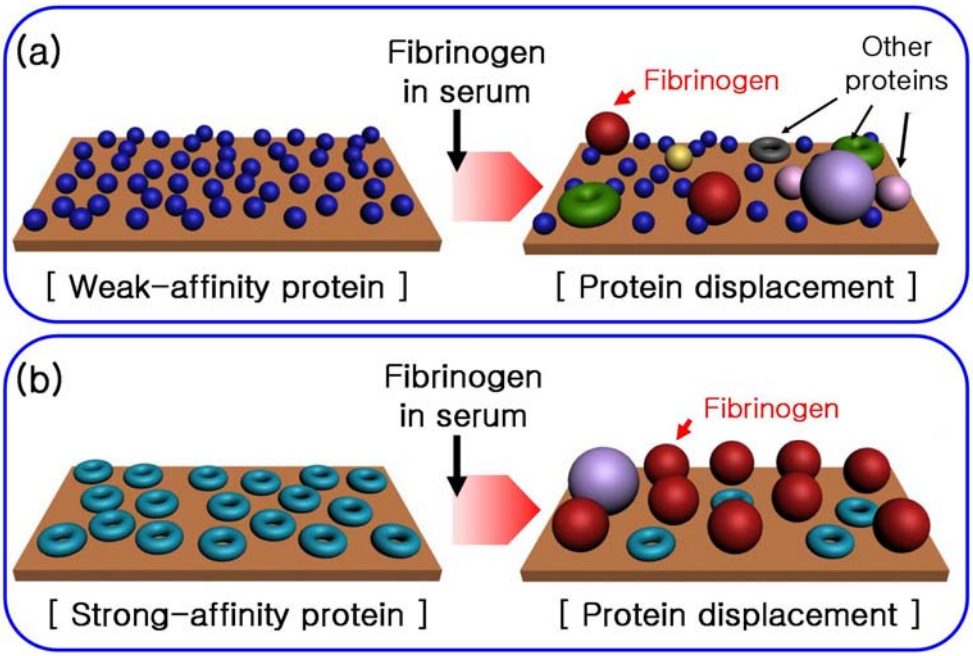

Figure 4.8 Operating principle of measuring fibrinogen in human serum based on the competitive protein adsorption.

In equation (4.1), the equilibrium association constant K_A and dissociation constant K_D can be acquired from SPR kinetic analysis. K_D of albumin, IgM, and fibrinogen were 13.2 μM, 9.2 μM, and 2.0 μM, respectively, and their respective ΔG were -6.6 Kcal/mol, -6.9 Kcal/mol, -7.8 Kcal/mol. Albumin has relatively small Gibbs free energy, which means that the albumin pre-adsorbed surface has a high chance of being displaced by other proteins in serum, and thus may not offer any selectivity for fibrinogen measurements. However, IgM has large Gibbs free energy, which may offer high selectivity of fibrinogen measurements in serum. Adsorption of proteins and their subsequent displacement behaviors were monitored by SPR in real time. Two samples were prepared: 3.0 mg/ml and 3.2

mg/ml of fibrinogen in undiluted human serum. 3.0 mg/ml and 3.2 mg/ml suggest, respectively, normal and abnormal fibrinogen levels in human blood.

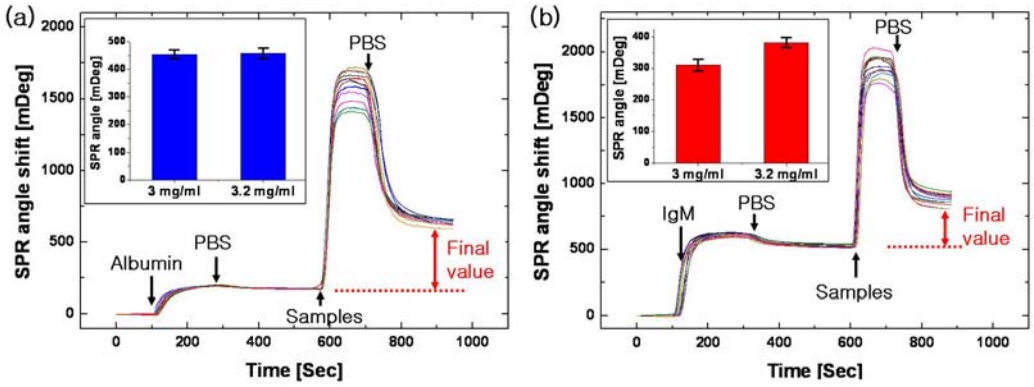

Figure 4.9 SPR profile of the displacement behaviors upon injection of two fibrinogen samples spiked in human serum. Each sample was introduced onto two surfaces that were pre-adsorbed by two different proteins; (a) albumin and (b) IgM.

Figure 4.9 shows SPR sensorgrams of displacement behaviors upon injection of the two serum samples. Each sample was introduced onto two surfaces at the speed of 30 μl/min, and pre-adsorbed by two different proteins (albumin and IgM). The experiments were repeated six times. Initially, phosphate-buffered saline (PBS) was circulated until the SPR signal stabilized. Once it stabilized, the gold surfaces were pre-adsorbed by flowing albumin and IgM at a concentration of 0.1 % (w/v), generating SPR angle shifts as shown in Figure 4.9. During the pre-adsorption procedure, the surface needs to be saturated by albumin or IgM before the protein exchange. If they do not form a fully packed protein monolayer, a later protein tends to adsorb on the space between the pre-adsorbed proteins. In this experiment, the surface was saturated using 0.05 % (w/v) proteins to form a fully

packed monolayer (Green et al., 1997), and verified by re-injecting higher-than-0.05% (w/v) protein concentrations (Figure 4.10).

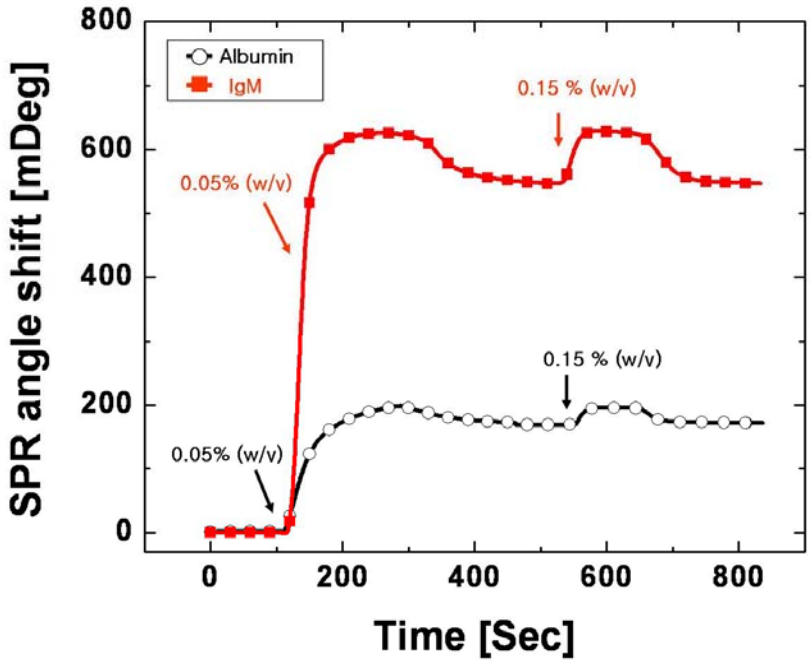

Figure 4.10 SPR sensorgrams of a fully packed protein monolayer. 0.05 % (w/v) proteins saturated the surface

When the protein adsorption was complete, PBS was flowed to wash the surfaces to remove excess weakly-bound proteins to establish the baseline. The angle shifts of albumin and IgM pre-adsorbed on each gold surface averaged 172.7±3.2 mDeg and 526.5±10.5 mDeg, respectively, which suggests that higher molecular weight proteins produce a thicker monolayer. When fibrinogen-spiked samples flew onto the two pre-adsorbed surfaces, the SPR angle values rapidly increased on both surfaces and reached an equilibrium plateau. Finally, PBS washed out all proteins not involved in the interaction or displaced by serum samples. When the angle shift stabilized, the final angle shift was measured from the baseline where

albumin and IgM pre-adsorbed on the surface. The final angle shift measurements were recorded all six times, and these are shown as inserts in Figure 4.9 (a) and (b), respectively. The inserts indicate how sensitively and selectively two fibrinogen-spiked samples can be differentiated by the measurements. The albumin pre-adsorbed surface does not provide distinct SPR angle shifts between 3.0 mg/ml and 3.2 mg/ml, and this suggests that many serum proteins, including fibrinogen, were involved in the displacement reaction. On the other hand, the surface covered by IgM shows enough sensitivity and selectivity to differentiate two different fibrinogen concentrations in serum samples SPR produced an average of 310.3 and 381.3 mDeg for 3.0 mg/ml and 3.2 mg/ml, respectively, which correspond to 4.58×10^{11} molecules/cm^2 and 5.63×10^{11} molecules/cm^2 (120 mDeg corresponds to 1ng/mm^2). The limit of detection and dynamic range were characterized by measuring the angle changes over a range of fibrinogen loadings (200 μg/ml to 3.2 mg/ml), shown in Figure 4.11 (a). The biosensor has a detection limit of ~ 200 μg/ml and a sensitivity of 63.0 mDeg/ml. The selectivity of the biosensor was characterized by spiking 1 mg/ml albumin and transferrin in human serum samples (figure 4.11 (b)).

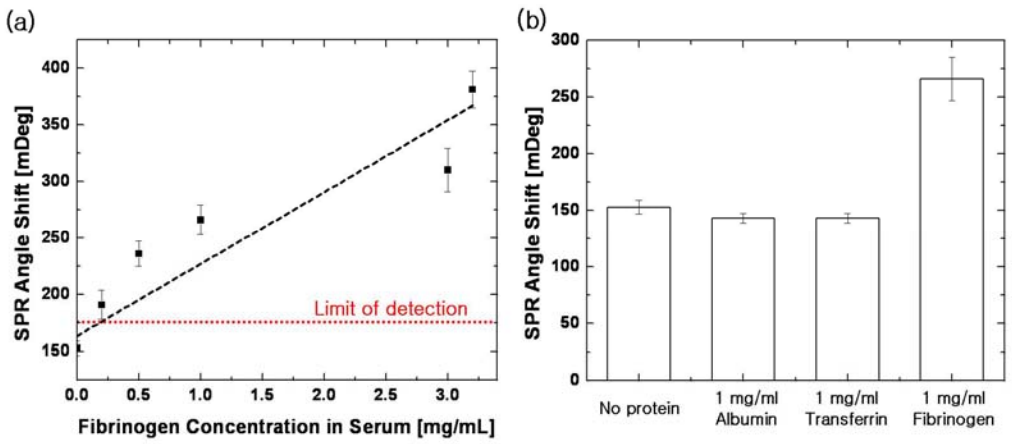

Figure 4.11 (a) Sensitivity and (b) selectivity of the biosensor

The IgM pre-adsorbed surface was evaluated after exposing it to fibrinogen-spiked serum samples. By flowing anti-fibrinogen antibodies onto the surface, permanent SPR angle shifts were generated on both 3.0 mg/ml and 3.2 mg/ml samples, as shown in Figure 4.12. This permanent shift demonstrates that a majority of proteins displacing the IgM were fibrinogen.

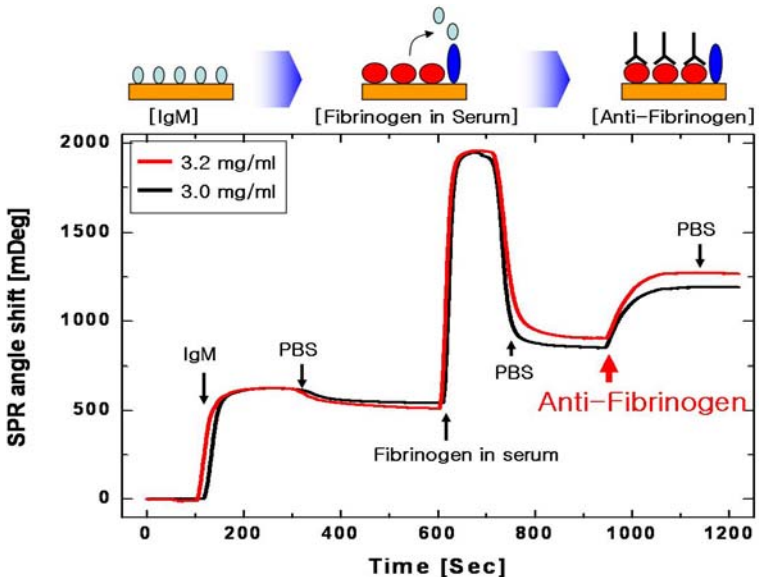

Figure 4.12 SPR sensorgrams of the interaction of anti-fibrinogen and fibrinogen after the competitive protein adsorption/exchange.

4.3.4 Conclusion

This section demonstrated that protein adsorption can be used as a sensing mechanism, and offered proof of concept by differentiating two different concentration fibrinogen-spiked samples (3.0 mg/ml vs. 3.2 mg/ml) in undiluted human serum. Two pre-adsorbed surfaces were tested: one covered with albumin and one covered with IgM. Each set of experiments was repeated six times. Results shows that the IgM pre-adsorbed surface has large Gibbs free energy, so only strong-affinity proteins--including fibrinogen—can displace the pre-adsorbed IgM. This new method obviates the need for complicated assay configurations to measure proteins, and complements the use of affinity-based immunosensors.

5 A NOVEL METHOD OF PROTEIN IDENTIFICATION BASED ON PATTERNS GENERATED BY PROTEIN ADSORPTION BEHAVIOR AND ITS DEMONSTRATION USING C-REACTIVE PROTEIN

5.1 Introduction

Proteins in human serum are considered effective diagnostic sources (Sahab et al., 2007). This is because proteins are the final form of the gene product and hence directly associated with biological functions (Choi et al., 2011, Sahab et al., 2007). Two different protein sensing techniques are generally employed: (1) a "lock-and-key" approach to detect a specific analyte and (2) a "cross-reactive" or "pattern-generation" technique to monitor the overall levels of proteins in serum (Albert et al., 2000; Wilson, 2009). The "Lock-and-key" design immobilizes a specific bio-receptor on a sensing surface, which enables the surface to form a strong and specific chemical bond with target analytes (Lavigne and Anslyn, 2001). In practice, however, most biosensors based on the "Lock-and-key" design suffer from interference caused by molecules that are structurally or chemically similar to the desired analyte. This is an unavoidable consequence of the "lock" being able to fit many imperfect "keys" (Albert et al., 2000). Additionally, biomarkers themselves are an imperfect measure, as most biomarkers are non-specific to particular diseases, and most diseases have more than one biomarker associated with their incidence (Wu et al., 2007). Furthermore, concentration changes of biomarkers in serum may cause unexpected interactions with other proteins making their detection much more difficult, as in the case of prostate antigen serum, for example (Sarkar et al., 2002). These challenges lead to adopt efficient

identification of total protein distributions, rather than aiming to detect a specific protein, in serum for disease diagnosis. The “cross-reactive” technique has been developed as an alternative approach for this purpose (De et al., 2009). This method is inspired by the sense of taste and smell, and utilizes an array of differentially responsive receptors to create response patterns to identify and quantify target analytes when they are present at elevated levels in media (Turner and Magan, 2004; De et al., 2009). The distinct advantage of the "cross-reactive" method is that the individual receptors do not need to be highly specific or selective to an analyte unlike the “lock-and-key” method which requires time-consuming and labor intensive synthesis and design of the receptors (Kusnezow and Hoheisel, 2002) (Figure 5.1).

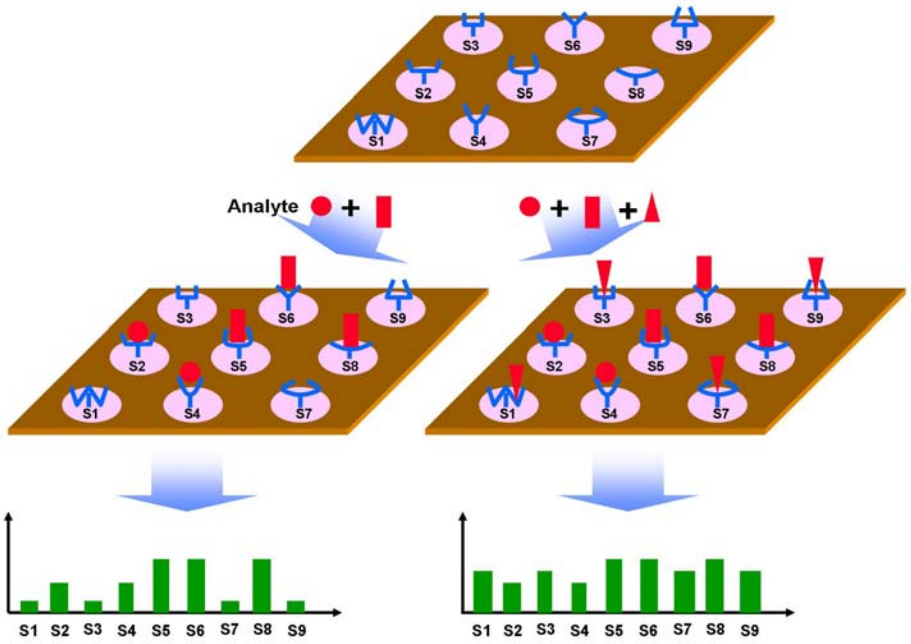

Figure 5.1 A general scheme for a “Pattern-recognition”-based sensor.

To date, various receptors have been employed for "cross-reactive"-based sensing of proteins. Zhou *et al.* utilized 8 array cells out of a 35-member receptor library of tetraphenyl porphyrin derivatives, functionalized with amino acids resulting in charge differences (Zhou et al., 2006). Rotello and co-workers (You et al., 2007; De et al., 2009) reported the use of nanoparticle conjugated with groups capable of making electrostatic and hydrophobic non-covalent interactions with analytes. Although they are highly effective at identifying proteins and can even be applied to sensing in a complex matrix such as human serum, the method still suffers from the requirement of a large number of receptors relative to the number of target analytes. In this sense, the method may not be very practical since the size of array of receptors or sensing surfaces should be very large to effectively generate responsive array to an analyte. The nature of protein adsorption on a surface is presented to address these issues effectively. By using physical adsorption of proteins on a sensing surface, a set of individually-tailored receptors generate an array of response patterns without any additional chemical modification. Moreover, since several thousands of proteins are found in nature and individually possess different characteristics on their own (Latour, 2005), an individual protein itself can be employed as one of the potential receptors providing responsive interactions with other target proteins. This is because it retains its own size, morphology, and charged and hydrophobic characteristics. The previous work showed that competitive protein adsorption could be potentially utilized as a sensing mechanism using the "lock-and-key" approach (Choi and Chae, 2009a; Choi et al., 2010). In a two-channel surface plasmon

resonance (SPR) system, two surfaces covered by two known proteins form a selective protein sensor by being displaced by a target protein on only one of the surfaces. The target protein displaces a weakly-bound protein; however, a strongly-bound protein is not displaced by the target protein. IgG and thyroglobulin successfully were detected in cocktail proteins and fibrinogen in undiluted human serum (Choi and Chae, 2009; Choi and Chae, 2010a; Choi et al., 2010). However, this technique is based on different adsorption properties of various proteins and does not provide enough selectivity for the "lock-and-key" mechanism. This limitation motivated us to take advantage of the protein adsorption behavior instead in a "cross-reactive" protein sensing mechanism. This chapter presents a proof-of-concept "cross-reactive"-based biosensor based on protein adsorption behavior that includes protein displacement and multi-layer formation. It is shown that a sample mixture of proteins generates a distinctive composite pattern of SPR angle shifts upon interaction with a sensing platform consisting of multiple surfaces whereby each surface consists of a distinct type of protein pre-adsorbed on the surface. Then this "cross-reactive" type of sensing mechanism is verified through its recognition of a particular biomarker, C-reactive protein (CRP), in the cocktail sample mixture. CRP is an important marker for the diagnosis of infection and inflammation (Vikholm-Lundin and Albers, 2006). The concentration level of CRP can rise from a normal level of less than 40 nM to above 850 nM for most infections and inflammations (Tsai et al., 2007). The sensing platform comprises a set of eight different surfaces, four of which are bare gold surfaces and the remaining four are self-assembled

monolayer (SAM)-modified gold surfaces, with one of four proteins (lysozyme, albumin, transferrin, and IgG) pre-adsorbed on each surface. This compilation of surfaces generates a signature when interacted with a sample of proteins. This response signature can then be employed to identify a matrix of various sample protein mixtures (α1-antitrypsin, haptoglobin, CRP, and IgM). SPR was used to monitor adsorption of proteins on the surface and their subsequent interactions in real time. The generated SPR angle patterns were subjected to linear discriminant analysis (LDA) to classify each sample and identify CRP selectively.

5.2 Experimental methods

5.2.1 Chemicals

Four proteins were pre-adsorbed on a surface: lysozyme (14.7 kDa), albumin (66 kDa), transferrin (80 kDa), and IgG (150 kDa) (Sigma-Aldrich), which were received as lyophilized powders and used without further purification. The proteins were made up to 0.1 % (w/v) concentration in phosphate buffered saline (PBS, 1.15 g/L−Na_2HPO_4, 0.20 g/L−KCl, 0.20 g/L−KH_2PO_4, 8.0 g/L−NaCl, pH 7.4) immediately prior to injection. Target mixture samples include five different proteins with different concentration in PBS: α1-antitrypsin (54 kDa), haptoglobin (86 kDa), CRP (118 kDa), and IgM (900 kDa) (Sigma-Aldrich). Tables 5.1 and 5.2 show a matrix of five samples for selectivity characterization of the sensor and another matrix of four samples for the detection of CRP, respectively. 11-mercaptoundecanoic acid was purchased from Sigma-Aldrich to form COOH-terminated SAM.

Table 5.1 Sample matrix for selectivity characterization

	α1-antitrypsin	Haptoglobin	CRP	IgM
Sample 1 (S1)	20 nM	20 nM	20 nM	20 nM
Sample 2 (S2)	**50 nM**	20 nM	20 nM	20 nM
Sample 3 (S3)	20 nM	20 nM	20 nM	**50 nM**
Sample 4 (S4)	20 nM	20 nM	**50 nM**	20 nM
Sample 5 (S5)	20 nM	**50 nM**	20 nM	20 nM

Table 5.2 Sample matrix for sensitivity characterization

	α1-antitrypsin	Haptoglobin	CRP	IgM
Sample 6 (S6)	20 nM	20 nM	**1 nM**	20 nM
Sample 7 (S7)	20 nM	20 nM	**5 nM**	20 nM
Sample 8 (S8)	20 nM	20 nM	**20 nM**	20 nM
Sample 9 (S9)	20 nM	20 nM	**50 nM**	20 nM

5.2.2 Fabrication of sensing surfaces

Glass substrates (BK7, n = 1.517, 150 μm) were first cleaned in piranha solution (a 3:1 ration of H_2SO_4 and H_2O_2) for 10 min. The substrates were then rinsed with water and ethanol sequentially and were dried under N_2 stream. Using a sputter, Cr layer was deposited first on the glass substrates to a thickness of 2 nm followed by Au to a thickness of 48 nm. The slides were then cleaned by a hydrogen flame for several seconds. The bare gold surface showed moderately hydrophobic (82.6 ± 0.77° of contact angle). For a COOH-SAM modified surface, the cleaned gold surface was immersed in an ethanol solution of 1 mM alkane-thiols for 24 hours at room temperature. Finally, the substrate was rinsed with ethanol and water, and thoroughly dried using nitrogen. The COOH-SAM

modified surface was negatively charged and showed hydrophilic (41.4 ± 0.63° of contact angle) (Yu and Golden, 2007), which led to different interaction with proteins compared to that on the hydrophobic bare gold surface (More et al., 2003).

5.2.3 SPR setup

The sensing surface was mounted to the semi-cylindrical prism of SPR instrument (Bi SPR 2000, Biosensing Instrument Inc.) by using a refractive index matching liquid. Each solution was delivered through the fluidic channels by an external syringe pump at the rate of 30 μl/min. The experimental setup is equipped with a computer-controlled data acquisition system. The SPR produces two sensorgrams in real time. Throughout the experiment, temperature was maintained at 25 °C.

5.2.4 Experimental procedure

Figure 5.2 illustrates a SPR sensorgram upon proteins displacement or multi-layer formation on pre-adsorbed sensing surfaces. One of the four pre-adsorbed proteins was first injected into either of two channels to form baseline of the sensing surfaces. When protein adsorption completes, PBS was flowed through the surface to remove excess weakly bound proteins. Then, a target sample was introduced to interact with the pre-adsorbed protein. Some of protein components in the sample might displace the pre-adsorbed proteins or bind to form a multi-layer structure, both of which increase SPR angle. The final angle shift subtracted from the baseline was monitored. Each mixture sample was tested six times on a protein pre-adsorbed surface, generating distinctive response patterns. SPR was calibrated each time to maintain the sensitivity, 60 mDeg at 1 % ethanol solution.

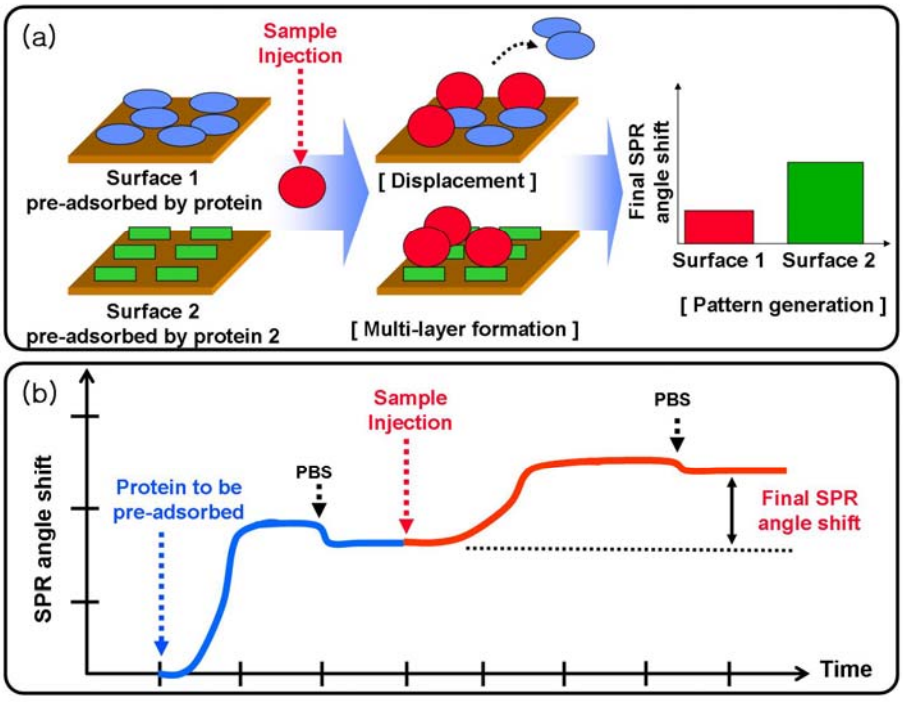

Figure 5.2 Schematic of (a) the biosensor based on protein adsorption behaviors and (b) the SPR sensorgram with step-by-step protein behaviors on a sensing surface.

5.2.5 Linear discriminant analysis (LDA)

LDA was used to quantitatively differentiate the SPR angle patterns on the sensing surfaces with pre-adsorbed proteins. LDA is a statistical method that maximizes the ratio of between-class variance to within-class variance thereby guaranteeing maximal separability (Jurs et al., 2000). Specifically, with K classes, LDA seeks K-1 canonical factors that maximally separate the K classes. The canonical factors are linear combinations of the features in the dataset. In this case, each "class" is a protein mixture sample and each "feature" is a protein pre-adsorbed on a surface. The classification accuracy of LDA is computed using the jackknife method, in which one case (i.e., one repetition in a sample) at a time is

omitted from the LDA and treated as an unknown. This unknown case is then classified based on the LDA model generated from the remaining cases in the dataset. This "leave-one-out" scheme is then repeated for every case. The classification accuracy with respect to each sample is the proportion of cases in this sample that are correctly identified. The jackknife method has the merit of avoiding overestimating the classification accuracy, as classification of each case is independent of the LDA model generation. Furthermore, LDA can compute the posteriors probability of a case in its own class, which represents the confidence for classifying each case as its true identity. A higher the confidence (i.e., closer to 1) results in a higher the classification accuracy, which is computed based on the specific experimental dataset and can be generalized for future cases. The following section reports both the jackknife classification accuracy and confidence

5.3 Results and discussion

5.3.1 Cross-reactivity

This sensing strategy relies on the protein adsorption behavior including protein displacement (Choi et al., 2008) and multi-layer formation (Choi and Chae 2010b) through electrostatic force. Proteins in a sample mixture interact with pre-adsorbed proteins to different extents depending on the size of protein, the type of amino acids composing the protein, isoelectric point (*p*I) of the proteins, characteristics of the sensing surface, and *p*H of the surrounding solution (Latour 2005; Choi and Chae 2009a). The composite interactions of a sample mixture results in a set of SPR angle shifts on individual surfaces. The uniqueness of this

approach is that it does not matter which proteins in a sample interacts with pre-adsorbed proteins or how many proteins are involved in the event. These properties are irrelevant because the composite response of any given sample will be distinct. The protein adsorption behavior is led by thermodynamics: proteins with different characteristics adsorb differently to a surface based upon their thermodynamic energy preferences, and behave in ways that minimize the overall system energy (Latour 2005; Choi and Chae 2009a). Therefore, when proteins in a sample reach a surface that is packed with pre-adsorbed proteins, the equilibrium of their total energy is achieved through protein displacement or multi-layer formation with the pre-adsorbed proteins on the surface. While hydrophobic attraction dominates those protein adsorption behaviors, one can control electrostatic forces among those proteins to obtain distinctive response patterns. Lysozyme (pI = 9.2) is positively charged at physiological conditions (pH = 7.4) while albumin (pI = 5.2), transferrin (pI = 5.6), and IgG (pI = 7.6) are negatively charged. Two surfaces were compared: bare-gold and COOH-SAM surfaces, which obviously show different distinctive response patterns to a given set of proteins, governed by hydrophobic and electrostatic attractions among proteins.

5.3.2 Characteristics of sensing surfaces

Four proteins were chosen to be pre-adsorbed on a sensing surface and used two (bare-gold and COOH-SAM modified) sensing surfaces in order to obtain provide differential responsive bio-receptors. The hypothesis is that proteins pre-adsorbed surfaces have distinctive binding characteristics to a mixture of proteins and the

binding characteristics can be monitored by SPR in real time to generate distinctive patterns. Table 5.3 shows a matrix of surfaces prepared to convey the experiments, having different equilibrium dissociation constant, K_D, and Gibbs free energy change, ΔG, between four pre-adsorbed proteins and the two surfaces.

Table 5.3 Properties of eight surfaces. Equilibrium dissociation constants (K_D) and Gibbs free energy changes ($\triangle G$) between four proteins and two surfaces as determined by SPR angle shifts.

	K_D	ΔG
Surface 1 Lysozyme on a bare-gold	**(7.2 ± 2.5) x 10^{-5} M**	**(-5.6 ± 0.2) Kcal/mol**
Surface 2 Albumin on a bare-gold	**(6.3 ± 2.2) x 10^{-5} M**	**(-5.7 ± 0.2) Kcal/mol**
Surface 3 Transferrin on a bare-gold	**(6.0 ± 1.7) x 10^{-5} M**	**(-5.8 ± 0.2) Kcal/mol**
Surface 4 IgG on a bare-gold	**(3.3 ± 0.7) x 10^{-5} M**	**(-6.1 ± 0.1) Kcal/mol**
Surface 5 Lysozyme on a COOH-SAM	**(1.6 ± 0.8) x 10^{-4} M**	**(-5.2 ± 0.3) Kcal/mol**
Surface 6 Albumin on a COOH-SAM	**(1.0 ± 0.4) x 10^{-4} M**	**(-5.4 ± 0.2) Kcal/mol**
Surface 7 Transferrin on a COOH-SAM	**(1.2 ± 0.3) x 10^{-4} M**	**(-5.3 ± 0.1) Kcal/mol**
Surface 8 IgG on a COOH-SAM	**(1.4 ± 0.5) x 10^{-4} M**	**(-5.2 ± 0.2) Kcal/mol**

As mentioned in section 5.2.4, since protein adsorption behaviors are governed by thermodynamic energy preferences, their reactions can be interpreted as a natural outcome of surface reorganization to achieve the equilibrium interphase composition. Therefore, the change in the free energy of the protein adsorption

process on a certain surface reflects the protein reactions, which can be expressed as

$$\Delta G = \Delta G° + RT \ln(\frac{[AB]}{[A][B]}) = -RT \ln K_A = RT \ln K_D, \quad (5.1)$$

where ΔG and $\Delta G°$ represent the changes in adsorption free energy and in standard-state adsorption free energy, respectively; R is the ideal gas constant [1.985 cal/K·mol]; T is the absolute temperature [298K]. *[A]* is the molar concentration of the protein in solution and *[B]* and *[AB]* are the mole fraction of surface sites occupied by a surface and adsorbed protein, respectively (Schubert et al. 2003; Schasfoort and Tudos 2008). Figure 5.3 shows the equilibrium association constant K_A and dissociation constant K_D can be acquired from SPR angle values by fitting the data using Langmuir equation (Forzani et al., 2005) given by

$$\Delta\theta = \frac{\Delta\theta_{\max} C}{K_D + C}, \quad (5.2)$$

where $\Delta\theta$ is the SPR angle shift; $\Delta\theta_{max}$ is the SPR angle shift at the saturation; C is the protein concentration (Forzani et al., 2007). Proteins on the hydrophobic bare-gold surface (Surface 1~4) have adsorption strengths proportional to their own molecular weight because proteins are mainly governed by hydrophobic attractions on the gold surface and their hydrophobicities are typically depending on their sizes (Choi et al., 2008).

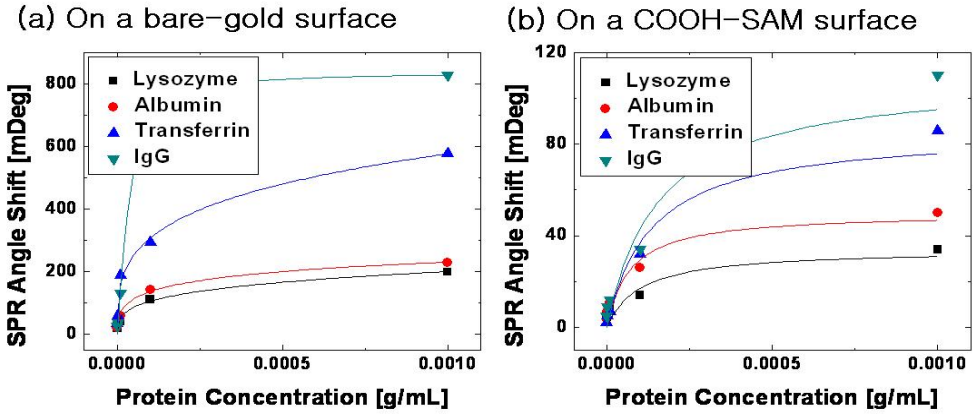

Figure 5.3 SPR angle shifts as a function of protein concentration either (a) on a bare-gold or (b) on a COOH-SAM modified surface.

On the bare-gold surfaces, the smallest protein, lysozyme (15 kDa), has the lowest adsorption strength while the largest protein, IgG (150 kDa), shows the highest adsorption strength. On the contrary, COOH-modified surface provides different adsorption results because of the additional electrostatic force and hydrophilic hindrance (More et al. 2003). Migration of positively charged lysozyme (15 kDa, *p*I = 9.2) and IgG (150 kDa, *p*I = 7.6) in PBS (*p*H, 7.4) to the negatively-charged COOH-SAM surface hampers their consecutive unfolding and spreading process which make their adsorption much weaker on the surface. That is probably why albumin and transferrin have stronger adsorption on the COOH-modified surface than IgG even though IgG has higher molecular weight than albumin and transferrin. More studies need to be performed to investigate their behaviors in detail. However, eight different surfaces each with different adsorption strengths will suffice in characterizing the protein biosensor and giving

us distinctive response patterns for a mixture of multiple proteins as shown in the following sections.

5.3.3 Identification of protein samples

Four human serum proteins were selected to prepare a matrix of five cocktailed samples to characterize the protein biosensor. The detailed sample specifications are in Table 5.1. The sample proteins (S1~S5) were injected on to the eight surfaces (Surface 1~8), respectively, to interact with the pre-adsorbed proteins and SPR was used to monitor the reaction in real time to generate angle shift. SPR responses were collected six times for each sample from the eight different surfaces (Table 5.4). Figure 5.4 (a) shows SPR angle patterns of the five samples. As interactions of the sample proteins increase through displacement or multi-layer formation, SPR angle responses increase. Moreover, the small difference of a protein's concentration in a sample induces a large impact on the composite signal of the pattern. By comparing the pattern of the standard (S1) to those of other samples (S2-S5), the sample proteins were discriminated. The power of the "pattern-generation" approach is obvious here as it is unlikely that a single bio-receptor ("lock-and-key") could have adequately discriminated the five samples.

LDA was used to differentiate quantitatively the composite patterns. After the analysis, four canonical factors were generated (94.0 %, 4.0 %, 1.6 %, and 0.4 %) that represent linear combinations of the response matrices obtained from the pattern (five samples x eight surfaces x six replicates).

Table 5.4 Training matrix of SPR response signals of five samples in Table 5.1

	SPR angle shift [mDeg]							
	Surface 1	**Surface 2**	**Surface 3**	**Surface 4**	**Surface 5**	**Surface 6**	**Surface 7**	**Surface 8**
Sample 1	53	34	11	10	17	7	4	11
	54	33	12	9	9	3	6	6
	51	30	10	9	10	6	4	7
	50	29	11	8	15	4	6	9
	49	34	16	7	14	5	8	10
	47	35	11	9	13	6	10	11
Sample 2	60	39	4	9	12	9	7	11
	66	40	6	20	7	8	6	14
	70	42	5	15	16	8	7	13
	75	46	6	16	14	7	9	16
	59	30	9	18	15	6	10	15
	58	40	10	19	12	8	9	14
Sample 3	151	50	16	12	31	14	16	22
	144	66	20	8	30	17	18	21
	148	60	18	15	28	15	20	20
	159	60	16	12	24	16	18	19
	160	62	14	10	26	17	14	25
	162	64	15	6	27	15	15	24
Sample 4	68	29	8	7	10	5	5	11
	60	29	6	16	8	8	4	13
	62	31	4	8	9	6	5	15
	65	30	5	10	10	7	6	14
	67	26	6	16	12	4	7	13
	70	25	8	15	13	5	5	14
Sample 5	52	19	5	7	12	2	3	5
	49	22	9	4	4	5	5	6
	50	15	8	8	10	6	6	5
	48	16	6	7	5	4	4	4
	47	18	7	5	6	3	3	3
	50	19	5	6	8	5	2	2

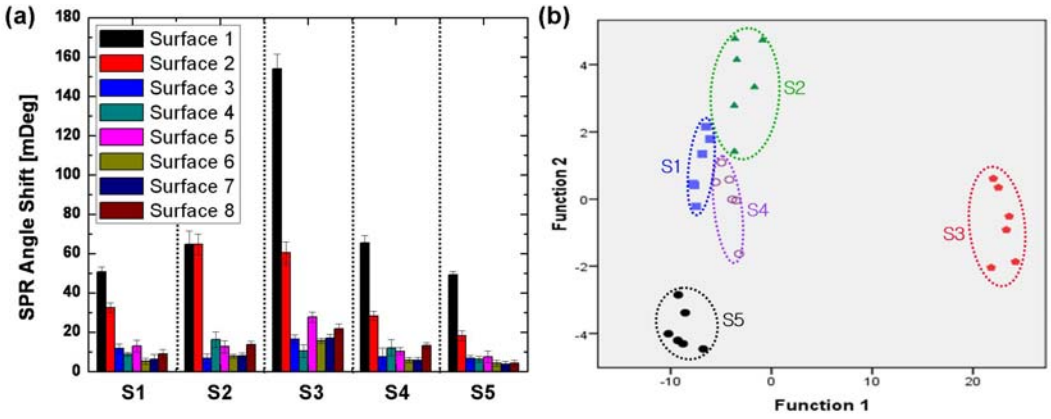

Figure 5.4 (a) SPR response patterns of interaction between the five samples and eight surfaces with pre-adsorbed proteins. (b) Canonical score plot for the patterns as obtained from LDA with 95 % confidence ellipses.

Table 5.5 LDA classification accuracy of five samples by using a single surface and eight surfaces. The values are taken from the Jackknifed classification matrix based on LDA analysis

	Surface1	Surface2	Surface3	Surface4	Surface5	Surface6	Surface7	Surface8	Surface1-8
Sample 1	50%	66.7%	83.3%	66.7%	33.3%	16.7%	33.3%	50%	83.3%
Sample 2	0%	83.3%	0%	83.3%	33.3%	83.3%	50%	66.7%	66.7%
Sample 3	100%	83.3%	83.3%	16.7%	100%	100%	100%	100%	100%
Sample 4	33%	83.3%	66.7%	0%	33.3%	16.7%	50%	33.3%	100%
Sample 5	50%	100%	0%	83.3%	66.7%	50%	66.7%	100%	100%
Average	46.7%	83.3%	46.7%	50%	53.3%	53.3%	60%	70%	90%

The two factors that were most significant were plotted in 2D (Figure 5.4(b)). The 30 training cases (five samples x six replicates) were separated into five respective groups, with 90 % average classification accuracy over the five samples using the jackknife method (please see the last column of Table 5.5). Notably, the classification accuracy for sample 4 (i.e., the target protein, CRP) is 100 %. For a single surface, however, the average classification accuracies range only from 46.7 % to 83.3 % (please see other columns of Table 5.5), indicating

that a set of different sensing surfaces is essential for protein discrimination. In addition, the confidence of classifying each case as its true identity is shown in Table 5.6.

Table 5.6 Detection and identification of five unknown samples by applying LDA to the data of both bare gold and SAM modified surfaces (*confidence of the classification: the probability that an observation is classified as the "true sample".)

	Observation #	True sample	Classified sample	Confidence of the classification*
Sample 1	Observation 1	S1	S1	1
	Observation 2	S1	S1	1
	Observation 3	S1	S1	1
	Observation 4	S1	S1	1
	Observation 5	S1	S1	1
	Observation 6	S1	**S2**	**0.1869**
Sample 2	Observation 7	S2	**S4**	**0.1849**
	Observation 8	S2	S2	1
	Observation 9	S2	S2	1
	Observation 10	S2	S2	1
	Observation 11	S2	**S4**	**< 0.01**
	Observation 12	S2	S2	1
Sample 3	Observation 13	S3	S3	1
	Observation 14	S3	S3	1
	Observation 15	S3	S3	1
	Observation 16	S3	S3	1
	Observation 17	S3	S3	1
	Observation 18	S3	S3	1
Sample 4	Observation 19	S4	S4	1
	Observation 20	S4	S4	1
	Observation 21	S4	S4	1
	Observation 22	S4	S4	1
	Observation 23	S4	S4	1
	Observation 24	S4	S4	1
Sample 5	Observation 25	S5	S5	1
	Observation 26	S5	S5	1
	Observation 27	S5	S5	1
	Observation 28	S5	S5	1
	Observation 29	S5	S5	1
	Observation 30	S5	S5	1

The confidence is 1 for all cases that are correctly classified. Furthermore, LDA was applied to the partial data that correspond to the four proteins pre-adsorbed on only one surface, e.g., the COOH-SAM modified surface. The resulting classification and confidence values are summarized in table 5.7.

Table 5.7 Detection and identification of five unknown samples by applying LDA to the data of SAM modified surfaces (*confidence of the classification: the probability that an observation is classified as the "true sample".)

	Observation #	True sample	Classified sample	Confidence of the classification*
Sample 1	Observation 1	S1	S1	0.5055
	Observation 2	S1	**S5**	**< 0.01**
	Observation 3	S1	**S5**	**0.1227**
	Observation 4	S1	S1	0.9849
	Observation 5	S1	S1	0.9408
	Observation 6	S1	**S2**	**< 0.01**
Sample 2	Observation 7	S2	S2	0.6996
	Observation 8	S2	**S4**	**0.0432**
	Observation 9	S2	S2	0.8643
	Observation 10	S2	S2	0.9239
	Observation 11	S2	S2	0.9043
	Observation 12	S2	S2	0.9757
Sample 3	Observation 13	S3	S3	1
	Observation 14	S3	S3	1
	Observation 15	S3	S3	1
	Observation 16	S3	S3	1
	Observation 17	S3	S3	1
	Observation 18	S3	S3	1
Sample 4	Observation 19	S4	S4	0.5820
	Observation 20	S4	S4	0.7148
	Observation 21	S4	S4	0.9607
	Observation 22	S4	S4	0.6393
	Observation 23	S4	S4	0.7999
	Observation 24	S4	S4	0.9192
Sample 5	Observation 25	S5	S5	0.8759
	Observation 26	S5	S5	0.8713
	Observation 27	S5	**S1**	**0.0382**
	Observation 28	S5	S5	1
	Observation 29	S5	S5	1
	Observation 30	S5	S5	1

It can be seen that the classification accuracy varies only slightly regardless of whether data were used from the bare-gold or COOH-SAM modified surfaces. However, if only using the data from the bare gold surface, the classification accuracy decreases significantly, indicating that the COOH-SAM modified surface improves the classification. Therefore, if only one surface is to be used in order to save experimental resources and efforts, the COOH-SAM modified surface should be adopted.

5.3.4 Detection of CRP

After selective detection of five samples (S1~S5), the next challenge was to detect a protein at various concentration levels. One of the limitations of "lock-and-key" sensors, as well as other approaches, is to differentiate between various concentration levels of a single protein. To characterize the sensitivity of the sensor, four samples were prepared with different concentrations of CRP (1 nM, 5 nM, 20 nM, and 50 nM) as shown in Table 5.2. Only four bare-gold surfaces (Surface 1~4) were employed for this procedure. Figure 5.5 (a) shows SPR angle patterns obtained from the individual SPR angle values of four samples (S6~S9) (Table 5.8). LDA plots for various concentrations of CRP were not random, but rather followed certain patterns and thus can be differentiated from each other. Noticeably, the responses from four samples form clusters around a common center with 95 % accuracy (Figure 5.5 (b)). This result demonstrates that the biosensor can detect CRP at a concentration of as low as 1 nM, providing adequate resolution.

Table 5.8 Training matrix of SPR response signals of four samples in Table 5.2

	SPR angle shift [mDeg]			
	Surface 1	Surface 2	Surface 3	Surface 4
Sample 6	53	34	11	10
	54	33	12	9
	51	30	10	9
	50	29	11	8
	49	34	16	7
	47	35	11	9
Sample 7	68	29	16	7
	60	29	6	16
	62	31	4	8
	65	30	5	10
	67	26	6	16
	70	25	8	15
Sample 8	46	15	4	8
	53	15	5	4
	45	14	4	5
	39	16	3	7
	42	14	6	5
	40	17	2	6
Sample 9	49	20	6	8
	47	18	10	5
	43	16	10	8
	52	19	6	6
	53	18	8	8
	51	21	6	6

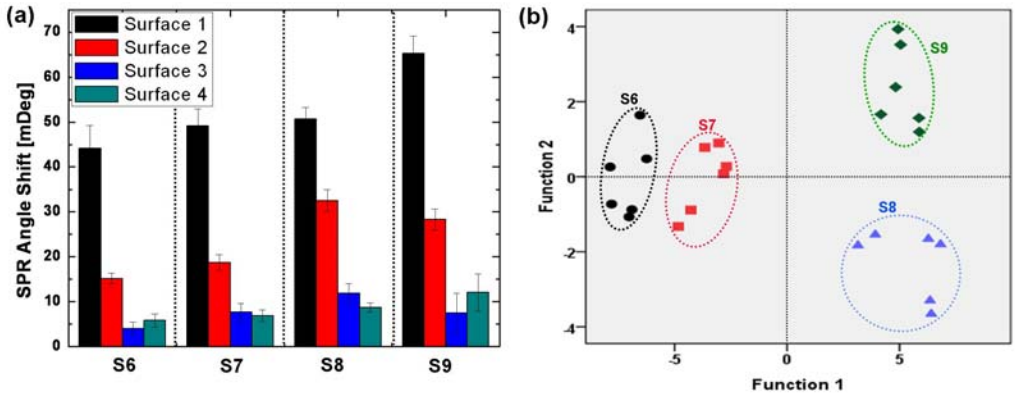

Figure 5.5 (a) SPR response patterns of interaction between the four samples and four surfaces with pre-adsorbed proteins. (b) Canonical score plot for the patterns as obtained from LDA with 95 % confidence ellipses.

Table 5.9 LDA classification accuracy of four samples by increasing the number of surfaces. The values are taken from the Jackknifed classification matrix based on LDA analysis

	Sample 6	Sample 7	Sample 8	Sample 9	Average
Surface 1	66.7%	100%	83.3%	33.3%	**70.8%**
Surface 2	66.7%	83.3%	83.3%	83.3%	**79.2%**
Surface 3	100%	0%	83.3%	16.7%	**50%**
Surface 4	83.3%	50%	66.7%	0%	**50%**
Surface 1 & 2	100%	83.3%	83.3%	83.3%	**87.5%**
Surface 1 & 3	100%	83.3%	83.3%	66.7%	**83.3%**
Surface 1 & 4	66.7%	100%	66.7%	33.3%	**66.7%**
Surface 2 & 3	66.7%	83.3%	100%	100%	**87.5%**
Surface 2 & 4	66.7%	66.7%	83.3%	83.3%	**75.0%**
Surface 3 & 4	100%	50%	100%	50%	**75%**
Surface 1, 2 & 3	100%	83.3%	83.3%	83.3%	**87.5%**
Surface 1, 2 & 4	100%	100%	83.3%	83.3%	**91.7%**
Surface 1, 3 & 4	100%	66.7%	83.3%	83.3%	**83.3%**
Surface 2, 3 & 4	66.7%	83.3%	100%	100%	**87.5%**
Surface 1~4	100%	83.3%	100%	83.3%	**91.7%**

Sensitivity of the “lock-and-key” approach greatly depends on the performance of associated transducers. That is, the transducers are responsible for decreasing noise and amplifying the signal. However, there are often a number of limitations of developing the transducers to detect target biomarkers which are normally at the very low concentrations of down to atto molar levels. On the other hand, the “pattern generation” technique enables sensors to enhance their sensitivity by increasing the number of bio-receptors without solely relying on enhancements of the transducer. As shown in Table 5.9, the jackknife classification accuracies increase up to 91.7 % from 50 % by increasing the number of surfaces. Moreover,

even though only three surfaces are employed, Surface 1, 2, & 4 combination generates 91.7 % accuracy; two surfaces, i.e., Surface 1 & 2 combination or Surface 2 & 3 combination generates 87.5 % accuracy. These results also show that the selection of surfaces is critical for the effective biosensor. In addition, the confidence of classifying each case as its true identity is shown in table 5.10. The confidence is close to 1 for all cases that are correctly classified.

Table 5.10 Detection and identification of four unknown samples using LDA

	Observation #	True sample	Classified sample	Confidence of the classification*
Sample 6	Observation 1	S6	S6	1
	Observation 2	S6	S6	1
	Observation 3	S6	S6	1
	Observation 4	S6	S6	1
	Observation 5	S6	S6	1
	Observation 6	S6	S6	1
Sample 7	Observation 7	S7	**S6**	**< 0.01**
	Observation 8	S7	S7	1
	Observation 9	S7	S7	1
	Observation 10	S7	S7	1
	Observation 11	S7	S7	1
	Observation 12	S7	S7	1
Sample 8	Observation 13	S8	S8	1
	Observation 14	S8	**S9**	0.7817
	Observation 15	S8	S8	1
	Observation 16	S8	S8	1
	Observation 17	S8	S8	1
	Observation 18	S8	S8	1
Sample 9	Observation 19	S9	S9	1
	Observation 20	S9	S9	1
	Observation 21	S9	**S8**	**0.2187**
	Observation 22	S9	S9	1
	Observation 23	S9	S9	1
	Observation 24	S9	S9	1

5.4 Conclusion

This work reports “pattern generation”-based protein identification method utilizing protein adsorption behavior for a highly selective and sensitive sensor system. It demonstrated the identification of five sample proteins using only eight surfaces and differentiated between four concentration levels of CRP using four surfaces. The surfaces were tailored either by physically placing proteins or by modifying the sensing surface with SAM. The “pattern generation” method allows the analysis of complex analytes and mixtures. Here, cocktail samples in buffer were used, but current studies are underway to explore the use of this approach to profile serum samples for the diagnosis of disease states.

6 SUMMARY AND SIGNIFICANCE

The first project described in this dissertation resulted in a reusable/reconfigurable microfluidic biosensor via in-situ electrochemical surface regeneration that was effective even in a physiologically relevant medium. Viable reusable biosensors for enclosed microfluidics are challenging because regeneration methods must ensure precision and sensitivity after recycle. Electrochemical desorption method is a very attractive option for regenerating biosensors in microfluidic environments because it can be controlled by applying a small voltage, and individual electrodes can be flexibly implemented within array formats. However, there are three severe problems to be solved; re-adsorption of the detached molecules, electrode peeling-off and electrolysis occurring at a similar potential to the potential of the SAM desorption. The potential for the reductive desorption of thiol SAMs depends on the length of the alkyl chin, the type of terminal groups and the binding of proteins and that this approach using short chain SAMs ($n<3$) can be a good candidate to minimize these limitations. Results confirmed short-chain SAM formation in enclosed microfluidic devices, and desorption promoted "clean" surface recycling for up to 50 cycles. Sensor reusability was evaluated in situ and in real time by Surface Plasmon Resonance (SPR), with a Relative Standard Deviation (RSD) of less than 1.86 %, suggesting reusable microfluidics biosensors are finally within reach.

In tandem, this research also explored one of the persistent challenges in conventional biosensors: *Non-specific adsorption (NSA) of biomolecules.* Microfluidic biosensors often have immobilized bioreceptors such as antibodies,

enzymes, DNA, etc., via linker molecules such as self-assembled monolayers (SAMs) to enhance immobilization. However, the linker molecules are very susceptible to NSA, causing false responses and decreasing sensitivity. This dissertation discussed design methods that reduce the NSA of alkanethiol SAMs, which are popular linker molecules on microfluidic biosensors. Three design parameters were studied for two different chain-length SAMs (n=2 and 10): i) SAM incubation time, ii) surface roughness [0.8 nm and 4.4 nm RMS (root mean square)], and iii) gold crystal re-growth along (111) the target orientation. NSA was monitored by surface plasmon resonance (SPR). Results suggest that increased SAM incubation time reduces NSA, and that short-chain SAMs respond more favorably than the long-chain SAMs. Both SAMs were shown to be sensitive to surface roughness, and long-chain SAMs reduced NSA by 75%. Gold crystal re-growth along (111) the target orientation profoundly reduced NSA on the short-chain SAM. On a gold surface where surface roughness was 0.8 nm and there was strong directional alignment along the (111) gold crystal, final concentrations of nonspecifically bound proteins were 0.05 ng/mm^2 (fibrinogen) and 0.075 ng/mm^2 (lysozyme)—significantly lower than other known methods. Results show that optimizing three parameters (SAM incubation time, gold surface roughness, and gold crystal orientation) improved SAM sensitivity for fibrinogen–anti-fibrinogen conjugates by a factor of five in 2.94 pM, suggesting the methods are effective for reducing NSA in microfluidic biosensors.

SPR (Surface plasmon resonance) affinity-based biosensors are a promising technique for biomarker detections, and in recent years, a large number of

previously referenced SPR studies have shown that these sensors enable direct and label-free specific detection of various analytes below the nano-molar level with real-time monitoring of various biomolecular interactions. The assays, however, are quite complex; they require multi-component, multi-step configurations that are time-consuming and labor intensive, and this is often the bottleneck for high yield sensors. Further, SPR-based, label-free biosensors are prone to high background noise from non-specific binding in the complex mixtures (e.g. serum contains 40-80 mg/ml protein). Until now, the key to allowing surface sensors to be used in complex media has been reducing the non-specific binding of proteins to the surface. Protein adsorption to surfaces, however, is practically unavoidable, since every surface is hydrophobic, ionic, or polar, and proteins have hydrophobic, ionic, and polar domains. To date, few alternative platforms for protein detection have been active in biosensor communities. This dissertation described a fundamentally different protein detection method that relies on the competitive nature of protein adsorption onto a surface. The method can be a complementary solution to the existing affinity-based biosensor. A new conceptual biosensor has been developed using protein adsorption on a surface instead of immobilized molecular probes to detect these biomarkers in human serum. The dissertation described work to demonstrate that a specific human serum protein, thyroglobulin (Tg), in a protein mixture of albumin, haptoglobin and Tg, can be selectively detected based on the adsorption/exchange reaction. Also, by using this technique, fibrinogen was monitored even in undiluted human serum. Two different concentrations of fibrinogen spiked in human serum (3.0

mg/ml (normal concentration) vs. 3.2 mg/ml (abnormal concentration with heart disease)) were successfully differentiated by monitoring real-time SPR signals as fibrinogen displaced a pre-adsorbed protein, IgM. The technique provides a selective detection of fibrinogen; the relatively strong-affinity protein, IgM, was dominantly displaced by fibrinogen, and significantly less by other proteins in human serum.

Finally the dissertation described work to expand this idea (protein displacement) into a unique protein identification technique based on distinctive patterns generated by protein adsorption behavior. Conventional approaches to biosensors make use of a "Lock-and-Key" design, wherein a specific bio-receptor is immobilized on the sensing surface. In theory, this process strongly and highly selectively binds target analytes within the sensor. In practice, however, most biosensors suffer from interference caused by molecules that are structurally or chemically similar to the desired analyte. Therefore, the best tool for disease diagnosis is rapid and efficient identification of total protein imbalances in serum.

Bare gold and COOH-modified self-assembled monolayer (SAM) sensing surfaces were pre-adsorbed with one of four different proteins: lysozyme, albumin, transferrin, or IgG. Each surface provides a thermodynamically governed platform for immobilizing proteins and generates analyte-specific response patterns. Each surface has hydrophobic and electrostatic forces governing pre-adsorbed protein behaviors, so that sample proteins are either displaced, or they form multi-layer protein structures. Modified surfaces were mounted and monitored in real time with surface plasmon resonance (SPR). Buffer-prepared

sample matrices (α1-antitrypsin, haptoglobin, C-reactive protein (CRP), and IgM) characterized protein response patterns. Each surface generated different patterns based on individual SPR angle shifts. Each sample was classified with 95% accuracy using linear discriminant analysis (LDA). Also, C-reactive protein (CRP), an inflammatory marker associated with higher risk of cardiovascular disease, was identified with 90% accuracy. The method also discriminated between different concentrations of CRP in the cocktail sample, detecting concentrations as low as 1 nM with 91.7% accuracy.

Despite the high volume of academic research to date, only a handful of biosensors have become viable in commercial applications. The main reason is that, traditionally, research has been done by individuals and research groups, and this fragmented approach supports an unbalanced view of biosensors—one that lends itself more to science fiction than immediate solutions. At this point, academic research achievements must focus on practical uses for biosensors. Broadly, my research interests centered on integrating a unique set of skills to bridge the academia-industry gap. This work specifically explored innovative technologey for detecting cancer biomarkes and developed a new conceptual biosenosr that uses protein adsorption behaviors on a surface instead of immobilized biomolecular recognition elements. Developing a pattern recognition strategy for detecting biomolecules will revolutionize the field and open up market opportunities for biosensor technology since it can provide rapid efficient identification of total protein imbalances in complex media.

REFERENCES

Aizawa, H., Kurosawa, S., Ogawa, K., Yoshimoto, M., Miyake, J., Tanaka, H, 2001, Conventional diagnosis of C-reactive protein in serum using latex piezoelectric immunoassay, Sensors and Actuators B. 76, 173-176.

Albert, K.J., Lewis, N.S., Schauer, C.L., Sotzing, G.A., Stitzel, S.E., Vaid, T.P., Walt, D.R., 2000, Cross-Reactive Chemical Sensor Arrays, Chem. Rev. 100, 2595-2626.

Anderson, M.R., Baltzersen, R., 2003, Reductive desorption of 11-mercaptoundecanoic acid monolayers modified by covalent attachment of 1,3- and 1,4-phenylenediamine, Journal of Colloid and Interface Science, 263, 516-521.

Anandan, V., Gangadharan, R., Zhang, G., 2009, Role of SAM Chain Length in Enhancing the Sensitivity of Nanopillar Modified Electrodes for Glucose Detection, Sensors, 9, 1295-1305.

Asanov, A.N., Wilson, W.W., Oldham, P.B., 1998, Regenerable biosensor platform: a total internal reflection fluorescence cell with electrochemical control, Anal. Chem. 70, 1156-1163.

Bain, C.D., Troughton, E.B., Tao, Y.T., Evall, J., Whitesides, G.M., Nuzzo, R.G., 1989 Formation of monolayer films by the spontaneous assembly of organic thiols from solution onto gold, J. Am. Chem. Soc. 111, 321-335.

Balasubramanian, S., Revzin, A., Simnian, A., 2006, Electrochemical desorption of proteins from gold electrode surface, Electroanalysis, 18, 1885-1892.

Billah, M., Hays, H.C.W., Millner, P.A., 2008, Development of a myoglobin impedimetric immunosensor based on mixed self-assembled monolayer onto gold, Microchimica Acta, 160, 447-454.

Bloth, B., Bergquist, R., 1968, The Ultrastructure of human thyroglobulin, J. Exp. Med. 128, 1129-1136.

Bolduc, O.R., Masson, J., 2008, Monolayers of 3-Mercaptopropyl-amino Acid to Reduce the Nonspecific Adsorption of Serum Proteins on the Surface of Biosensors, Langmuir, 24, 12085-12091.

Bryant, M.A., Pemberton, J.E., 1991, Surface Raman scattering of self-assembled monolayers formed from 1-alkanethiols at silver, J. Am. Chem. Soc. 113, 3629-3637.

Buck, M., Eisert, F., Fischer, J., Grunze, M., Traeger, F., 1991, Investigation of self-organizing thiol films by optical second harmonic generation and X-ray photoelectron spectroscopy, Appl. Phys. A. 53, 552-556.

Canaria, C.A., So, J., Maloney, J.R., Yu, C.J., Smith, J.O., Roukes, M.L., Fraser, S.E., Landsford, R., 2006, Formation and removal of alkylthiolate self-assembled monolayers on gold in aqueous solutions, Lab on a Chip, 6, 289-295.

Chaki, N.K., Vijayamohanan, K., 2002, Self-assembled monolayers as a tunable platform for biosensor applications, Biosensors and Bioelectronics, 17, 1-12.

Chapman, R.G., Ostuni, E., Takayama, S., Holmlin, R.E., Yan, L., Whitesides, G.M., 2000, Surveying for Surfaces that Resist the Adsorption of Proteins, J. Am. Chem. Soc. 122, 8303-8304.

Chen, C.H., Hwang, R.Z., Huang, L.S., Lin, S., Chen, H.C., Yang, Y.C., Lin, Y.T., Yu, S.A., Wang, Y.H., Chou, N.K., Lu, S.S., 2006, A Wireless Bio-MEMS Sensor for C-Reactive Protein Detection Based on Nanomechanics, IEEE International Solid-State Circuits Conference, 2298-2307.

Choi, S., Chae, J., 2009a, A microfluidic biosensor based on competitive protein adsorption for thyroglobulin detection, Biosensors and Bioelectronics, 25, 118-123.

Choi, S., Chae, J., 2009b, A Regenerative Biosensing Surface in Microfluidics using Electrochemical Desorption of Short-Chain Self-Assembled Monolayer, Microfluidics and Nanofluidics, 7, 819-827.

Choi, S., Chae, J., 2010a, A Physisorbed Interface Design of Biomolecules for Selective and Sensitive Protein Detection, Journal of the Association for Laboratory Automation, 15, 172-178.

Choi, S., Chae, J., 2010b, Methods of reducing non-specific adsorption in microfluidic biosensors, Journal of Micromechanics and Microengineering, 20, 075015.

Choi, S., Goryll, M., Sin, L.Y.M., Wong, P.K. Chae, J., 2011, Microfluidic-based biosensors toward point-of-care detection, Microfluidics and Nanofluidics, 10, 232-247.

Choi, S., Wang, R., Lajevardi-Khosh, A., Chae, J., 2010, Using competitive protein adsorption to measure fibrinogen in undiluted human serum, Applied Physics Letters, 97, 253701.

Choi, S., Yang, Y., Chae, J., 2008, Surface plasmon resonance protein sensor using Vroman effect, Biosensors and Bioelectronics, 24, 893-899.

Chambers, J.P., Arulanandam, B.P., Matta, L.L., Weis, A., Valdes, J.J., 2008, Biosensor recognition elements, Curr. Issues Mol. Biol. 10, 1-12.

Damos, F.S., Luz, R.C.S., Kubota, L.T., 2005, Determination of Thickness, Dielectric Constant of Thiol Films, and Kinetics of Adsorption Using Surface Plasmon Resonance, Langmuir, 21, 602-609.

De, M. Rana, S., Akpinar, H., Miranda, O.R., Arvizo, R.R., Bunz, U.H.F., Rotello, V.M., 2009, Sensing of proteins in human serum using conjugates of nanoparticles and green fluorescent protein, Nature Chemistry, 1, 461-465.

de Feijter, J.A., Benjamins, J., Veer, F.A., 1978, Ellipsometry as a tool to study the adsorption behavior of synthetic and biopolymers at the air-water interface. Biopolymers, 17, 1759-1772.

Deshpande, V., Venkatesh, S.G., 1999, ochimica et Biophysica Acta (BBA)/Protein Structure and Molecular Enzymology, Biochimica et Biophysica Acta, 1430, 157-178.

Desikan, R., Armel, S., Meyer, III H.M., Thundat, T., 2007, Effect of chain length on nanomechanics of alkanethiol self-assembly, Nanotechnology, 18, 424028.

Deval, J., Umali, T.A., Lan, E.H., Bunn, B., Ho, C., 2004, Reconfigurable hydrophobic/hydrophilic surfaces in microelectromechanical systems (MEMS), Journal of Micromechanics and Microengineering, 14, 91-95.

Forzani, E.S., Foley, K., Westerhoff, P., Tao, N., 2007, Detection of arsenic in groundwater using a surface plasmon resonance sensor, Sensors and Actuators B. 123, 82-88.

Forzani, E.S., Zhang, H., Chen, W., Tao, N., 2005, Detection of Heavy Metal Ions in Drinking water using a high-resolution differential surface plasmon resonance sensor, Environ. Sci. Technol. 39, 1257-1262.

Frasoldati, A., Pesenti, M., Gallo, M., Caroggio, A., Salvo, D., Valcavi, R., 2002, Diagnosis of neck recurrences in patients with differentiated thyoid carcinoma, Cancer, 97, 90-96.

Frederix, F., Bonroy, K., Laureyn, W., Reekmans, G., Campitelli, A., Dehaen, W., Maes, G., 2003, Enhanced performance of an affinity biosensor interface based on mixed self-assembled monolayers of thiols on gold, Langmuir, 19, 4351-4357.

Frederix, F., Bonroy, K., Reekmans, G., Laureyn, W., Campitelli, A., Abramov, M.A., Dehaen, W., Maes, G.J., 2004, Reduced nonspecific adsorption on covalently immobilized protein surfaces using poly(ethylene oxide) containing blocking agents, Biochem. Biophys. Methods, 58, 67-74.

Furuya, M., Haramura, M., Tanaka, A., 2006, Reduction of nonspecific binding proteins to self-assembled monolayer on gold surface, Bioorganic & Medicinal Chemistry, 14, 537-543.

Gau, J., Lan, E.H., Dunn, B., Ho, C., Woo, J.C.S., 2001, MEMS Based Amperometric Detector for E.Coli Bacteria Using Self-Assembled Monolayers, Biosensors and Bioelectronics, 16, 745-755.

Gervais, L., Delmarche, E., 2009, Toward one-step point-of-care immunodiagnostics using capillary-driven microfluidics and PDMS substrates, Lab on a Chip, 9, 3330-3337.

Glokler, J., Angenendt, P., 2003, Protein and antibody microarray technology, Journal of Chromatography B. 797, 229-240.

Green, R.J., Davies, J., Davies, M.C., Roberts, C.J., Tendler, S.J.B., 1997, Surface plasmon resonance for real time in situ analysis of protein adsorption to polymer surfaces, Biomaterials, 18, 405-413.

Green, R.J., Davies, M.C., Roberts, C.J., Tendler, S.J.B., 1999, Competitive protein adsorption as observed by surface plasmon resonance, Biomaterials, 20, 385-391.

Haab, B.B., 2003, Methods and applications of antibody microarrays in cancer research, Proteomics, 3, 2116-2122.

Han, Y., Uosaki, K., 2008, Effects of concentration and temperature on the formation process of decanethiol self-assembled monolayer on Au(111) followed by electrochemical reductive desorption, Electrochimica Acta, 53, 6196-6201.

Hemmersam, A.G., Foss, M., Chevallier, J., Besenbacher, F., 2005, Adsorption of fibrinogen on tantalum oxide, titanium oxide and gold studied by the QCM-D technique, Colloids and Surfaces B: Biointerfaces, 43, 208-215.

Henderson, A.P., Seetohul, L.N., Dean, A.K., Russell, P., Pruneanu, S., Ali, Z., 2009, A Novel Isotherm, Modeling Self-Assembled Monolayer Adsorption and Structural Changes, Langmuir, 25, 931-938.

Himmelhaus, M., Eisert, F., Fischer, J., Grunze, M., 2000, Self-Assembly of n-Alkanethiol Monolayers. A Study by IR−Visible Sum Frequency Spectroscopy, J. Phys. Chem. B. 104, 576-584.

Holden, M., Cremer, P.S., 2005, Microfluidic tools for studying the specific binding, adsorption, and displacement of proteins at interfaces, Annu. Rev. Phys. Chem. 56, 369-387.

Horbett, T.A., Brash, J.L., 1995, Proteins at Interfaces II:Fundamentals and Applications, American Chemical Society,Washington DC, 112–128.

Huber, L.A., 2002, Preface: Proteomics and Genomics Technologies, Journal of Mammary Gland Biology and Neoplasia, 7(4), 357-358.

Ince, R., Narayanaswamy, R., 2006, Analysis of the performance of interferometry, surface plasmon resonance and luminescence as biosensors and chemoscensors, Analytica Chimica Acta. 569, 1-20.

Imabayashi, S., Iida, M., Hobara, D., Feng, Z.Q., Niki, K., Kakiuchi, T., 1997, Reductive desorption of carboxylic-acid-terminated alkanethiol monolayers from Au(111) surfaces, Journal of Electroanalytical Chemistry, 428, 33-38.

Jakubowicz, A., Jia, H., Wallace, R.M., Gnade, B.E., 2005, Adsorption Kinetics of p-Nitrobenzenethiol Self-Assembled Monolayers on a Gold Surface, Langmuir, 21, 950-955.

Jang, L., Keng, H., 2008, Modified fabrication process of protein chips using a short-chain self-assembled monolayer, Biomed. Microdevices. 10, 203-211.

Jung, L.S., Campbell, C.T., 2000, Sticking Probabilities in Adsorption of Alkanethiols from Liquid Ethanol Solution onto Gold, J. Phys. Chem. B. 104, 11168-11178.

Jurs, P.C., Bakken, G.A., McClellan, H.E., 2000, Computational methods for the analysis of chemical sensor array data from volatile analytes, Chem. Rev., 100, 2649-2678.

Kamahori, M., Ishige, Y., Shimoda, M., 2007, A novel enzyme immunoassay based on potentiometric measurement of molecular adsorption events by an extended-gate field-effect transistor sensor, Biosensors and Bioelectronics, 22, 3080-3085.

Kamath, S., Lip, G.Y.H., 2003, Fibrinogen: biochemistry, epidemiology and determinants, Q. J. Med. 96, 711-729.

Khan, J., 2003, Genomic & Proteomic Technological Advances in Cancer Research, Pharmacogenomics, 4(3), 245-249.

Kim, J.P, Lee, B.Y., Hong, S., Sim, S.J., 2008, Ultrasensitive carbon nanotube-based biosensors using antibody-binding fragments, Analytical Biochemistry, 381, 193-198.

Kim, D.J., Pitchimani, R., Snow, D.E., Hopeweeks, L.J., 2008, A simple method for the removal of thiols on gold surfaces using an $NH_4OH–H_2O_2–H_2O$ solution, Scanning, 30, 118-122.

Kissinger, P.T., 2005, Biosensors-a perspective, Biosensors and Bioelectronics, 20, 2512-2516.

Krahn, J., Dembinski, T., 2009, Thyroblobulin and anti-thyroglobulin assays in thyroid cancer monitoring, Clinical Biochemistry, 42, 416-419.

Kusnezow, W., Hoheisel, J.D., 2002, Antibody Microarray: Promises and Problems, Bio Techniques, 33, S14-S23.

Kurosawa, S., Nakamura, M., Park, J.W., Aizawa, H., Yamada, K., Hirata, M., 2004, Evaluation of a high-affinity QCM immunosensor using antibody fragmentation and 2-methacryloyloxyethyl phosphorylcholine (MPC) polymer, Biosensors and Bioelectronics, 20, 1134-1139.

Noh, H., Vogler, E.A., 2007, Volumetric interpretation of protein adsorption: Competition from mixtures and the Vroman effect, Biomaterials, 28, 405-422.

Lahiri, J., Isaacs, L., Tien, J., Whitesides, G.M., 1999, A Strategy for the Generation of Surfaces Presenting Ligands for Studies of Binding Based on an Active Ester as a Common Reactive Intermediate: A Surface Plasmon Resonance Study Anal. Chem. 71, 777-790.

Lam, P., Kumar, K., Wnek, G.E., Przybycien, T.M., 1999, A Prototype Electrochemical Chromatographic Column for Use with Proteins, Anal. Chem. 71, 4272-4277.

Latour, R.A. Jr., 2005, Biomaterials: Protein–Surface Interactions. Encyclopedia of Biomaterials and Biomedical Engineering, 1-15.

Lavigne, J.J., Anslyn, E.V., 2001, Sensing A Paradigm Shift in the Field of Molecular Recognition: From Selective to Differential Receptors, Angewandte Chemie International Edition, 40, 3119-3130.

Lee, H.J., Yan, Y., Marriott, G., Corn, R.M., 2005, Quantitative functional analysis of protein complexes on surfaces, J. Physiol., 563(1), 61-71.

Lee, K., Su, Y., Chen, S., Tseng, F., Lee, G., 2007, Microfluidic systems integrated with two-dimensional surface plasmon resonance phase imaging systems for microarray immunoassay, Biosensors and Bioelectronics, 23, 466-472.

Lee, L.Y.S., Lennox, R.B., 2007, Electrochemical Desorption of n-Alkylthiol SAMs on Polycrystalline Gold: Studies Using A Ferrocenylalkylthiol Probe, Langmuir, 23, 292-296.

Li, Y., Xiang, J., Zhou, F., 2007, Toward one-step point-of-care immunodiagnostics using capillary-driven microfluidics and PDMS substrates, Plasmonics, 2, 79-87.

Limbut, W., Kanatharana, P., Mattiasson, B., Asawatreratanakul, P., Thavarungkul, P., 2006, A comparative study of capacitive immonosensors based on self-assembled monolayer from thiourea, thioctic acid and 3-mercaptopropioic acid, Biosensors and Bioelectronics, 2006, 22, 233-240.

Love, J.C., Estroff, L.A., Kriebel, J.K., Nuzzo, R.G., Whitesides, G.M., 2005, Self-Assembled Monolayers of Thiolates on Metals as a Form of Nanotechnology, Chem. Rev. 105, 1103-1169.

Luderer, F., Walschus, U., 2005, Immobilization of Oligonucleotides for Biochemical Sensing by Self-Assembled Monolayers: Thiol-Organic Bonding on Gold and Silanization on Silica Surfaces, Top Curr. Chem. 260, 37-56.

Lukaszewski, M., Czerwinski, A., 2006, Dissolution of noble metals and their alloys studied by electrochemical quartz crystal microbalance, Journal of Electroanalytical Chemistry, 589, 38-45.

Luo, Y., Yu, F., Zare, R.N., 2008, Microfluidic device for immunoassays based on surface plasmon resonance imaging, Lab on a Chip, 8, 694-700.

Masson, J., Battaglia, T.M., Cramer, J., Beaudoin, S., Sierks, M., Booksh, K.S., 2006, Reduction of nonspecific protein binding on surface plasmon resonance biosensors, Anal.Bioanal. Chem. 386, 1951-1959.

Minunni, M., Tombelli, S., Gullotto, A., Luzi, E., Mascini, M., 2004, Development of biosensors with aptamers as bio-recognition element: the case of HIV-1 Tat protein, Biosensors and Bioelectronics, 20, 1149-1156.

Mirsky, V.M., 2002, New electroanalytical applications of self-assembled monolayers, Trends in Analytical Chemistry, 21, 439-450.

Mohammed, M., Desmulliez, M.P.Y., 2011, Lab-on-a-chip based immunosensor principles and technologies for the detection of cardiac biomarkers: a review, Lab on a chip, 11, 569-595.

Mohanty, S.P., Kougianos, E., 2006, Biosensors: a tutorial review, IEEE Potentials, 25, 35-40.

More, S.M., Hudecek, J., Urisu, T., 2003, Hydrophobic/hydrophilic interactions of cytochrome c with functionalized self-assembled monolayers on silicon, Surface Science, 532-535, 993-998.

Nakamura, H., Karube, I., 2003, Current research activity in biosensors, Anal. Bioanal. Chem., 377, 446-468.

Noh, H., Vogler, E.A., 2007, Volumetric interpretation of protein adsorption: Competition from mixtures and the Vroman effect, Biomaterials, 28, 405-422.

O'Dwyer, C., Gay, G., Viaris de Lesegno, B., Weiner, J., 2004, The Nature of Alkanethiol Self-Assembled Monolayer Adsorption on Sputtered Gold Substrates, Langmuir, 20, 8172-8182.

Ogi, H., Fukunishi, Y., Nagai, H., Okamoto, K., Hirao, M., Nishiyama, M., 2009, Nonspecific-adsorption behavior of polyethylenglycol and bovine

serum albumin studied by 55-MHz wireless–electrodeless quartz crystal microbalance, Biosensors and Bioelectronics, 24, 3148-3152.

Oldham, P.B., Asanov, A.N., 1999, Control of antibody-antigen binding or dissociation by electric field, The SPIE Conference on Clinical Diagnostic Systems and Technologies, 156-162.

Oliva, A.G., Cruz, H.J., Rosa, C.C., 2001, Immunosensors for Diagnostics, Sensors update, 9, 283-312.

Oyamatsu, D., Fujita, T., Arimoto, S., Munakata, H., Matsumoto, H., Kuwabata, S., 2008, Electrochemical desorption of a self-assembled monolayer of alkanethiol in ionic liquids, Journal of Electroanalytical Chemistry, 615, 110-116.

Pan, W., Durning, C.J., Turro, N.J., 1996, Kinetics of Alkanethiol Adsorption on Gold. Langmuir, 12, 4469-4473.

Park, J.S., Oh, K.K., Kim, E., Chang, H., Hong, S.W., 2006, Sonographic Screening for Thyroid Cancer in Females Undergoing Breast Sonography, American Journal of Roentgenology, 186, 1025-1028.

Pavlickova, P., Schneider, M., Hug, H., 2004, Advances in recombinant antibody microarrays, Clinica Chimica Acta, 343, 17-35.

Pesika, N.S., Stebe, K.J., Searson, P.C., 2006, The Kinetics of Desorption of Alkanethiolates on Gold, Langmuir, 22, 3474-3476.

Peterlinz, K.A., Georgiadis, R., 1996, In Situ Kinetics of Self-Assembly by Surface Plasmon Resonance Spectroscopy, Langmuir, 12, 4731-4740.

Powner, E.T., Yalcinkaya, F., 1997, Intelligent biosensors, Sensor Review, 17, 107-116.

Predki, P.F., Mattoon, D., Bangham, R., Schweitzer, B., Michaud, G., 2005, Protein microarray: A new tool for profiling antibody cross-reactivity, Human Antibodies, 14, 7-15.

Qu, D., Morin, M., 2001, An EQCM study of the oxidative deposition of alkylthiolates on gold, Journal of Electroanalytical Chemistry, 517, 45-53.

Raiber, K., Terfort, A., Benndorf, C., Krings, N., Strehblow, H., 2005, Removal of self-assembled monolayers of alkanethiolates on gold by plasma cleaning, Surface Science, 595, 56-63.

Riepl, M., Mirsky, V.M., Wolfbeis, O.S., 1999, Electrical Control of Alkanethiols Self-Assembly on a Gold Surface as an Approach for Preparation of Micro-Electrode Arrays, Mikrochim. Acta. 131, 29-34.

Rifai, N., Gillette, M.A., Carr, S.A, 2006, Protein biomarker discovery and validation: the long and uncertain path to clinical utility, Nature biotechnology 24(8), 971-983.

Sahab, Z. J., Semaan, S.M., Sang, Q.A., 2007, Methodology and Applications of Disease Biomarker Identification in Human Serum, Biomarker Insights, 2, 21-43.

Saerens, D., Huang, L., Bonroy, K., Muyldermans, S., 2008, Antibody Fragments as Probe in Biosensor Development, Sensors, 8, 4669-4686.

Santini, J.T., Richards, A.C., Scheidt, R., Chima, M.J., Langer, R., 2000, Microchips as controlled drug-delivery devices, Angew. Chem. Int. Ed. 39, 2396-2407.

Sarkar, P., Pal, P.S., Ghosh, D., Setford, S.J., Tothill, I.E., 2002, Amperometric biosensors for detection of the prostate cancer marker (PSA), International Journal of Pharmaceutics, 238, 1-9.

Sasaki, S., Kai, E., Miyachi, H., Muguruma, H., Ikebukuro, K., Ohkawa, H., Karube, I., 1998, Direct determination of etofenprox using surface plasmon resonance, Analytica Chimica Acta, 363, 229-233.

Schasfoort, R.B.M., Tudos, A.J., 2008, Handbook of Surface Plasmon Resonance. The Royal Society of Chemistry.

Schilardi, P.L., Dip, P., dos Santos Claro, P.C., Benitez, G.A., Fonticelli, M.H., Azzaroni, O., Salvarezza, R.C., 2006, Electrochemical Deposition onto Self-Assembled Monolayers: New Insights into Micro- and Nanofabrication, Chem. Eur. J., 12, 38-49.

Schubert, F., Zettl, H., Hafner, W., Krauss, G., Krausch, G., 2003, Comparative thermodynamic analysis of dna-protein interactions using surface plasmon resonance and fluorescence correlation spectroscopy, Biochemistry, 42, 10288-10294.

Shepherd, J.L., Kell, A., Chung, E., Sinclar, C.W., Worentin, M.S., Bizzotto, D., 2004, Selective Reductive Desorption of a SAM-Coated Gold Electrode Revealed Using Fluorescence Microscopy, J. Am. Chem. Soc., 126, 8329-8335.

Simon, E., 2010, Biological and chemical sensors for cancer diagnosis, Measurement Science and Technology, 21, 112002.

Skottrup, P.D., Nicolaisen, M. Justesen, A.F., 2008, Towards on-site pathogen detection using antibody-based sensors, Biosensor and Bioelectronics, 24, 339-348.

Taussig, M., Landegren, U., 2003, Progress in antibody arrays, Targets, 2, 169-176.

Tsai, H.Y., Hsu, C.F., Chiu, I.W., Bor Fuh, C., 2007, Detection of C-reactive protein based on immunoassay using antibody-conjugated magnetic nanoparticles, Anal. Chem., 79, 8416-8419.

Tsuneda, S., Ishida, T., Nishida, N., Hara, M., Sasabe, H., Knoll, W., 1999, Tailoring of a smooth polycrystalline gold surface as a suitable anchoring site for a self-assembled monolayer, Thin Solid Film, 339, 142-147.

Twardowski, M., Nuzzo, R.G., 2002, Chemically Mediated Grain Growth in Nanotextured Au, Au/Cu Thin Films: Novel Substrates for the Formation of Self-Assembled Monolayers, Langmuir, 18, 5529-5538.

Tyers, M., Mann, M., 2003, From genomics to proteomics, Nature, 422, 193-197.

Turner A.P.F., Magan, N., 2004, Electronic noses and disease diagnostics, Nature Reviews Microbiology, 2, 161-166.

Van der Veen, M., Norde, W., Stuart, M.C., 2004, Electrostatic interactions in protein adsorption probed by comparing lysozyme and succinylated lysozyme, Colloids and surfaces B, 35, 33-40.

Vericat, C., Andreasen, G., Vela, M.E., Martin, H., Salvarezza, R.C., 2001, Following transformation in self-assembled alkanethiol monolayers on Au(111) by in situ scanning tunneling microscopy, Journal of Chemical Physics, 115 , 6672-6678.

Vikholm-Lundin, I., Albers, W.M., 2006, Site-directed immobilization of antibody fragments for detection of C-reactive protein, Biosensors and Bioelectronics, 21, 1141-1148.

Vroman, L., Adams, A.L., 1969, Findings with the recording ellipsometer suggesting rapid exchange of specific plasma proteins at liquid/solid interfaces, Surface Science, 16 , 438-446.

Xu, W., Choi, S., Chae, J., 2010, A contour-mode film bulk acoustic resonator of high quality factor in a liquid environment for biosensing applications, Applied Physics Letters, 96, 053703.

Wano, W., Uosaki, K., 2001, In Situ, Real-Time Monitoring of the Reductive Desorption Process of Self-Assembled Monolayers of Hexanethiol on Au(111) Surfaces in Acidic and Alkaline Aqueous Solutions by Scanning Tunneling Microscopy, Langmuir, 17, 8224-8228.

Wartofsky, L., Nostrand, D.V., 2005, Thyroid Cancer: A Comprehensive Guide to Clinical Management, Humana Press (2nd edition)

Widrig, C.A., Chung, C., Porter, M.D., 1991, The electrochemical desorption of n-alkanethiol monolayers from polycrystalline Au and Ag electrodes, Journal of Electroanalytical Chemistry, 310, 335-359.

Wilson, A.J., 2009, Nanonose for sniffing out proteins, Nature Chemistry, 1, 429-430.

Wink, Th., van Zuilen, S.J., Bult A, van Bennekom, W.P., 1997, Self-assembled Monolayers for Biosensors, Analyst, 122, 43R-50R.

Wu, G., Datar, R.H., Hansen, K.M., Thundat, T., Cote, R.J., Majumdar, A., 2001, Bioassay of prostate-specific antigen using microcantilevers, Nature Biotechnology, 19, 856-860.

Wu, J., Fu, Z., Yan, F., Ju, H., 2007, Biomedical and clinical applications of immunoassays and immunosensors for tumor markers, Trends in Analytical Chemistry, 26, 679-688.

Yang, D.F., Al-Maznai, H., Morin, M., 1997, Vibrational Study of the Fast Reductive and the Slow Oxidative Desorptions of a Nonanethiol Self-Assembled Monolayer from a Au(111) Single Crystal Electrode, J. Phys. Chem. B. 101, 1158-1166.

Yang, J., Han, J., Isaacson, K., Kwok, D.Y., 2003, Effects of Surface Defects, Polycrystallinity, and Nanostructure of Self-Assembled Monolayers for Octadecanethiol Adsorbed onto Au on Wetting and Its Surface Energetic Interpretation, Langmuir, 19, 9231-9238.

You, C., Miranda, O.R., Gider, B., Ghosh, P.S., Kim, I., Erdogan, B., Krovi, S.A., Bunz, U.H.F., Rotello, V.M., 2007, Detection and identification of proteins using nanoparticle-fluorescent polymer chemical nose sensors, Nature Nanotechnology, 2, 318-323.

Yu, Q., Golden, G., 2007, Probing the protein orientation on charged self-assembled monolayers on gold nanohole array by SERS, Langmuir, 23, 8659-8562.

Yu, X., Xu, D., Cheng, Q., 2006. Label-free detection methods for protein microarrays, Proteomics, 6, 5493–5503.

Yuan, M., Zhan, S., Zhou, X., Liu, Y., Feng, L., Lin, Y., Zhang, Z., Hu, J., 2008. A method for removing self-assembled monolayers on gold, Langmuir. 24, 8707-8710.

Zhang, X., Wu, Y., Tu, Y., Liu, S., 2008, A reusable electrochemical immunosensor for carcinoembryonic antigenvia molecular recognition of glycoproteinantibody by phenylboronic acid self-assembly layer on gold, Analyst, 133, 485-492.

Zheng, G., Patolsky, F., Cui, Y., Wang, W.U., Lieber, C.M., 2005, Multiplexed electrical detection of cancer markers with nanowire sensor arrays, Nature Biotechnology, 23, 1294-1301.

Zhou, H., Baldini, L., Hong, J., Wilson, A.J., Hamilton, A.D., 2006, Pattern recognition of proteins based on an array of functionalized porphyrins, J. Am. Chem. Soc., 128, 2421-2425.